

Aus dem Walter Brendel Zentrum für Experimentelle Medizin
Institut der Ludwig-Maximilians-Universität München
Direktor: Prof. Dr. med. Ulrich Pohl

Control of lymphocyte trafficking through lymph nodes by the circadian clock

DISSERTATION

zum Erwerb des Doctor of Philosophy (Ph.D.)
an der Medizinischen Fakultät der
Ludwig-Maximilians-Universität München

Vorgelegt von

David Jakob Druzd

aus
Knurow

am

.....2017.....



Mit Genehmigung der Medizinischen Fakultät
Der Universität München

Betreuer: Dr. Christoph Scheiermann
Zweitgutachter (in): Prof. Dr. Markus Sperandio
Prof. Dr. Oliver Söhnlein
Prof. Dr. Sussan Nourshargh
Dekan: Prof. Dr. med. dent. Reinhard Hickel

Tag der mündlichen Prüfung: 25.07.2017

Acknowledgment

I would like to thank my supervisor Dr. Christoph Scheiermann for his excellent guidance and supervision throughout the whole project.

Furthermore, I would like to thank my thesis advisory committee, Prof. Dr. Markus Sperandio and Prof. Dr. Steffen Massberg for their constructive suggestions on my PhD study.

I would further like to thank the members of our lab and the institute, in particular Kerstin Kraus, Michael Lorenz and Susanne Bierschenk for their continuous help and advice.

I benefited greatly from being enrolled in the graduate program of the SFB914. Throughout the last years it provided valuable seminars and courses and helped me a lot in broaden my horizon and becoming a scientist. In particular, I would like to thank Dr. Verena Kochan, for coordinating the program.

I would also like to thank my family, for their tremendous support and trust. From early on, they encouraged me in any activity I was fascinated about (and there were many) and never stopped to believe in me. With all your effort (and money!) you made it possible that I graduate and I will be forever grateful for that.

Finally, to my wife, Clara. You made me never lose faith in my work and gave me the best support one can imagine. Although you might not have understood much about immunology, you were the best listener and gave me the best advises of all. Thank you for everything!

And to our son Jakob, may you always stay curious and never stop to question how things work.

Abstract

Leukocyte recruitment from blood to tissues is a critical step of the immune system to protect against pathogens and provide tissue repair. While myeloid cell recruitment is a hallmark in inflammatory conditions, lymphocyte recirculation through tissues is an important feature of immune surveillance of an organism at steady state. Thus far, various molecules have been implicated in these migratory processes including chemokines and adhesion molecules. However, how this fundamental process of immunity is being regulated at the organismal level at different times is unknown. Here, we describe mechanisms that govern a non-continuous but oscillatory behavior in the infiltration of lymphoid and myeloid cells to different tissues in the mouse. Our data indicate the existence of a leukocyte- and tissue-specific oscillatory molecular signature in the expression of pro-migratory factors. Specifically, robust circadian oscillations, exhibiting a period length of ~24h, occur in cellular numbers in murine lymph nodes, showing a ~2-fold difference with a trough at the onset of the behavioral rest phase (light) and a peak at the onset of the active phase (dark). Oscillations were observed in the capacity of lymphocytes to home to lymph nodes, peaking at the onset of the activity phase, and to exit lymph nodes via efferent lymph, peaking during the rest phase. Using lineage-specific genetic ablation of circadian rhythmicity in T and B cells we demonstrate this to be dependent on both lymphocyte and endothelial oscillations in cell surface receptors. Taken together, our data show discrete tissue and leukocyte mechanisms that control rhythmic leukocyte trafficking and provide new insights into the temporal control of innate and adaptive immunity.

Table of Contents

ACKNOWLEDGMENT	- 1 -
ABSTRACT	- 2 -
TABLE OF CONTENTS	- 3 -
TABLE OF FIGURES AND TABLES	- 6 -
ABBREVIATIONS	- 8 -
1 INTRODUCTION	- 11 -
1.1 THE LYMPHATIC SYSTEM.....	- 12 -
1.1.1 <i>The lymphatic vasculature</i>	- 12 -
1.2 HOMING OF CELLS INTO LYMPH NODES.....	- 15 -
1.2.1 <i>Checkpoint for Lymph node homing: High endothelial venules</i>	- 15 -
1.2.2 <i>The leukocyte adhesion cascade</i>	- 17 -
1.3 LEUKOCYTE EGRESS FROM LYMPHOID ORGANS.....	- 19 -
1.3.1 <i>Egress of cells into efferent lymphatic vessels</i>	- 19 -
1.3.2 <i>Control of leukocyte egress</i>	- 21 -
1.3.3 <i>Pharmacological blockade of leukocyte egress</i>	- 22 -
1.4 CIRCADIAN RHYTHMS	- 24 -
1.4.1 <i>Biological rhythms</i>	- 24 -
1.4.2 <i>The molecular clock machinery</i>	- 25 -
1.4.3 <i>Central and peripheral clocks</i>	- 27 -
1.4.4 <i>Circadian rhythms in immune cell trafficking</i>	- 30 -
1.4.5 <i>Circadian rhythms in the immune response</i>	- 31 -
2 MATERIAL AND METHODS	- 33 -
2.1 ANIMAL HUSBANDRY	- 34 -

2.2 GENOTYPING BY PCR	- 34 -
2.3 SURGICAL TECHNIQUES	- 37 -
2.3.1 <i>Lymph cannulation</i>	- 37 -
2.4 PHARMACOLOGICAL INHIBITION OF LYMPH NODE EGRESS.....	- 38 -
2.5 ADOPTIVE TRANSFER STUDIES AND HOMING BLOCK.....	- 38 -
2.6 BLOOD SAMPLE COLLECTION	- 39 -
2.7 FLOW CYTOMETRY.....	- 39 -
2.8 T CELL ISOLATION.....	- 41 -
2.9 QUANTITATIVE RT-PCR	- 41 -
2.10 IMMUNOFLUORESCENCE MICROSCOPY	- 44 -
2.11 QUANTITATIVE IMAGING ANALYSIS	- 45 -
2.12 MASS SPECTROMETRY	- 47 -
2.13 STATISTICAL ANALYSES	- 48 -
3 RESULTS	- 49 -
3.1 LEUKOCYTE NUMBERS IN LYMPH NODES OSCILLATE IN A TIME-OF-DAY-DEPENDENT FASHION	- 50 -
3.1.1 <i>Steady-state oscillations in skin draining and mesenteric lymph nodes</i>	- 50 -
3.1.2 <i>Lymph node oscillations persist under altered light regimes</i>	- 52 -
3.1.3 <i>Dynamic egress and homing of cells into lymph nodes</i>	- 52 -
3.2 HOMING OF CELLS INTO LYMPH NODES IS UNDER CIRCADIAN CONTROL	- 54 -
3.2.1 <i>Homing of cells into lymph nodes is time-of-day dependent</i>	- 55 -
3.2.2 <i>Rhythmic leukocyte homing is regulated by leukocyte- and endothelium-derived factors</i>	- 55 -
3.2.3 <i>Rhythmic homing is dependent on circadian CCR7 expression</i>	- 60 -
3.3 ROLE OF CLOCK GENES IN LEUKOCYTE TRAFFICKING	- 62 -
3.3.1 <i>Clock genes oscillate in lymph nodes</i>	- 62 -

3.3.2 <i>Phenotype of T- and B-cell specific Bmal1 knock-out mice</i>	- 63 -
3.4 LEUKOCYTE EGRESS INTO EFFERENT LYMPHATIC IS UNDER CIRCADIAN CONTROL	- 66 -
3.4.1 <i>Circadian oscillations in leukocyte numbers in lymph fluid</i>	- 66 -
3.4.2 <i>Leukocyte half-life in LNs is time-of-day dependent</i>	- 68 -
3.4.3 <i>Leukocyte egress and half-life is non-rhythmic in CD4 T lymphocytes lacking Bmal1</i>	- 70 -
3.5 RHYTHMIC LEUKOCYTE EGRESS IS DEPENDENT ON CIRCADIAN S1PR1 EXPRESSION	- 72 -
3.5.1 <i>Modulation of lymphocyte trafficking in S1pr1 gene-targeted mice</i>	- 75 -
4 DISCUSSION	- 78 -
4.1 CELLULAR OSCILLATIONS OF LEUKOCYTE NUMBERS IN LYMPH NODES	- 80 -
4.2 CONTROL OF LYMPH NODE CELLULARITY BY THE CIRCADIAN CLOCK	- 81 -
4.2.1 <i>Homing of cells into lymph nodes is under circadian control</i>	- 81 -
4.2.2 <i>Leukocyte egress into efferent lymphatic vessels is under circadian control</i> ... - 84 -	
4.2.3 <i>Rhythmic leukocyte egress is dependent on circadian S1pr1 expression</i> - 85 -	
4.3 OUTLOOK.....	- 87 -
5 REFERENCES	- 89 -
6 APPENDIX	- 99 -
6.1 PUBLICATIONS ARISING FROM THIS WORK	- 99 -
AFFIDAVIT	- 100 -

Table of Figures and Tables

Figure 1.1 The lymphatic system.....	- 13 -
Figure 1.2 Major Trunks and Ducts of the Lymphatic System	- 14 -
Figure 1.3 Organization of the vessel system in lymph nodes.....	- 16 -
Figure 1.4 The leukocyte adhesion cascade.....	- 18 -
Figure 1.5 S1P and S1P1 control leukocyte trafficking.....	- 20 -
Figure 1.6 Factors promoting leukocyte retention versus egress.....	- 21 -
Figure 1.7 Mode of Action of FTY720.....	- 23 -
Figure 1.8 The circadian clock	- 25 -
Figure 1.9 Entrainment and synchronization of peripheral clocks by the central clock.....	- 27 -
Figure 2.1 PCR genotyping gel.....	- 36 -
Figure 2.2 Cannulation of mesenteric lymphatic vessels.....	- 37 -
Figure 2.3 Surface expression measurements on lymph node sections.....	- 45 -
Figure 2.4 MFI data points from software analysis.....	- 46 -
Figure 2.5 CCL21 gradient measurement.....	- 47 -
Figure 3.1 Oscillations in total cell counts and leukocyte subsets in inguinal lymph nodes	- 50 -
Figure 3.2 Cellular oscillations and leukocyte subsets of different peripheral lymph nodes	- 51 -
Figure 3.3 Rhythms in cell counts are sustained under different light regimes	- 52 -
Figure 3.4 Homing and Egress block ablate oscillations in LN counts	- 53 -
Figure 3.5 Steady-state proliferation within lymph nodes does not occur rhythmically	- 54 -
Figure 3.6 Lymph node homing is time-of-day dependent.....	- 55 -
Figure 3.7 Leukocyte and endothelium-derived factors contribute to rhythmic LN homing.....	- 56 -
Figure 3.8 Integrin, selectin and chemokine receptor expression levels in blood	- 57 -
Figure 3.9 Integrin, selectin and chemokine receptor expression levels in lymph nodes...	- 58 -
Figure 3.10 Expression levels of adhesion molecules on HEVs.....	- 59 -
Figure 3.11 CCL21 expression levels oscillate within HEVs and lymph nodes	- 60 -
Figure 3.12 Rhythmic homing is blocked upon short PTX pre-treatment	- 61 -
Figure 3.13 Lymph node cellularity and homing of <i>Ccr7</i> KO mice	- 62 -

Figure 3.14 Expression profiles of clock genes in lymph nodes.....	- 63 -
Figure 3.15 Leukocyte counts in T-cell specific <i>Bmal1</i> knock-out mice.....	- 64 -
Figure 3.16 Leukocyte counts in B-cell specific <i>Bmal1</i> knock-out mice.....	- 64 -
Figure 3.17 Lymph node homing of leukocytes harvested from control and T-cell-specific <i>Bmal1</i> knock-out mice.....	- 65 -
Figure 3.18 CCR7 surface expression and mRNA levels of control and T-cell-specific <i>Bmal1</i> KO mice	- 66 -
Figure 3.19 Leukocyte and lymphocyte numbers oscillate in lymph fluid.....	- 67 -
Figure 3.20 Lymph cell counts under constant darkness.....	- 68 -
Figure 3.21 Lymph flow is constant at different Zeitgeber times.....	- 68 -
Figure 3.22 Analysis of remaining endogenous lymphocytes in lymph nodes and lymph after homing block	- 69 -
Figure 3.23 Half-life analysis of adoptively transferred cells in lymph nodes and lymph ...	- 70 -
Figure 3.24 Leukocyte counts in lymph of T-cell-specific <i>Bmal1</i> KO mice	- 71 -
Figure 3.25 Impaired leukocyte dwell time in <i>Bmal1</i> -deficient CD4 T-cells	- 72 -
Figure 3.26 Q-PCR analysis of S1P1-5 receptors	- 73 -
Figure 3.27 Time-of-day dependent sensitivity against FTY720.....	- 74 -
Figure 3.28 Q-PCR analysis of <i>S1pr1</i> levels in CD4 T-cells.....	- 74 -
Figure 3.29 Lymph and Plasma S1P levels over 24 hours	- 75 -
Figure 3.30 Leukocyte counts in T-cell-specific <i>S1pr1</i> heterozygous mice.....	- 76 -
Figure 3.31 Leukocyte counts in <i>S1pr1xCD4</i> inducible Cre mice	- 77 -
Table 2.1 PCR reaction mix used for genotyping	- 35 -
Table 2.2 PCR primers used for genotyping	- 36 -
Table 2.3 Antibody clones used for flow cytometry	- 40 -
Table 2.4 Quantitative RT-PCR primers.....	- 42 -
Table 2.5 Antibodies used for immunofluorescence microscopy.....	- 44 -

Abbreviations

ACTH	Adrenocorticotropic hormone
ANOVA	Analysis of variance
ARNTL	Aryl hydrocarbon receptor nuclear translocator-like protein
BMAL1	Brain and muscle aryl hydrocarbon receptor nuclear translocator (ARNT)-like 1
CCL	Chemokine (C-C motif) ligand
CCR	C-C chemokine receptor type
CD	Cluster of differentiation
CD62L	L-Selectin
CFSE	Carboxyfluorescein succinimidyl ester
CLOCK	Circadian Locomotor Output Cycles Kaput
CMTPX	CellTracker™ Red
CRY	Cryptochrome
CXCL	Chemokine (C-X-C motif) ligand
CXCR	C-X-C chemokine receptor type
DC	Dendritic cell
DD	Dark:dark
DL	Dark:light
EAE	Experimental autoimmune encephalomyelitis
EDG	Endothelial differentiation gene
EDTA	Ethylenediaminetetraacetic acid
FDA	U.S. food and drug association
FDC	Follicular dendritic cell
FRC	Fibroblast reticular cell
FTY720	Fingolimod (trade name Gilenya, Novartis)
GAPDH	Glyceraldehyde-3-phosphate dehydrogenase
GR	Glucocorticoid receptors
HEV	High endothelial venule
HPA	Hypothalamic-pituitary adrenal axis
HSC	Hematopoietic stem cell
HSPC	Hematopoietic stem and progenitor cell

ICAM	Intercellular adhesion molecule
IEC	Intestinal epithelial cell
KLF	Krüppel-like-factor
KO	Knock-out
LD	Light:dark
LEC	Lymphatic endothelial cell
LFA	Lymphocyte function-associated antigen
LN	Lymph node
LPA	Lysophosphatidic acid
LPS	Lipopolysaccharide
Lyve	Lymphatic vessel endothelial hyaluronan receptor
MAdCAM	Mucosal vascular addressin cell adhesion molecule
MEK	Mitogen-activated protein kinase kinase
MFI	Mean fluorescence intensity
MHC	Major Histocompatibility Complex
NADH	Nicotinamide adenine dinucleotide
NFIL3	Nuclear factor interleukin 3 regulated
NFkB	Nuclear factor kappa-light-chain-enhancer of activated B-cells
NK	Natural killer
PD-L	Programmed death-ligand
PECAM	Platelet endothelial cell adhesion molecule
PER	Period circadian protein
pLN	Peripheral lymph node
PNAd	Peripheral node addressin
PRX	Peroxiredoxin
PTX	Pertussis toxin
PVN	Paraventricular and arcuate nuclei
RT-PCR	Real-time polymerase chain reaction
S1P	Sphingosine-1-phosphate
S1PR	Sphingosine-1-phosphate receptor
SCN	Suprachiasmatic nucleus
SLO	Secondary lymphoid organs
SphK	Sphingosine kinase
SPL	Sphingosine-1-phosphate lyase

THI	2-acetyl-4-tetrahydroxybutylimidazole
TLR	Toll-like receptor
VCAM	Vascular cell adhesion molecule
WT	Wild-type
ZT	Zeitgeber time

1 Introduction

1.1 The lymphatic system

1.1.1 The lymphatic vasculature

In order to survey for antigens, leukocytes leave the bone marrow and thymus, from where they originate and circulate through blood, tissues, secondary lymphoid organs and lymph. Hippocrates and Aristoteles were the very first to mention the existence of lymphatic vessels, with Erasistratus from Alexandria being the first one who mentioned 'milky arteries' in the mesentery (Wigle & Oliver 1999; Banerji et al. 1999). But it took more than 2000 years to reveal the detailed characteristics and specific markers of the lymphatic system with the help of modern microscopy techniques.

The lymphatic vasculature is unique to vertebrates and is composed of tissue (afferent lymphatics) and lymph node (LN) (efferent lymphatics) draining lymphatic vessels. In contrast to blood vessels, tissue-draining lymphatic vessels are blind-ended, unidirectional absorptive vessels that can be found almost everywhere, except in the bone marrow. Even the central nervous system, which has long been thought not to be connected to the lymphatic system, does contain lymphatic vessel-like structures around the meninges (Louveau et al. 2015).

The basic principle of the lymphatic vessel system is that afferent lymphatic vessels absorb immune cells, interstitial solutes and macromolecules that extravasate for example from blood. These lymphatic capillaries are connected to bigger collecting vessels, which contain valves that help drive the lymph actively forward in concert with smooth muscle cell contraction. Multiple afferent vessels lead to a tissue draining lymph node, whereas efferent lymph vessels can also be directly connected to the venous circulation (Figure 1.1).

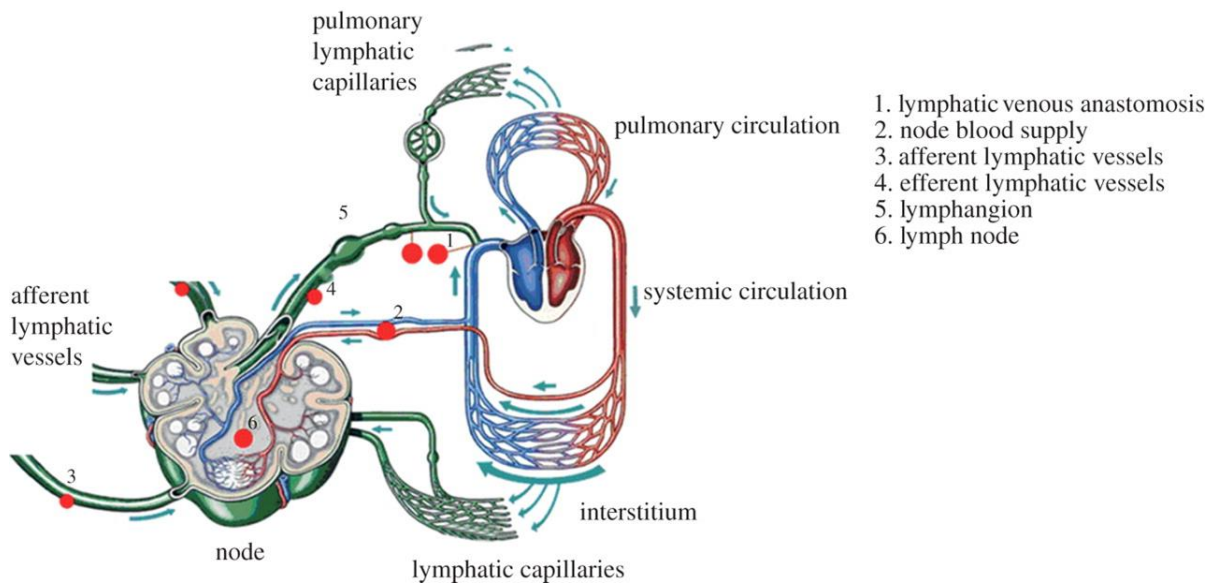


Figure 1.1 The lymphatic system

Lymphatic and pulmonary lymphatic capillaries absorb interstitial fluid and immune cells which extravasate from blood in peripheral tissues and transport these via afferent lymphatic vessels to a lymph node. Lymph fluid and accompanying cells exit the lymph node via an efferent lymphatic vessel, and finally drain back into blood, predominantly via the thoracic duct (Margaris & Black 2012).

After percolating through the lymph node, lymph fluid exits the lymph node via one efferent lymphatic vessel and flows either to another lymph node or enters collecting vessels, the lymphatic ducts. Most organs drain into the thoracic duct, while only the right arm and chest drain into the right lymphatic duct (Figure 1.2).

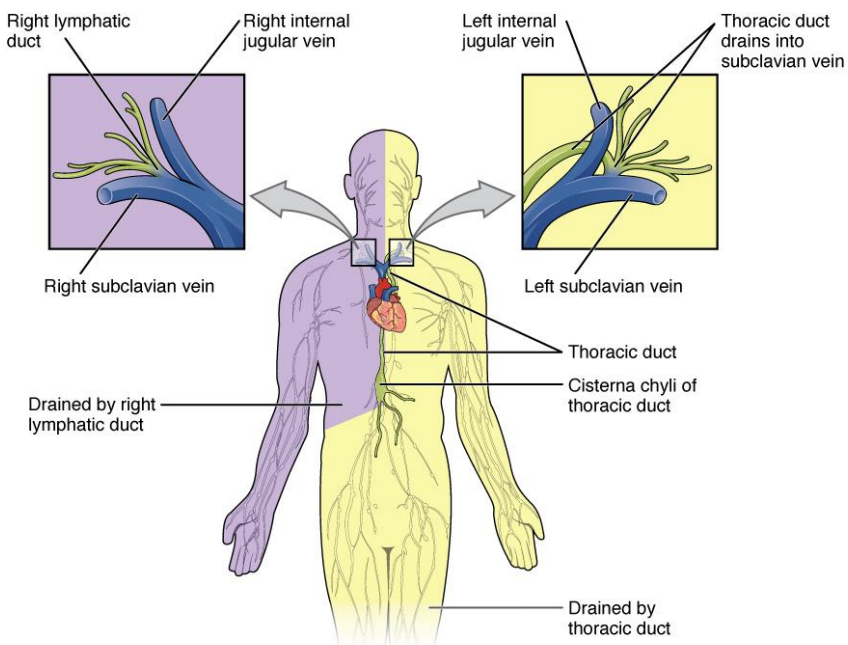


Figure 1.2 Major Trunks and Ducts of the Lymphatic System

Rough classification of body parts which drain either into the right lymphatic duct or the cisterna chyli of the thoracic duct (Fretham 2014).

The majority of plasma, which extravasates from blood is transported back through this system, highlighting its important role for body fluid homeostasis. Interestingly, lymphatic endothelial cells (LECs) which cover the inner walls of lymphatic vessels do not only play a passive role by serving as highways for lymph-borne cells, but also actively regulate several immune processes. For instance in the case of immune tolerance, LECs function as antigen-presenting cells: In some cases, leukocytes can escape thymic negative selection. By expressing tissue antigens such as MHC I or PD-L1, LECs are able to inactivate self-reactive CD8 T-cells, thereby serving as systemic mediators of peripheral immune tolerance (Cohen et al. 2010).

1.2 Homing of cells into lymph nodes

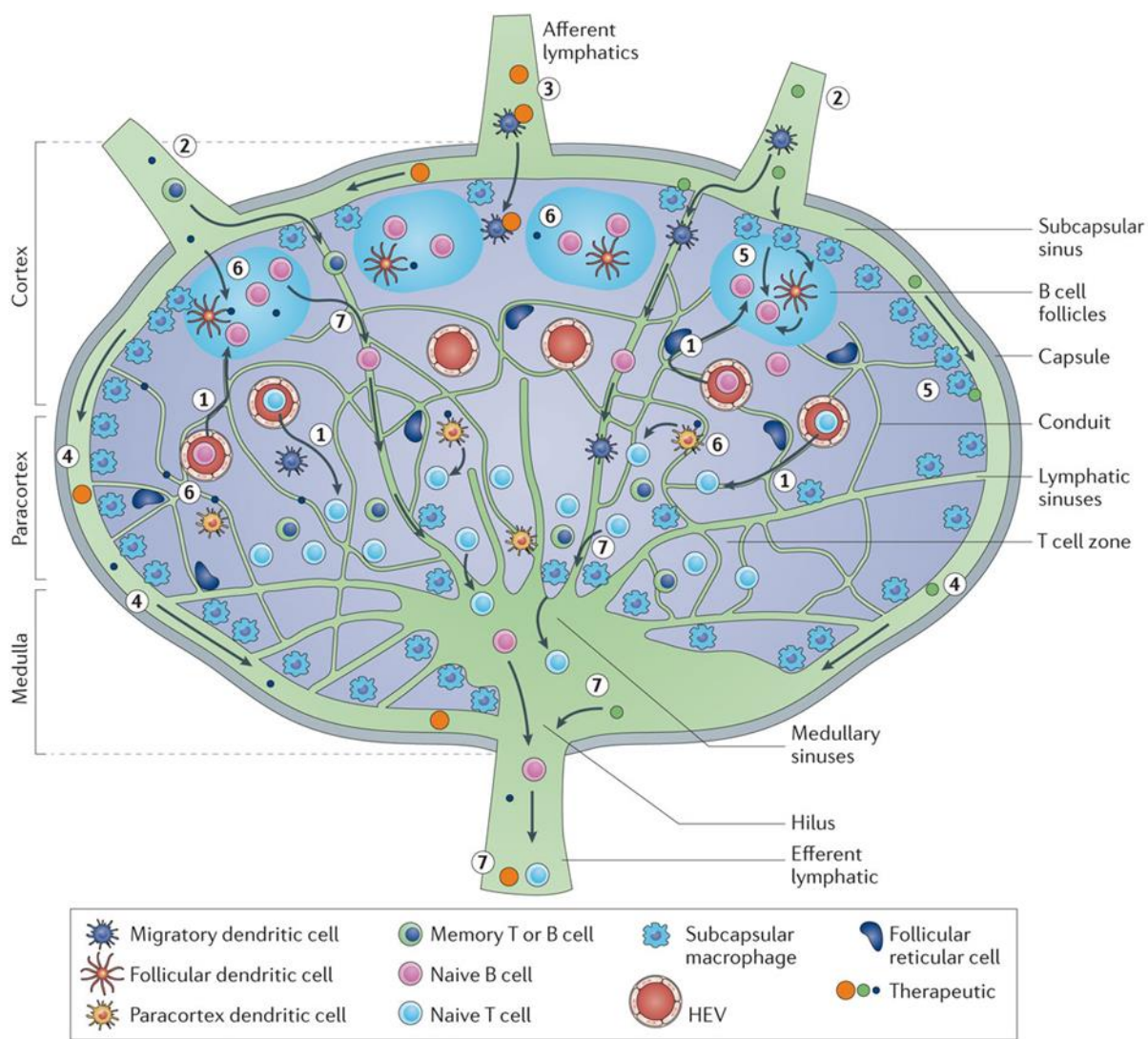
1.2.1 Checkpoint for Lymph node homing: High endothelial venules

Lymph nodes are key players in innate and adaptive immune responses. They are the sieve, where lymphocytes scan dendritic cells and fibroblastic reticular cells (FRCs) for activating, tolerogenic or homeostatic stimuli (Ager & May 2015).

In 1964, Sir James Gowan injected radioactively labelled cells into rats and could demonstrate that leukocytes continuously traffic from blood to secondary lymphoid organs (SLOs) and back to blood. He described post-capillary venules in lymphoid organs as the main entry sites for cells (J. L. Gowans 1964, Girard et al. 2012;). But it took decades to decipher the characteristics and the exact role of these venules in the regulation of cellular entry into SLOs. In the lymph node, due to their morphological features, they became known as high endothelial venules (HEVs).

HEVs are, as Sir James Gowan postulated, post-capillary venules, which lie downstream of incoming arteries of SLOs and can be found in the outer cortex or the B-cell area. They consist of a branched network of vessels that form circuits in order to connect incoming arteries with the collecting vein that exits lymph nodes. These vessels are relatively large in the paracortex and the T-cell area of lymph nodes and decrease in size towards cortical-paracortical junctions. In the medulla, these vessels merge with venules, which drain into the collecting vein and subsequently exit lymph nodes (Figure 1.3).

HEVs are characterized by a cuboidal morphology, referring to their tall (high) endothelium, a thick apical glycocalyx and a basal lamina that is coated with pericytes and follicular reticular cells (FRCs). The apical glycocalyx is made up of sialomucins, which are also known as peripheral node adressins (PNAd), and are specific for lymph nodes of peripheral tissues. In mucosal lymphoid organs another protein can be found on the apical side of HEVs, MAdCAM-1, which is a ligand for the leukocyte integrin $\alpha 4\beta 7$. In contrast to PNAd, MAdCAM-1 is not specific for lymph nodes, as it is also being expressed on blood vessels in the spleen.



Nature Reviews | Drug Discovery

Figure 1.3 Organization of the vessel system in lymph nodes

Lymph nodes have two different incoming vessel structures relevant for leukocytes, afferent lymphatic vessels and HEVs. Skin-draining cells (most prominently dendritic cells) enter lymph nodes via afferent lymphatic vessels, whereas blood-derived cells enter lymph nodes via HEVs (see text for details). Skin-draining and blood-derived cells leave lymph nodes via an efferent lymphatic vessel or as is the case for some dendritic cell populations that undergo apoptosis in the lymph node (Trevaskis et al. 2015).

1.2.2 The leukocyte adhesion cascade

Although HEVs can also be found during chronic inflammation in non-lymphoid organs (Martinet et al. 2011), their general role is to serve as checkpoints and facilitate the entry of leukocytes from the bloodstream into lymph nodes.

Homing of leukocytes into lymph nodes follows a complex multistep adhesion and migration cascade, including leukocyte tethering and rolling, followed by firm adhesion, crawling and transmigration (Figure 1.4).

The leukocyte adhesion cascade is initiated by L-selectin (CD62L) on the side of the homing cell. CD62L recognizes the carbohydrate determinant sialic acid α 2-3Gal β 1-4(Fuca1-3(sulpho-6)) GlcNAc β 1-R (6-sulpho sialyl Lewis X), which is expressed by HEVs and presented by PNAd. This apically expressed carbohydrate supports tethering and rolling of CD62L^{high} leukocytes and is crucial for homing, as blocking of this interaction with the anti-L-selectin antibody MECA-79 results in a functional block of leukocyte homing to the lymph node (Umemoto et al. 2006).

In the next step, lymphocyte arrest is mediated via chemokine-induced activation of integrins. The most important chemokines for lymph node migration are CCL21 for T-cells, which is produced by HEVs and FRCs and presented by heparane sulfate, and CXCL12 and CXCL13 for T- and B-cells respectively, which are produced by follicular dendritic cells (FDCs) and FRCs and then transcytosed to the luminal surface of HEVs (von Andrian & Mempel 2003). These chemokines are recognized by their respective chemokine receptors (CCR7 for CCL21, CXCR4 for CXCL12 and CXCR5 for CXCL13) on the leukocyte and initiate binding of LFA-1 to ICAM-1 and ICAM-2, or MAdCAM-1 in mesenteric lymphoid organs. This interaction of ICAM-1 with LFA-1 supports the arrest of cells on the inner luminal surface of HEV and enables leukocytes to crawl along HEV (Warnock et al. 1998).

In the final step leukocytes cross the venule either via paracellular migration or transcellular transmigration (Nieminne et al. 2006). For the latter mode of migration, leukocytes accumulate in extracellular HEV pockets, before they enter the lymph node parenchyma. This process is regulated by HEV-derived lysophosphatidic acid (LPA), which increases cell motility for transmigration and might control together with

sphingosine-1-phosphate (S1P) the accumulation of leukocytes in an HEV pocket (Bai et al. 2013; Mionnet et al. 2011).

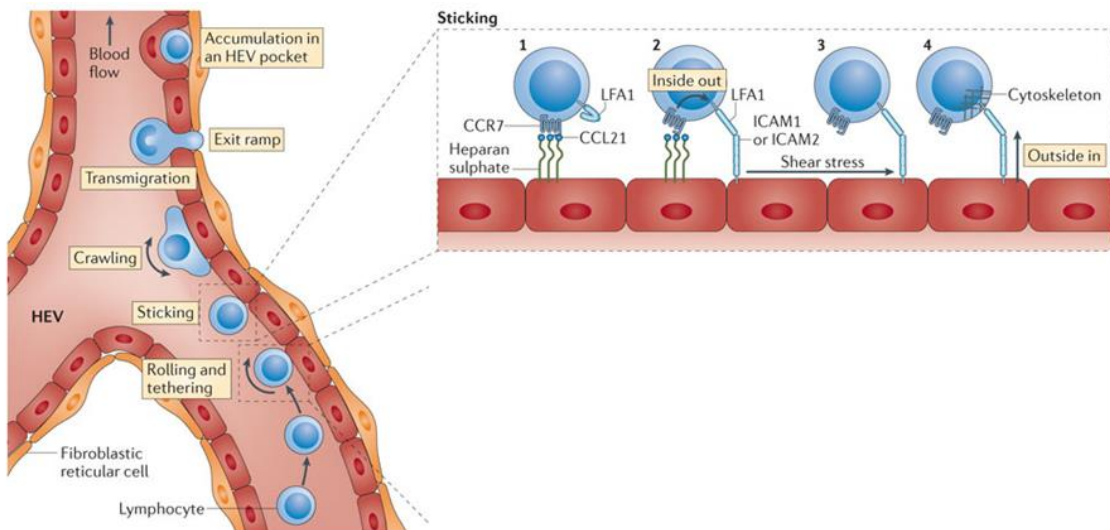


Figure 1.4 The leukocyte adhesion cascade

Schematic illustration of the coordinated steps of leukocyte recruitment from HEVs into lymph nodes. CD62L and PNAd mediated rolling and tethering is followed by adhesion and crawling of leukocytes, which involves chemokines, chemokine receptors and adhesion molecules. After finding an exit point, leukocytes transmigrate and accumulate in HEV pockets, before finally extravasating into the lymph node parenchyma (Girard et al. 2012).

Depending on the cell type, leukocytes move to different areas within the LN. After crossing HEVs, T-cells are retained in perivascular channels that are surrounded by FRCs. This temporal lingering has been hypothesized to most likely increase the chance for T-cell DC encounters (Mempel et al. 2004). Afterwards, T-cells crawl along stromal networks to T- and B-cell areas of the lymph node (Bajénoff et al. 2006). These stromal networks are made up of FRCs, which produce the chemokines CCL21 and CCL19 and are responsible for the random migration pattern of T-cells (Miller et al. 2002).

In contrast to T-cells, B-cells remain significantly longer close to their HEV entry site, as they survey locally for DCs at these points (Qi 2006). After three to four hours, they start crawling towards the T-cell area or the B-cell follicle (Bajénoff et al. 2006). This process is mediated by the chemokine CXCL13, which is produced by FDCs and binds to CXCR5 on the B-cell (Ansel et al. 2000).

1.3 Leukocyte egress from lymphoid organs

1.3.1 Egress of cells into efferent lymphatic vessels

After immune cells have homed to SLOs and have scanned for antigen, leukocytes leave the lymph node to continue their quest for antigen survey in other areas – in case they have not encountered it (Cahalan & Parker 2008).

For this process, sphingosine-1-phosphate (S1P) plays a crucial role. S1P is a chemoattractant lipid, whose biosynthesis starts with serine and palmitoyl coenzyme A in the endoplasmic reticulum. After reduction and dehydrogenation, ceramide is formed, which is metabolised in the Golgi-apparatus to sphingosine. Sphingosine can then either be phosphorylated by sphingosine kinase 1 (SphK1) or SphK2 to S1P (Maceyka & Spiegel 2014).

Fundamental studies have shown that S1P is involved in many physiological processes, including vascular integrity (Herzog et al. 2013), hematopoietic stem cell trafficking (Golan et al. 2012; Juarez et al. 2012), ubiquitin functions (Alvarez et al. 2010), histone deacetylation (Harikumar et al. 2009) and immune cell trafficking (Pappu et al. 2007) (Figure 1.5).

The main sources for blood S1P are erythrocytes and vascular endothelial cells (Pappu et al. 2007; Venkataraman et al. 2008), whereas lymph S1P is produced by lymphatic endothelial cells (Pham et al. 2010). For a proper function of immune cell trafficking, the maintenance of a S1P gradient is crucial, with a high S1P concentration in blood (~1 μ M) and lymph (~100 nM) and low levels in tissues (~nM) (Cyster & Schwab 2012). This gradient is ensured by a relative short plasma half-life of S1P (~15min) and a fast enzymatic degradation of S1P in tissues. Therefore plasma S1P does not reach lymph nodes or lymph. This maintenance can be disturbed, when mice are administered food colorant 2-acetyl-4-tetrahydroxybutylimidazole (THI). THI inhibits the S1P degrading enzyme Sphingosine-1-phosphate lyase (SPL), leading to a more than 100-fold increase of lymphoid tissue S1P. This results in lymphopenia as leukocytes do not leave lymph nodes anymore and a defect in immune cell trafficking (Schwab et al. 2005).

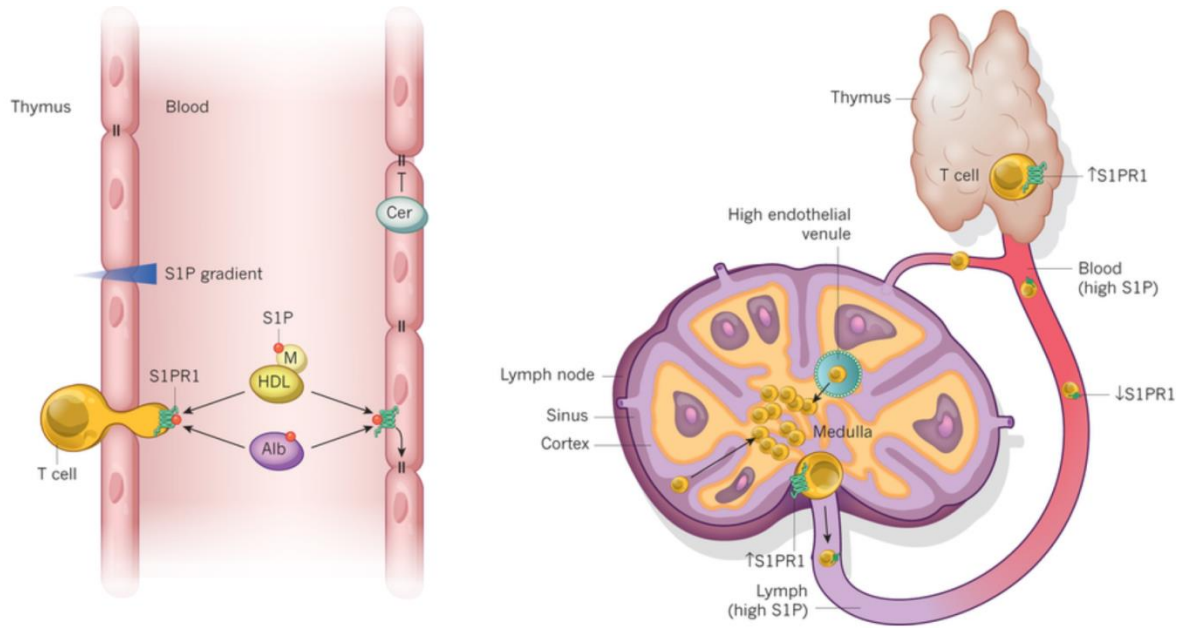


Figure 1.5 S1P and S1P1 control leukocyte trafficking

S1P is bound to apolipoprotein M in high-density lipoprotein and albumin, forming a gradient between blood and lymphoid tissues. High S1P levels in blood lead to downregulation of S1P1. After cells have homed to lymphoid tissues, low S1P levels cause S1P1 upregulation, thus promoting S1P1-dependent leukocyte egress (Maceyka & Spiegel 2014).

S1P mediates its cell-type dependent functions via five specific cell surface receptors (S1P1-5), all G-protein-coupled receptors that trigger downstream signalling pathways and numerous physiological processes. Although the general consensus is that S1P signalling is mediated in a paracrine and/or autocrine fashion, it might be feasible that S1P does not need to be secreted for proper function, as the molecule enters the binding pocket of the receptor by sliding in the plane of the membrane (Hanson et al. 2012). This might suggest, that S1P does not need to be secreted at all for proper function.

S1P was first shown in 1998 to activate the heterotrimeric guanine nucleotide binding protein (G-protein)-coupled orphan receptor EDG-1, also known as S1P1 (Lee et al. 1998). S1P1 is being expressed throughout the body and thus many physiological functions of the receptor have been identified, being critical in embryonic development, as *S1pr1*^{-/-} embryos die from haemorrhage due to incomplete vascular maturation (Liu et al. 2000), and in maintaining the vascular integrity of HEVs (Herzog et al. 2013). The binding of S1P to S1P1 leads to Rac activation, trans-endothelial migration of T-cells and LN egress (Faroudi et al. 2010).

This pathway functions for S1P concentrations from 0.1-1nM, as they occur in lymph nodes. For locations with higher concentrations of S1P, the receptor is being downregulated as it is the case for blood or lymph (Schwab et al. 2005). Experiments with *Sphk1*^{-/-} mice emphasized the importance of the S1P gradient. Knocking out *Sphk1* in lymphatic endothelial cells, leads to a loss of S1P in lymph. Although S1P levels in plasma remain normal, the S1P gradient is impaired and leukocytes are not able to leave the lymph node any longer (Pham et al. 2010).

1.3.2 Control of leukocyte egress

Besides the importance in vascular functions, S1P1 plays a crucial role in leukocyte trafficking, where it is responsible for the egress of T- and B-cells from thymus and lymph nodes. The major S1P1 function in the lymph node is to overcome the retention signal mediated by the chemokine receptor CCR7 as shown by Pham and colleagues (Figure 1.6).

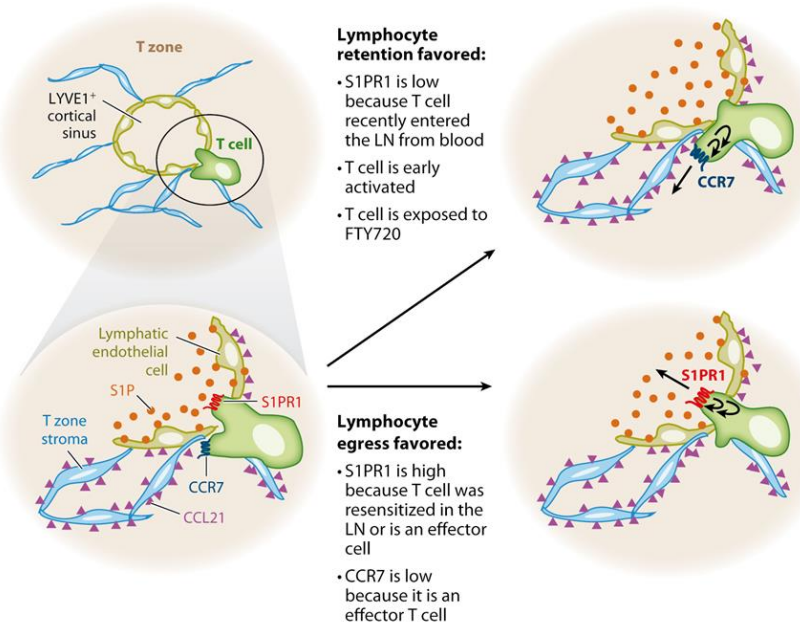


Figure 1.6 Factors promoting leukocyte retention versus egress

The fine-tuned counter play between S1P1 and CCR7 decides the fate of lymphocytes. When the CCR7 signal overrides S1P1, retention of the leukocyte is favored. In the other case, leukocyte egress is promoted (Cyster & Schwab 2012).

When *S1pr1*^{-/-} T and B-cells were adoptively transferred, they homed into the lymph node, but did not egress the lymph node. After incubation with PTX, a reagent that inactivates Gai-mediated signalling as promoted by chemokine receptors, these cells were able to exit the lymph node again (Pham et al. 2008).

In some cases, S1P1 is being downregulated to ensure proper immune function. For example under inflammatory conditions, it is necessary that lymphocyte retention takes place in LNs in order for T-cells to have more time to scan DCs and encounter cognate antigen (Cyster & Schwab 2012).

This process is mediated by CD69, a cell surface glycoprotein, which associates and forms a complex with S1P1 and in this manner downregulates S1P1 expression levels. Thus, T- and B-cells do not leave the inflamed lymph node anymore and have more time for scanning the lymph node and producing a productive immune response (Shiow et al. 2006). Another mechanism, by which surface expression of S1P1 can be modulated, is via transcriptional modulation by Krüppel-like Factor 2 (KLF2). In T-cells but not B-cells, KLF2 binds to and activates the promoter region of S1P1 (Carlson et al. 2006; Bai et al. 2007). As a consequence, T-cells can egress from the thymus and SLOs.

1.3.3 Pharmacological blockade of leukocyte egress

For many decades, researchers strived for a method to modulate leukocyte egress from LNs using pharmacological reagents to prevent pathogenic T-cells from leaving the lymph node and thus stopping the cells from causing damage to other organs.

This was finally achieved with the discovery of fingolimod, a drug that plays a major role in the treatment of multiple sclerosis. Multiple sclerosis is a chronic autoimmune disease and the leading cause of neurological disability in young and middle-aged adults. It is characterized by lesions, due to astrogliosis and a loss of oligodendrocytes, and demyelination. Fingolimod (FTY720/Gilenya; Novartis), was first described in 1995 and approved by the FDA (U.S. food and drug administration) in 2010 as the first orally available drug against multiple sclerosis (Brinkmann et al. 2010).

FTY720 is a drug that interferes with the S1P₁ levels on the surface of leukocytes (Figure 1.7). When FTY720 is given orally, it is being phosphorylated by SphK2 into its active form. FTY720-P can bind to all S1P receptors, except S1P₂, which leads to S1P receptor down regulation. FTY720 therefore acts as a functional antagonist of S1P₁ (Mandala et al. 2002). Pharmacologically, FTY720 can inhibit MS on two frontiers. By retaining pathogenic T-cells in lymph nodes, which as a consequence do not cross the blood brain barrier any more (Brinkmann et al. 2010) and by downmodulation of S1P₁ on astrocytes, leading to reduced astrogliosis and recovery of nerve conduction (Choi et al. 2011).

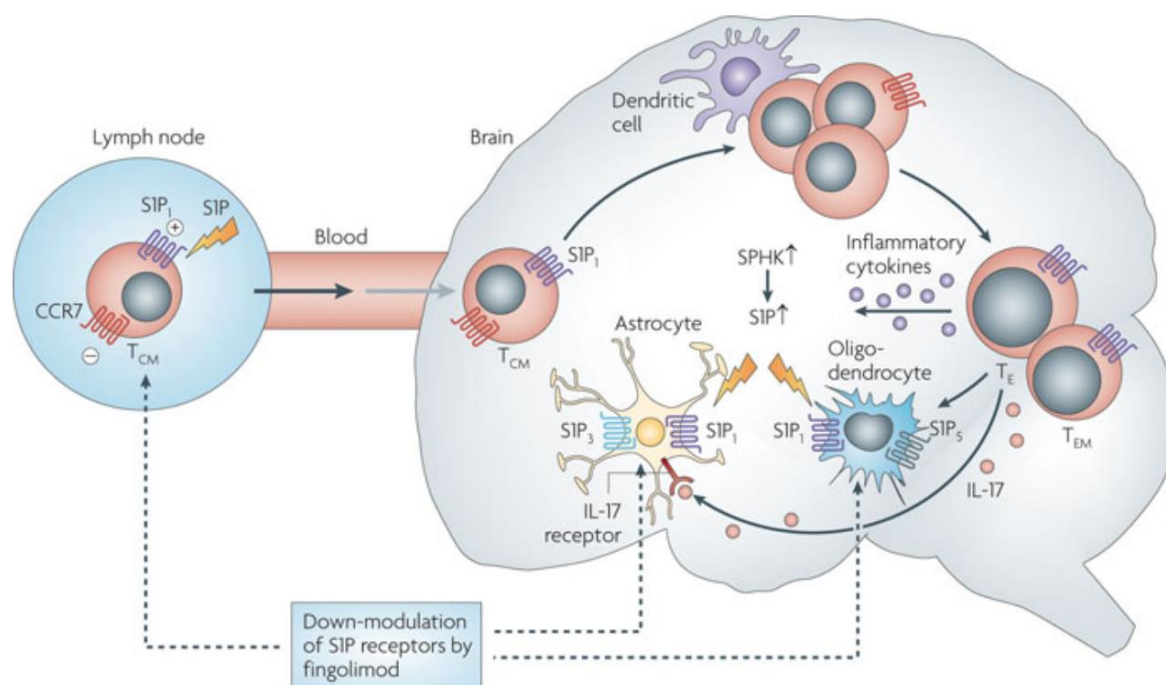


Figure 1.7 Mode of Action of FTY720

After FTY720 is taken up orally, S1P receptors are being down-modulated in lymph nodes and the brain. Thus, pathogenic lymphocytes do not infiltrate into the central nervous system but stay in the lymph node. In the brain, down-modulation of S1P₁ reduces demyelination, axonal loss and astrogliosis (Brinkmann et al. 2010).

1.4 Circadian rhythms

1.4.1 Biological rhythms

Most animals have developed biological clocks in order to adapt optimally to the environment they are being exposed to. These clocks are defined by their frequency (period length τ), which can range from seconds to years. Among mammals, ultradian, circadian and infradian biological rhythms play a major role.

Ultradian (inner-day) rhythms have a relatively short period length of milliseconds to several hours and can be found in various patterns. Heart beat (average $\tau=1$ s), the nasal cycle, e.g. the partial congestion and decongestion of the nasal cavities (with a period length of 30 minutes till 14 hours, average $\tau=2.4$ h) are just two examples. In contrast to ultradian rhythms, infradian rhythms are described by long period lengths, ranging from several days, e.g. the human menstrual cycle (average $\tau=29.1$), to years, such as the emerge cycles of cicada insects (average $\tau=17$ years) (Gachon et al. 2004).

Circadian rhythms exhibit a period length of approximately 24 hours and play a crucial role in the regulation of immune cell trafficking (Druzd et al. 2014).

Bona fide circadian rhythms can be entrained, i.e. they adjust to different geophysical environments and persist over a range of physiological temperatures. They are also independent from external factors, such as light or food, which are the most important *Zeitgebers* or synchronizers of circadian rhythmicity (Green et al. 2008). Thus, a circadian rhythm can be entrained to different *Zeitgebers* (e.g. lighting regimes after jetlag), yet these *Zeitgebers* are not required for the oscillation *per se*, they are only required for the synchronization of the organism to the environment. Oscillations would also occur in constant conditions such as constant darkness. These circadian criteria are fulfilled for instance by core body temperature oscillations as well as plasma cortisol or plasma melatonin levels, which are therefore classical markers of circadian rhythms in mammals (Brown et al. 2002). Thus, non-circadian rhythms, observed for example only under a rhythmic 12h light/dark cycle but not under constant conditions are referred to as diurnal rhythms.

For mammals, two clock systems are responsible for the regulation of circadian rhythms, the central clock and the peripheral clocks.

1.4.2 The molecular clock machinery

Gene expression analyses revealed that a surprising amount of genes oscillate over the course of a day with approximately 10% of genes showing circadian expression patterns in liver and heart (Panda et al. 2002; Storch et al. 2002).

Since circadian rhythms can be also observed for unicellular organisms as prokaryotes (Kondo et al. 1993), circadian oscillators must rely on intracellular mechanisms. Further analysis led to the identification of the core complex of the molecular clock, which consists of multiple transcription factors that interact together and form autoregulatory transcription-translation feedback loops (Figure 1.8).

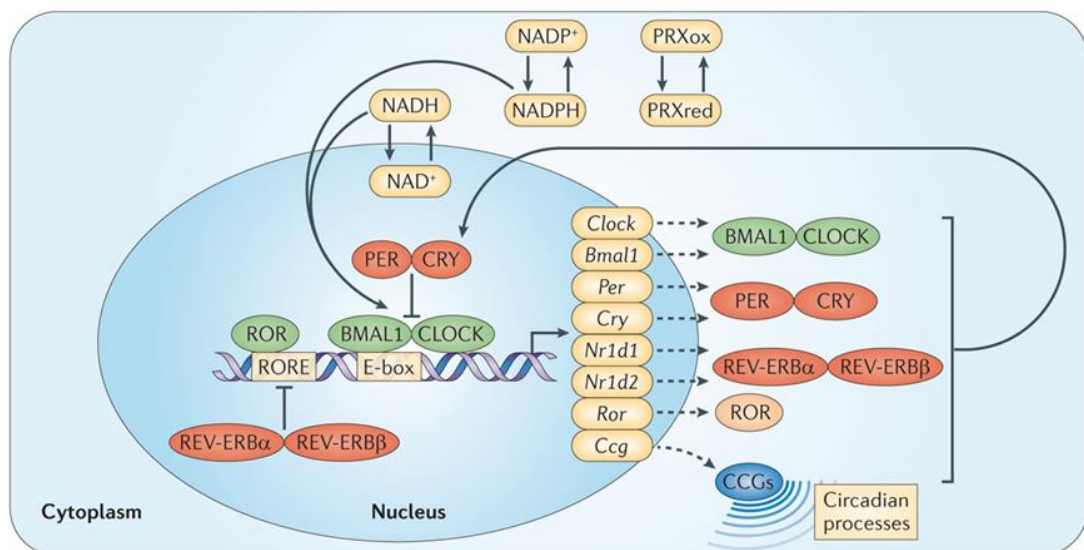


Figure 1.8 The circadian clock

BMAL1 and CLOCK form a heterodimer complex which binds to E-box motifs in clock controlled genes and drives the auto regulatory feedback loop by activating the transcription of negative regulators, as Per and Cry. Further molecules, as for example NADH or peroxiredoxins (PRX) interfere in the molecular machinery dependent on their oxidation status (Scheiermann et al. 2013).

The key transcription factors that operate the positive branch of the feedback loop are BMAL1 (brain and muscle aryl hydrocarbon receptor nuclear translocator (ARNT)-like 1, also known as ARNTL or MOP3) and CLOCK (circadian locomotor output cycles kaput) (Dunlap 1999). CLOCK-BMAL1 form a heterodimer complex, which binds to DNA E-Box response elements containing the nucleotide sequence CACGTG. They are thus able to induce the transcription of other clock genes or clock controlled genes (Darlington et al. 1998; Ueda et al. 2005; Hogenesch et al. 1998). These genes are fundamental components of the molecular clock machinery, as knocking out *BMAL1* in mice is the only single gene deficiency that results in complete loss of circadian rhythmicity in constant darkness (Bunger et al. 2000).

CLOCK-BMAL1 is regulating its own expression by promoting the negative branch of the feedback loop via two different paths. One is to induce the expression of three PERIOD proteins (PER, period circadian protein 1-3), and two CRY flavoproteins (cryptochrome 1 and 2). These proteins form PER-CRY heterodimer complexes, translocate to the nucleus and interact directly with the CLOCK-BMAL1 complex, leading to an inhibition of CLOCK and BMAL1 transcription (Jin et al. 1999; Griffin et al. 1999; Gekakis et al. 1998).

The second one is to activate another transcriptional cycle, which is made up of REV-ERB α and REV-ERB β (encoded by *Nr1d1* and *Nr1d2*) proteins. The REV-ERB α /REV-ERB β heterodimer complex inhibits *BMAL1* transcription via Rev-Erb/ROR response elements (Preitner et al. 2002).

Transcription, translation and degradation of clock genes are under tight epigenetic control. Epigenetic histone modifications, like histone acetylation or methylation, are able to regulate both the development of whole T-cell subset and the expression of specific genes (Ramming et al. 2012). Crosio et al. showed that light itself is able to induce histone acetylation in neurons of the SCN. As a result, this leads to dynamic chromatin remodeling and higher transcription rates in circadian genes (Crosio et al. 2000).

1.4.3 Central and peripheral clocks

In order to orchestrate the billions of cells that are present in the body, an organism needs to orchestrate its cellular clocks. Lesion experiments in the brain led to the identification of an area, called the suprachiasmatic nucleus (SCN), which is essential for rhythmic activity and functions as the central clock of the body in mammals (Ralph et al. 1990; Silver et al. 1996) (Figure 1.9).

This master pacemaker, situated directly above the optic chiasm in the anterior hypothalamus, consists of around 20.000 neurons. The key role of the SCN is to establish phase coherence with the environment and peripheral clocks of the body via direct and indirect signals. The SCN is the only clock system that is directly influenced by light input, which it receives via the retinohypothalamic tract. Light therefore functions as the main *Zeitgeber* (i.e. time giver) of the body (Golombek & Rosenstein 2010).

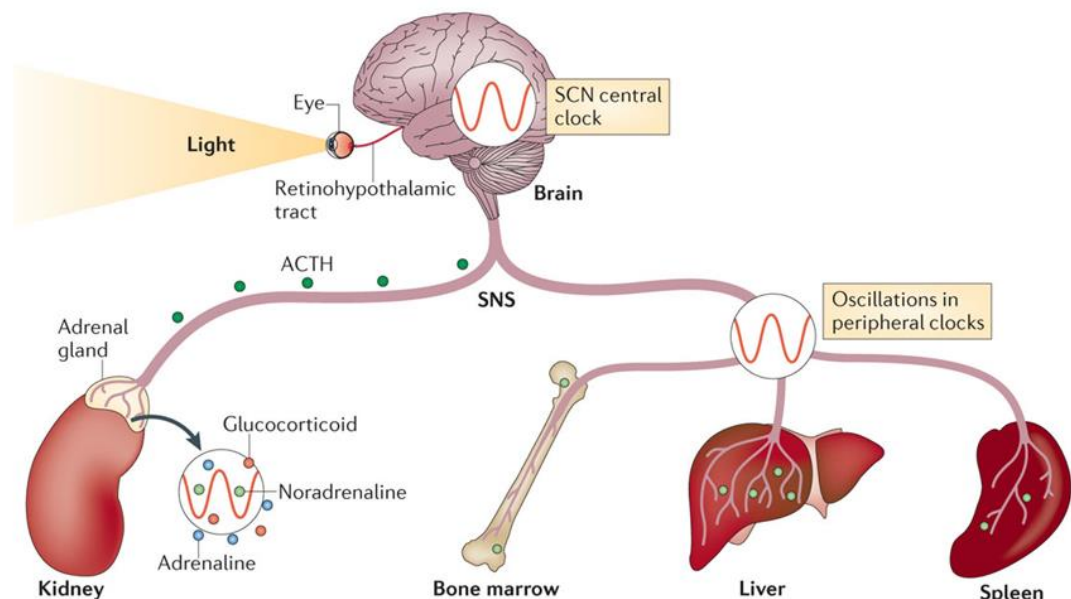


Figure 1.9 Entrainment and synchronization of peripheral clocks by the central clock
 Light signals are being perceived via the eye and processed via the retinohypothalamic tract into the SCN. From here, the SCN orchestrates the circadian release of glucocorticoids from the adrenal gland or hematopoietic stem cells from the bone marrow via the release of adrenocorticotrophic hormone (ACTH) over the humoral axis or the sympathetic nervous system (Scheiermann et al. 2013).

Moreover, feeding-fasting cycles and body temperature are important indirect *Zeitgebers* (Brown et al. 2002). For example, the SCN is able to entrain peripheral clocks in the liver by regulating the rest-activity cycle leading to different timing of feeding behavior (Damiola et al. 2000; Stokkan et al. 2001). As shown by Saini and colleagues, body temperature cycles can synchronize gene expression, a process that is heat shock factor 1-dependent (Saini et al. 2012). These data provide strong evidence for a link between metabolism and the circadian clock.

Another key pathway of the SCN to entrain peripheral clocks and thus organs and cells that are not under direct environmental control in an opaque organism is via humoral and neuronal means. These pathways are mediated by the hypothalamus-pituitary-adrenal (HPA) axis: The PVN (paraventricular and arcuate nuclei, located in the hypothalamus), which are controlled by excitatory and inhibitory SCN efferents, are able to induce the release of ACTH from the pituitary (Arjona & Sarkar 2008). This induces the production of glucocorticoids in the adrenal gland in a circadian manner, which can then bind to GR receptors. This process is also under direct circadian clock gene control as CLOCK regulates the transcriptional activity of the glucocorticoid receptor by acetylating its hinge region lysine cluster (Dickmeis 2009; Nader et al. 2009). In addition, glucocorticoids play an essential role in inflammatory processes, as they are known to up-regulate the expression of anti-inflammatory proteins and inhibit the synthesis of pro-inflammatory proteins (Elenkov et al. 2000).

The glucocorticoid synthesis is also known to be regulated by intestinal epithelial cells (IECs), as IECs show a temporal circadian expression of clock genes (Asfeldt 1971). Mukherji et al (Cell 2013) found that microbiota can modulate the circadian clock in IEC. During the behavioral active phase ROR α activity is dominant, resulting in expression of toll-like receptors (TLRs) and low cortisone production. Furthermore, the intestine microbiota can interact with TLR, leading to low expression of REV-ERB α . In the resting phase, REV-ERB α activity is dominant, resulting in high corticosterone production (Mukherji et al. 2013). This indicates the importance of entrainable oscillators like food and microbiota for circadian rhythmicity of non-brain tissues. As microbiota signaling deficiencies induce a prediabetic syndrome this is also important in the context of disease pathophysiology (Mukherji et al. 2013).

As mentioned before, oscillations in clock genes can be found in various tissues, such as the liver, adipose tissue and muscle (Yang et al. 2006). Interestingly, these peripheral clocks are not solely under control of the central clock. This was demonstrated by specifically disrupting circadian clock mechanism in hepatocytes. Although the majority of hepatic genes become arrhythmic, core clock components of the molecular clock as *Per2* remain to oscillate in the absence of the molecular feedback loop (Kornmann et al. 2007). This suggests that these peripheral clocks do not only rely on input from the central clock, but also on metabolic *Zeitgeber* signals (Thaiss et al. 2016). These represent peripheral pacemaker cues, which are able to regulate the molecular clock and serve as metabolic regulators of circadian clock components (Albrecht 2012).

Recent findings have provided evidence that peripheral clocks can also be found at the single cell level. With respect to the immune system, major clock genes and clock controlled transcription factors have been found to be expressed in natural killer cells, macrophages, dendritic cells, B cells and inflammatory monocytes (Silver, Arjona, Hughes, et al. 2012; Nguyen et al. 2013; Arjona & Sarkar 2005). In these cell the genes also show a rhythmic expression profile. In the case of macrophages, it could be even shown that roughly 8% of the macrophage transcriptome are under circadian control, including important regulators for pathogen recognition and cytokine secretion, such as ERK1, MEK1 and NF κ B expression (Keller et al. 2009). However, data for T lymphocytes has thus been sparse. So far, it has been only shown, that *Bmal1* and *Nr1d1* are expressed and oscillate in CD4 T cells, whereas the physiological relevance is currently unknown (Hemmers & Rudensky 2015).

In summary, a complex system of regulatory feedback loops exist which enables an organism to orchestrate its cellular clocks which can be found throughout the whole body.

1.4.4 Circadian rhythms in immune cell trafficking

Over the past decades, research has provided striking evidence that integral parts of the immune system are under circadian control. Among these are cytokines, chemokines, chemokine receptors and adhesion molecules (Druzd et al. 2014). All these factors fluctuate in accordance with the rest-activity phase of the species, which depends on whether the species is diurnal (such as humans) or nocturnal (such as rodents) (Scheiermann et al. 2013).

Regarding the circadian trafficking behavior of immune cells, the vast majority of research in this field has thus far focused on trafficking within blood, the bone marrow or tissues such as the cremaster muscle. It has been shown for hematopoietic stem and progenitor cells (HSPCs) that they oscillate in blood showing a peak during the behavioral rest phase (ZT5) and a trough at the beginning of the active phase (ZT13) (Méndez-Ferrer et al. 2008). For HSPCs, this is due to strong circadian modulation of the bone marrow microenvironment resulting in phases with higher egress of cells from the bone marrow and phases of stronger homing to the bone marrow. Specifically, enhanced homing to bone marrow is observed at ZT13, as the expression of P- and E-Selectins, VCAM-1 and CXCL12 peak towards the beginning of the active phase (Scheiermann et al. 2012). In contrast, the circadian homing behavior of leukocytes into other tissues is regulated more downstream of the leukocyte adhesion cascade, as ICAM-1 and CCL2 are the factors that regulate rhythmic leukocyte homing into mouse cremaster muscle tissue.

T-cells in blood fluctuate in a similar circadian manner, whereas the nature of T-cell affects the phase of oscillation. Central memory and naïve CD4+ and CD8+ T-cells peak at night in human blood, due to a cortisol-induced upregulation of CXCR4. This allows circulating naïve and central memory T-cells to redistribute to bone marrow. In contrast, effector CD8+ T-cells counts peak during the day, being positively correlated with epinephrine rhythms (Dimitrov et al. 2009).

Integral parts of adaptive immune response cells are also under tight control of clock genes: *Bmal1*-deficient mice show reduced levels of mature B-cells, as BMAL1 seems to exclusively regulate the development of pre-B cells to mature B-cells (Sun et al. 2006). In contrast, the development of Th17 cells is under control of REV-ERBa.

In this context, REV-ERB α can downregulate expression of the transcription factor NFIL3, which is itself a negative regulator of Th17 differentiation (Yu et al. 2013).

Natural killer (NK) cells are critical components of innate immunity against fungal, bacterial and viral infections. In addition to the existence of functional molecular clock mechanisms in NK cells, the release of granzyme B and Perforin, which are essential for granule mediated cytolytic activity of NK cells, are also under circadian control (Arjona & Sarkar 2005).

Taken together, the majority of myeloid and lymphoid cells exhibit a circadian oscillation with respect to numbers in blood. Regarding the relevance of these oscillations in some cell types, a benefit in the immune response is suggested, as described below.

1.4.5 Circadian rhythms in the immune response

The immune system itself represents a pivotal role in host defense, as its main task is to protect the organism against pathogens, such as parasites, bacteria or viruses. This difficult task is mediated via two defense systems, the innate and adaptive immune response.

In general, innate immunity leads to a nonspecific but rapid immune response, in which NK cells, mononuclear phagocytes (monocytes and macrophages) and granulocytes (neutrophils, eosinophils, basophils and mast cells) kill pathogens via phagocytosis or secreting antimicrobial substances. Furthermore, the innate immune system is able to activate the adaptive immune system, which leads to a slower but antigen-specific immune response. This process is mediated by T and B lymphocytes, and antigen-presenting cells such as dendritic cells.

As described above, most cell types, which take part in the immune response possess functional clock genes. Meanwhile, it is also known that these clock genes regulate the rhythmic expression of molecules, which are involved in immune responses.

Macrophages for example, display time-of-day-dependent secretion of TNF α and IL-6 production after treatment with lipopolysaccharide (LPS), a membrane compound of

gram-negative bacteria (Keller et al. 2009). When challenging macrophages with a TLR9-dependent model of sepsis, disease severity also depended on the timing of sepsis induction. The latter effect was mediated via rhythmic expression of TLR9, indicating an important link between the circadian system and innate immune response (Silver et al. 2012).

Another type of myeloid cells, monocytes, exhibit time-of-day dependent differences in the immune response following pathogen challenge. A study by Nguyen and colleagues reported that *Bmal1* regulates diurnal oscillations of Ly6C^{hi} inflammatory monocytes, which control their trafficking to sites of inflammation (Nguyen et al. 2013). When challenging mice with a lethal dose of *Listeria monocytogenes*, a gram-positive bacterium, towards the end of the active phase they observed higher survival rates compared to a challenge in the middle of the rest phase. Interestingly, mice, which lack *Bmal1* in myeloid cells, showed higher lethality than wild-type animals due to a higher pro-inflammatory state in these mice. Mechanistically, they unveiled that *Bmal1* in myeloid cells is able to suppress inflammation by regulating *Ccl2* and *Ccl8* expression, two important chemokines in acute and chronic inflammation (Druzd & Scheiermann 2013; Nguyen et al. 2013).

In the case of adaptive immunity, Fernandes and colleagues were the first ones to demonstrate, that the adaptive immune response is under circadian control (Fernandes et al. 1976; Labrecque & Cermakian 2015). Their findings showed higher antibody titers at specific times in mice after immunization with sheep red blood cells, were recently also confirmed in the human system, as Long et al. demonstrated that the antibody responses against certain flu strains is higher in the morning compared to afternoon immunization (Long et al. 2016). Whether this is due to higher T-cell proliferation, as has been shown for anti-CD3 stimulation and Th17 differentiation (Fortier et al. 2011; Yu et al. 2013), or due to other factors, such as higher rates of antigen presentation is currently not known.

In summary, it has been shown that integral parts of both innate and adaptive immune responses are under circadian control. However, little is known about the interplay between circadian rhythmicity and T-cell mediated immune responses in lymphoid organs.

2 Material and Methods

2.1 Animal husbandry

7-8 weeks old C57BL/6 wild type (WT) mice were obtained from Charles River Laboratories (Sulzfeld, Germany). *Bmal1*^{flox/flox}, *S1pr1*^{flox/flox}, *Cd4cre*, *Cd4creert2*, *Cd19cre*, mice were purchased from Jackson Laboratories and crossbred on-site to obtain *Bmal1*^{flox/flox} x *Cd4cre*, *Bmal1*^{flox/flox} x *Cd19cre*, *S1pr1*^{flox/+} x *Cd4cre*, *S1pr1*^{flox/+} x *Cd19cre*, *S1p1*^{flox/+} x *Cd4creert2* animals. All mice were maintained under a 12h light - 12h dark lighting schedule with food and water available ad libitum. In some experiments, mice were put in light cyclers to change light regime or were kept in constant darkness. For knockout experiments, age and gender matched littermates were used as a control. All mice were maintained and bred at the Walter-Brendel Center for Experimental Medicine, Ludwig Maximilians Universität, Munich, Germany. All work within this project was carried out in accordance with the German Law of Animal Welfare and approved by the Regierung of Oberbayern.

2.2 Genotyping by PCR

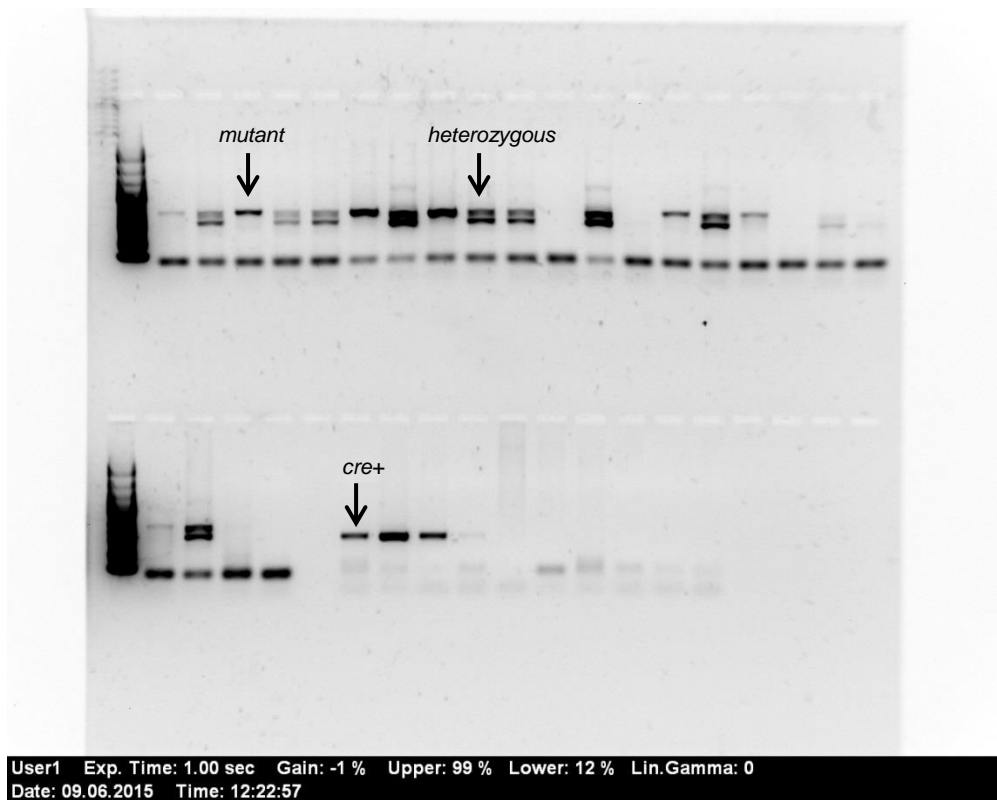
To determine the genotype of transgenic lines (*Bmal1*^{flox/flox} x *Cd4cre*, *Bmal1*^{flox/flox} x *Cd19cre*, *S1pr1*^{flox/+} x *Cd4cre*, *S1pr1*^{flox/+} x *Cd19cre*, *S1pr1*^{flox/+} x *Cd4creert2*), mice were genotyped by polymerase chain reaction (PCR). For this purpose, ear samples or tail tips were harvested and digested overnight at 55°C in 200µl lysis buffer (5mM EDTA, 200mM NaCl, 0.2% SDS in 100mM Tris-HCl, pH 8.5) containing proteinase K (1:200 units). On the next day, samples were gently mixed and centrifuged at 12,700g for 15 minutes. The supernatant was transferred to tubes containing 200µl isopropanol, mixed thoroughly and centrifuged at 12,700g for 10 minutes. Afterwards supernatant was removed and the pellet was dissolved in 100µl TE buffer and stored at -20°C. Samples were then incubated for 1 hour at 37°C before being used in the PCR reaction mix (Table 2.1)

Table 2.1 PCR reaction mix used for genotyping

Item	Volume (μl)
DNA	1
Dreamtaq	10
Forward primer	0.1
Reverse primer	0.2
Water	8.6

Samples were initially denatured at 94°C for 3 minutes, followed by 35 amplification cycles of DNA denaturation (94°C, 30 sec), primer annealing (55°C for *Bmal1*, 56°C for *S1pr1*, 30 sec), DNA polymerization (72°C, 30 sec) and a final primer extension (72°C, 2 minutes). Assessment of the *Cre* status was performed by a denaturation at 95°C for 3 minutes, followed by 38 cycles of DNA denaturation (95°C, 20 sec), primer annealing (62°C, 30 sec), DNA polymerization (72°C, 30 sec) and a final primer extension (72°C, 10 minutes).

Primer sequences were used as shown in Table 2.2. All PCR products were run on a 1% agarose-TAE gel containing gel red to visualize DNA bands and evaluated under ultraviolet light on a Gel iX20 Imager (Intas Science Imaging Instruments GmbH, Göttingen, Germany) (Figure 2.1).

**Figure 2.1** PCR genotyping gel

Exemplary genotyping of *Bmal1*^{flox/flox} and *Bmal1*^{flox/+} mice and their respective *Cd4cre* status. Mutant (431 bp), heterozygous (327bp and 431bp) and Cre⁺ (324bp) bands were detected.

Table 2.2 PCR primers used for genotyping

PCR Primers	Sequence
<i>S1pr1</i> flox forward	GAG CGG AGG AAG TTA AAA GTG
<i>S1pr1</i> flox reverse	CCT CCT AAG AGA TTG CAG CAA
<i>Bmal1</i> flox forward	ACT GGA AGT AAC TTT ATC AAA CTG
<i>Bmal1</i> flox reverse	CTG ACC AAC TTG CTA ACA ATT A
Generic Cre forward	GCG GTC TGG CAG TAA AAA CTA TC
Generic Cre reverse	GTG AAA CAG CAT TGC TGT CAC TT

2.3 Surgical techniques

2.3.1 Lymph cannulation

In order to obtain lymph from animals, lymph cannulation of the thoracic duct was performed on the basis of a protocol described by Ionac in 2013 (Ionac 2003). However, as the method established by Ionac often led to contamination of lymph with blood, the surgical approach had to be modified. 40 minutes prior to cannulation, 200 μ l olive oil was administered intragastrally. 10 minutes prior to cannulation, mice were anaesthetized intraperitoneally with 100 mg/kg ketamine, 20 mg/kg xylazine and 1% acepromazin. An incision was performed along the costal arch and the abdomen was opened as depicted (Figure 2.2).

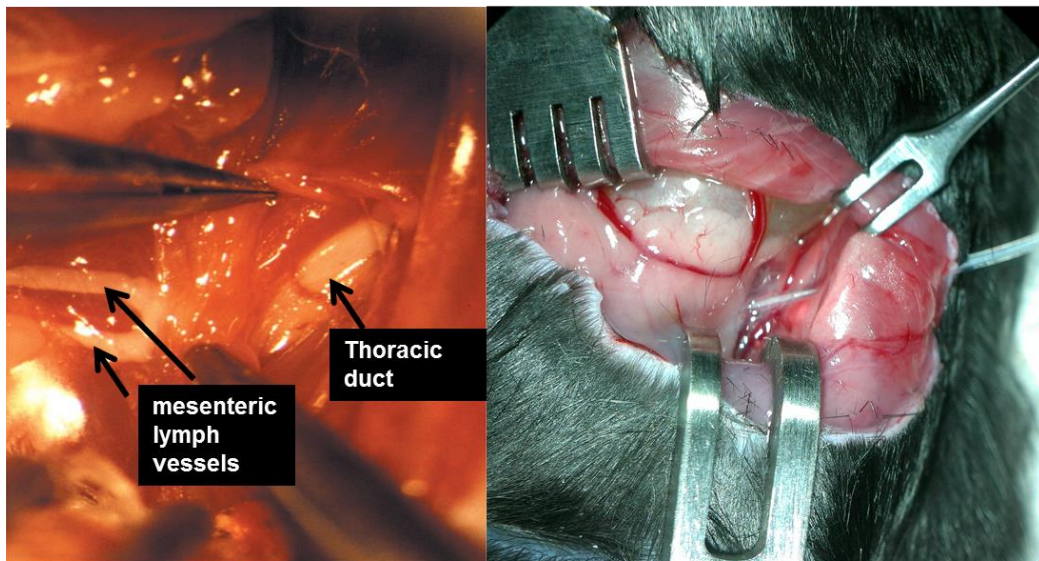


Figure 2.2 Cannulation of mesenteric lymphatic vessels
 (Left side) Lymphatic structures in a rat showing mesenteric lymph vessels and the thoracic duct. (Right side) Technique, which was established in the lab to cannulate mesenteric lymph vessels in the mouse.

The dorsum was perforated, slightly above the adrenal gland, using a 19G 1.1 x 40mm needle in order to implement the suction tube. The suction tube consisted on the one end of a syringe equipped with a 19G needle and a 130mm polyethylene

tube (LOT: 201600 REF:800/100/100 Smiths Medical). On the other end, the tip of a 30G 0.3 x 13mm needle was broken off and placed in the polyethylene tube. Before placing the suction tube into the 19G needle, the system was flushed with 20 μ l EDTA 0.5M to avoid clotting of the lymph. After placing the suction tube into the 19G needle, the needle was removed and mesenteric lymph vessels were cannulated by gently perforating the vessel in a flat angel. Lymph fluid was drawn for 40 minutes. On average 72.15 μ l was obtained, which equals a lymph flow rate of ~1.8 μ l/min. Lymph leukocyte counts were measured using a ProCyte DX cell counter (IDEXX, Ludwigsburg, Germany) and analyzed by flow cytometry as described below.

2.4 Pharmacological inhibition of lymph node egress

In order to study egress dynamics of lymphocytes from lymph nodes, chemical compounds were administered prior to lymph cannulation to inhibit lymph node egress. For FTY720 treatment, 1mg/kg FTY720 was given intraperitoneally one hour prior to cannulation. In some experiments, subsequent dilutions were used. For control mice, 200 μ l of 0.9% NaCl was injected. For SEW2871 treatment, 10mg/kg SEW2871 was injected two hours prior to cannulation and 25 μ l dimethylformamide was administered as a control.

2.5 Adoptive transfer studies and homing block

To investigate the dwell time of leukocytes in lymph nodes and the respective roles of leukocyte versus endothelial factors in lymph node homing, cell transfer experiments were performed. To achieve this, spleen and peripheral lymph nodes (pLN) were harvested from donor mice and processed through a cell strainer (40 μ m, Thermo Fisher Scientific, Waltham, USA). After red blood cell lysis (described below) for spleen, leukocytes from spleen and lymph nodes were counted with a Neubauer counting chamber and mixed with a ratio of 80:20 (spleen:pLN).

Subsequently, leukocytes were labeled with 1.5 μ M of carboxyfluorescein succinimidyl ester (CFSE, Thermo Fisher Scientific, Waltham, USA) or 2.5 μ M

CMTPX (Thermo Fisher Scientific, Waltham, USA) in PBS containing 0.2% BSA and 2mM EDTA for 20min at 37°C and washed 4 times. Finally, 10-20 x10⁶ cells were injected intravenously into recipient mice. Two hours later, inguinal lymph nodes of recipient mice were harvested and the amount of homed cells was analyzed by flow cytometry as described below. In some experiments, lymph node homing was inhibited to perform analyses of leukocyte transit by using blocking antibodies against CD11a (α L-integrin) and CD49d (α 4-integrin). To achieve this, lymph node entry was blocked two and 12 hours after adoptive cell transfer by administration of 100 μ g anti- α L (CD11a, clone M17/4; BioXCell) and 100 μ g anti- α 4 (CD49d, clone PS/2; BioXCell) antibodies in PBS intraperitoneally. To investigate the role of chemokine receptors in leukocyte homing, cells were labeled with CFSE or CMTPX and pre-incubated with a 200ng/ml pertussis toxin (PTX) pulse for 10 min at 37°C as described before (Lo et al. 2005). After 4 times washing, cells were co-injected with untreated cells into recipient mice and the amount of homed cells was analyzed as described before.

Between all adoptive transfer experiments, dyes were switched to avoid potential dye-specific effects.

2.6 Blood sample collection

Blood was taken by punctuation of the retrobulbar venous plexus of anaesthetized mice into EDTA-coated capillary tubes (Microvete 300). Blood leukocyte counts were measured using a ProCyte DX cell counter (IDEXX, Ludwigsburg, Germany) and analyzed by flow cytometry as described below.

2.7 Flow Cytometry

To decipher the distribution of leukocyte subsets, harvested organs, blood and lymph were analyzed via flow cytometry. Blood and Lymph was drawn as described above, lymph nodes and spleen were collected and cleared from fatty tissue under the dissecting microscope. Bone marrow cells were obtained by flushing tibias with PBS.

Prior to antibody staining, red blood cell lysis was performed twice for blood samples and once for spleen and bone marrow samples by mixing the samples with 5ml 0.8% NH₄Cl for 5 minutes on ice. 5ml PBS were added and the white blood cell population was separated by centrifugation. Lymph samples were washed once with 2ml PBS and centrifuged. Cells from lymph nodes were obtained by gently pushing lymph nodes through a cell strainer (40µm, Thermo Fisher Scientific, Waltham, USA) and washing them with 5ml PBS.

For surface staining of leukocyte markers or chemokine receptors, except CCR7, each sample was resuspended in 100µl PBS containing an antibody cocktail and incubated at 4°C for 30 minutes. For CCR7 staining, samples were initially resuspended in 100µl PBS supplemented with 2µl CD16 and CD32 antibodies and incubated at 4°C for 15 minutes to block unspecific Fc-receptor-mediated antibody binding. Without washing, 1µg anti-CCR7 antibody was added and cells were incubated at 37°C for 30 minutes. After a washing step with PBS, a secondary staining round was performed as described above. Antibody clones and dilutions are given in Table 2.3.

Finally, cells were washed once, resuspended in 150µl PBS and run on a flow cytometer (Gallios 10/3, Beckman Coulter, Brea, USA, equipped with three lasers, 405nm, 488nm and 635nm). Data was analyzed using FlowJo (Ashland, USA).

Table 2.3 Antibody clones used for flow cytometry

Antigen	Color	Species	Isotype	Clone	Company
CD 4	APC	anti-mouse	Rat IgG2b, κ	GK1.5	Biolegend
CD 4	PE	anti-mouse	Rat IgG2b, κ	GK1.5	Biolegend
CD 8a	PerCP/Cy5. 5	anti-mouse	Rat IgG2a, κ	53-6.7	Biolegend
CD 11b	PE	anti- mouse/human	Rat IgG2a, κ	M1/70	Biolegend

CD 16/32	Purified	anti-mouse	Rat IgG2a, λ	93	Biolegend
CD 44	APC/Cy7	anti-mouse/human	Rat IgG2b, κ	IM7	Biolegend
CD 45R/B220	PE/Cy7	anti-mouse/human	Rat IgG2a, κ	RA3-6B2	Biolegend
CD 62L	FITC	anti-mouse	Rat IgG2a, κ	MEL-14	Biolegend
CD 184 (CXCR4)	PE	anti-mouse	Rat IgG2b, κ	L276F12	Biolegend
CD 185 (CXCR5)	PE	anti-mouse	Rat IgG2b, κ	L138D7	Biolegend
CD 195 (CCR5)	PE	anti-mouse	Armenian Hamster IgG	HM-CCR5	Biolegend
CD 197 (CCR7)	PE	anti-mouse	Rat IgG2a, κ	4B12	Biolegend

2.8 T cell isolation

CD4 T-cells were purified for qPCR or adoptive transfer experiments from lymph nodes of WT mice, CD4cre x Bmal1flox/flox, CD4cre x S1P1flox/+ or littermate control mice using the EasySep Mouse CD4 T-cell enrichment kit (StemCell Technologies), in accordance with the manufacturer's instructions. Purity of isolated cells was confirmed via flow cytometry and was generally above 96 %.

2.9 Quantitative RT-PCR

RNA extraction from lymph nodes or isolated CD4 T-cells was performed using the RNeasy plus mini kit (Qiagen, Hilden, Germany), in accordance with the manufacturer's instructions. To determine RNA concentration and quantity after

extraction, RNA samples were analyzed using a NanoDrop 2000 (Thermo Fisher Scientific, Waltham, USA) and stored at -80°C.

100-200 ng RNA was used for reverse transcription into cDNA, using the High Capacity cDNA Reverse Transcription Kit (Applied Biosystems), in accordance with the manufacturer's instructions, and cDNA was stored at -20°C.

Quantitative real-time PCR was performed with SYBR GREEN on a StepOnePlus Real Time PCR System (Applied Biosystems). To determine the optimal primer concentrations and annealing temperatures, all primers were tested under different conditions. A primer concentration of 0.5 μ M was found optimal for each primer pair, whereas annealing temperatures differed depending on the primers. The sequences of oligonucleotides and annealing temperatures that were being used can be found in Table 2.4. All reactions were performed in duplicates or triplicates in a total reaction volume of 10 μ l, containing 5 μ l SYBR green, 1 μ l primer mix, 2 μ l H₂O and 2 μ l cDNA. The cycling conditions were one cycle at 95 °C (10 min) followed by 40 cycles of 95 °C (15 s) and 58-64 °C (1 min). Gene expression levels were normalized to the housekeeping gene glyceraldehyde-3-phosphate dehydrogenase (GAPDH) and the $\Delta\Delta CT$ method was used for relative quantification.

Table 2.4 Quantitative RT-PCR primers

Primers	Sequence	Annealing(°C)
<i>Bmal1_F</i>	AGA GGT GCC ACC AAC CCA TA	62
<i>Bmal1_R</i>	TGA GAA TTA GGT GTT TCA GTT CGT CAT	
<i>Clock_F</i>	CAA AAT GTC ACG AGC ACT TAA TGC	62
<i>Clock_R</i>	ATA TCC ACT GCT GGC CTT TGG	
<i>Per1_F</i>	TGA GAG CAG CAA GAG TAC AAA CTC A	60
<i>Per1_R</i>	CTC GCA CTC AGG AGG CTG TAG	
<i>Per2_F</i>	GTC CAC CTC CCT GCA GAC AA	60
<i>Per2_R</i>	TCA TTA GCC TTC ACC TGC TTC AC	
<i>Cry1_F</i>	CTC GGG TGA GGA GGT TTT CTT	62
<i>Cry1_R</i>	GAC TTC CTC TAC CGA GAG CTT CAA	

<i>Rev-Erb-alpha_F</i>	GAT AGC TCC CCT TCT TCT GCA TCA TC	60
<i>Rev-Erb-alpha_R</i>	TTC CAT GGC CAC TTG TAG ACT TC	
<i>Dbp_F</i>	AAT GAC CTT TGA ACC TGA TCC CGC T	
<i>Dbp_R</i>	GCT CCA GTA CTT CTC ATC CTT CTG T	60
<i>S1pr1_F</i>	CGG TGT AGA CCC AGA GTC CT	
<i>S1pr1_R</i>	AGC AGC AGA TGA GAA TGA AC	64
<i>S1pr2_F</i>	ATG GGC GGC TTA TAC TCA GAG	
<i>S1pr2_R</i>	GCG CAG CAC AAG ATG ATG AT	60
<i>S1pr3_F</i>	TTC CCG ACT GCT CTA CCA TC	
<i>S1pr3_R</i>	CCA ACA GGC AAT GAA CAC AC	62
<i>S1pr4_F</i>	TGC GGG TGG CTG AGA GTG	
<i>S1pr4_R</i>	TAG GAT CAG GGC GAA GAC C	62
<i>S1pr5_F</i>	CTT AGG ACG CCT GGA AAC C	
<i>S1pr5_R</i>	CCC GCA CCT GAC AGT AAA TC	62
<i>Ccr7_F</i>	TCA TTG CCG TGG TGG TAG TCT TCA	
<i>Ccr7_R</i>	ATG TTG AGC TGC TTG CTG GTT TCG	62
<i>Cxcr4_F</i>	TCA GTG GCT GAC CTC CTC TT	
<i>Cxcr4_R</i>	CTT GGC CTT TGA CTG TTG GT	60
<i>Cxcr5_F</i>	AAA CGA AGC GGA AAC TAG AGC C	
<i>Cxcr5_R</i>	GCC CAG CTT GGT CAG AAG CC	60
<i>Ccl19_F</i>	ATG TGA ATC ACT CTG GCC CAG GAA	
<i>Ccl19_R</i>	AAG CGG CTT TAT TGG AAG CTC TGC	62
<i>Ccl21_F</i>	ACA GCG GCC TCC AGA AGA ACA GCG G	
<i>Ccl21_R</i>	CGT GAA CCA CCC AGC TTG A	64
<i>Cxcl12_F</i>	CAG AGC CAA CGT CAA GCA	
<i>Cxcl12_R</i>	AGG TAC TCT TGG ATC CAC	58
<i>Cxcl13_F</i>	CAT AGA TCG GAT TCA AGT TAC GCC	
<i>Cxcl13_R</i>	TCT TGG TCC AGA TCA CAA CTT CA	62
<i>Klf2_F</i>	ACC AAG AGC TCG CAC CTA AA	
<i>Klf2_R</i>	GTG GCA CTG AAA GGG TCT GT	60
<i>Klf4_F</i>	CTG AAC AGC AGG GAC TGT CA	
<i>Klf4_R</i>	GTG TGG GTG GCT GTT CTT TT	60
<i>Gapdh_F</i>	TGT GTC CGT CGT GGA TCT GA	
<i>Gapdh_R</i>	CCT GCT TCA CCA CCT TCT TGA	60

2.10 Immunofluorescence microscopy

Inguinal lymph nodes were harvested and embedded in OCT (TissueTec), before being put on dry ice and stored at -80°C. Sections were obtained with a cryostat (Leica) at a thickness of 10 µm, which was found to be optimal.

For CCL21 staining, sections were left unfixed to be able to analyze the relevant extracellular protein levels and directly blocked with 0.1 % BSA solution at room temperature for 30 minutes. After blocking, the solution was carefully soaked up with facial tissues and sections were stained with 2000 µl staining solution, consisting of 1000µl 0.1% BSA, 960µl PBS, 20µl anti-PECAM-1-APC antibody, 20µl anti-Lyve-1-FITC antibody and 20µl biotinylated anti-CCL21 antibody at 4°C. After 24 hours, sections were washed with PBS and stained with 2000µl PBS containing 1:300 Streptavidin Cy3 at room temperature for 2 hours. After washing with PBS for 2 times sections were imaged on an Axio Examiner.D1 microscope equipped with 405, 488, 563 and 655 nm LED light sources (Zeiss).

For all other antibody stainings (Table 2.5), sections were fixed with ice-cold methanol for 10 minutes and washed with PBS. Afterwards, sections were permeabilized at room temperature for 30 minutes with 3800 µl PBS containing 0.5 % Triton and 20 % NGS and incubated at 4°C overnight with staining solution. After washing with PBS for 2 times sections were imaged on an Axio Examiner.D1 microscope (Zeiss).

Table 2.5 Antibodies used for immunofluorescence microscopy

Antigen	Color	Species	Isotype	Clone	Company
CD31 (PECAM)	Alexa Fluor® 647	anti-mouse	Rat IgG2a, κ	MEC13.3	Biolegend
CD106 (VCAM)	PE	anti-mouse	Rat IgG2a, κ	429 (MVCAM. A)	Biolegend
CD54 (ICAM)	Cy3	anti-mouse	Rat IgG2b, κ	YN1/1.7. 4	Biolegend

PNAd	PE	anti-mouse/human	Rat IGM, κ	MECA-79	Biolegend
Lyve-1	Biotin	anti-mouse	IgG1	ALY7	eBioscience
Streptavidin	Alexa Fluor® 488				Biolegend
Streptavidin	Cy3				Biolegend
CCL21	Biotin	anti-mouse	Goat IgG		R&D

2.11 Quantitative imaging analysis

Measurement of expression levels of chemokines or adhesion molecules on high endothelial venules was performed using the mask analysis tool provided within the Zeiss software as shown below. In the first step, a contour (yellow line) was drawn around HEVs to determine the area for mask analysis. Within this mask, PECAM-1 positive areas were determined based on their expression level (blue areas) (Figure 2.3).

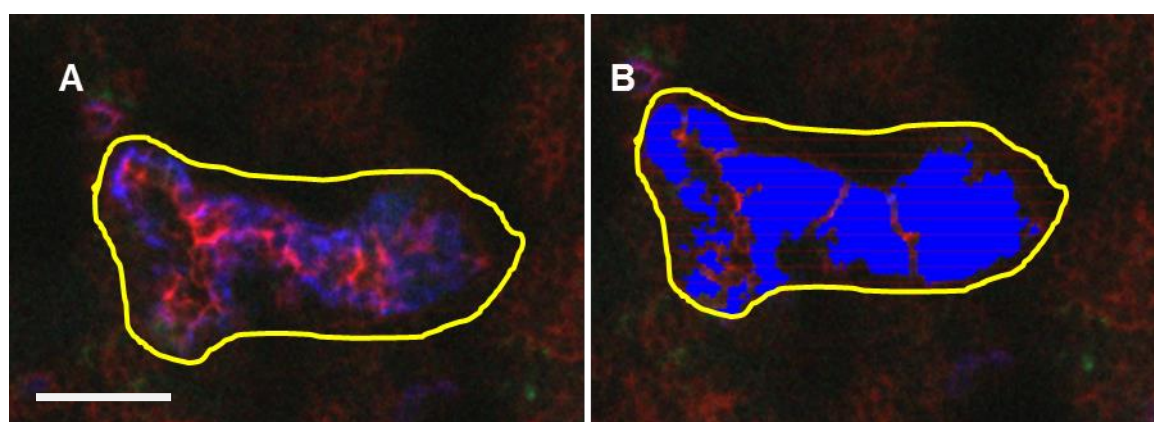


Figure 2.3 Surface expression measurements on lymph node sections

Representative image of a lymph node section stained for PECAM-1 (violet) and CCL21 (red) (A) A mask (yellow line) is drawn to determine the area for the mask analysis tool (B) PECAM-1 high endothelial cell areas (blue area) were determined for further analysis. Scale bar: 100μm

Within these PECAM-1 high areas, determining endothelial cells, expression levels of CCL21 and other adhesion molecules were calculated (Figure 2.4).

To minimize non-specific signals, PECAM-1 high areas smaller than $10 \mu\text{m}^2$ were excluded from analysis. The mean fluorescence intensity was calculated as a function of area and intensity and subtracted from isotype controls.

ID	Area[μm^2]	Intensity...	
		A	B
1	2	0.728	803.000
2	3	0.728	483.000
3	4	136.162	1,747.727
4	5	0.728	221.000
5	6	229.364	2,041.321
6	7	2.184	611.667
7	8	84.464	1,468.052
8	9	4.369	700.667
9	10	0.728	342.000
10	11	51.698	1,090.282
11	12	1.456	756.000
12	13	36.407	830.000
13	14	64.805	1,244.337
14	15	0.728	261.000
15	16	0.728	522.000
16	17	0.728	495.000
17	18	0.728	1,023.000
18	19	522.077	1,835.488
19	20	7.281	1,172.800
20	21	1218.179	1,510.830
21	22	871.584	1,634.952
22	23	61.892	1,290.482
			1,849.212

Figure 2.4 MFI data points from software analysis

PECAM-1 high areas are assigned to ID numbers (column A) and their respective size in μm^2 (column B). The corresponding MFIs of e.g. PECAM-1 and CCL21 are represented in column C (PECAM-1) and column D (CCL21).

For investigations of CCL21 gradients, a $10 \mu\text{m}$ thick and $100 \mu\text{m}$ long line was drawn starting from HEV borders and pointing towards the T cell area (Figure 2.5). An artificial HEV border was determined using a threshold level for PECAM-1 MFI above 1500. The MFI of CCL21 was calculated as a relative decrease starting from that border in $0.85 \mu\text{m}$ steps.

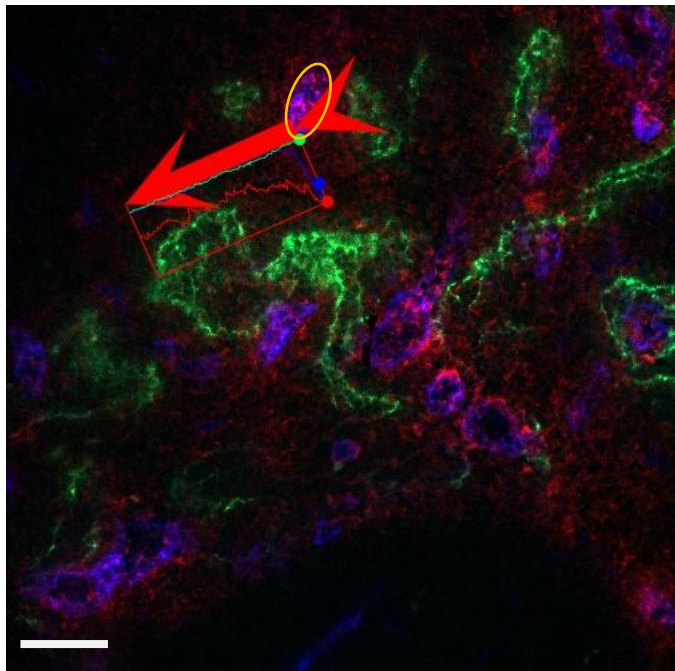


Figure 2.5 CCL21 gradient measurement

Representative image of a lymph node section stained for PECA-1 (violet), Lyve-1 (green) and CCL21 (red). A 10 μ m thick line was manually drawn to measure the MFI of CCL21 over a distance of 100 μ m, starting from a HEV (yellow line). Scale Bar: 50 μ m

2.12 Mass spectrometry

To determine levels of S1P in lymph and blood plasma, lymph and blood were collected as described above and centrifuged down at 2800rpm for 10 minutes. For each sample, 40 μ l lymph supernatant and 60 μ l blood plasma were stored at -80°C. After collection of all time points, samples were transferred to Dr. Olaf Uhl (Dr. von Hauner Children's Hospital, University of Munich Medical Center), who analyzed S1P levels using mass spectrometry on a 1200 SL HPLC system (Agilent) coupled to a 4000QTRAP tandem mass spectrometer (AB Sciex).

Proteins of 20 μ L sample matrix were precipitated by adding 200 μ L methanol including D-erythro-sphingosine-1-phosphate C17 base (860641P, Avanti Polar Lipids) as internal standard. After centrifugation, the supernatant was used for the analysis of S1P by liquid chromatography mass spectrometry (LC-MS/MS) analyses with a 1200 SL HPLC system (Agilent) coupled to a 4000QTRAP tandem mass spectrometer (AB Sciex). Separation was achieved with a Zorbax SB-C18, particle

size 3.5 μ m, 150 mm \times 2.1 mm HPLC column (Agilent) and water with 0.1% formic acid as mobile phase A and methanol/ isopropanol (1:1) with 0.1% formic acid as mobile phase B. A gradient elution was used for optimal separation from 60% B to 80% B within 7 minutes. After column cleaning at 100% B for 1 minute, the gradient was equilibrated for 2.5 min at 60% B before the next injection. The LC-MS/MS system operated in positive electrospray ionization with electron voltage of 5500V at 400 °C. Auxiliary gas was set to 50 psi and 60 psi was used for nebulizer gas. Curtain gas was set to 30 psi and collision gas was set to 8 psi. Mass transitions and individual energies (declustering potential, collision energy, collision cell exit potential) were optimized by direct infusion and set as follows: m/z 380.2 \blacktriangleright 264.2 (66, 23, 18) and 380.2 \blacktriangleright 82.1 (66, 49, 6) for S1P and 366.2 \blacktriangleright 250.2 (61, 23, 18) and 366.2 \blacktriangleright 82.0 (61, 45, 6) for internal standard. Mass transitions were detected in multiple reaction monitoring mode with a dwell time of 100 ms. Quantification was achieved by standard calibrating curves prepared from D-erythro-sphingosine-1-phosphate C18:1 base (860492P, Avanti Polar Lipids) at different concentration points in the range from 0.005 to 0.5 μ mol/L (Druzd et al. 2017).

2.13 Statistical analyses

Data was analyzed and plotted using Prism 6 (GraphPad). For comparison of two experimental groups, paired and unpaired student's t-test were performed. For comparisons between three or more experimental groups, either a one way analysis of variance (ANOVA) followed by Tukey's comparison or a two-way ANOVA analysis followed by Bonferroni's post hoc test were used.

3 Results

3.1 Leukocyte numbers in lymph nodes oscillate in a time-of-day-dependent fashion

3.1.1 Steady-state oscillations in skin draining and mesenteric lymph nodes

To assess whether lymph node cellularity oscillated over the course of a day, our initial experiment was to investigate lymph node cellularity in the physiologically occurring, rhythmic 12h light:12h dark environment. Every 4 hours, left and right inguinal lymph nodes were harvested, and pushed through a cell strainer. Afterwards, the samples were counted and leukocyte subsets were analyzed via flow cytometry. Surprisingly, strong oscillations could be observed in total leukocyte numbers, as well as in the major leukocyte subsets, peaking at ZT13 and exhibiting a trough at ZT1 (Figure 3.1).

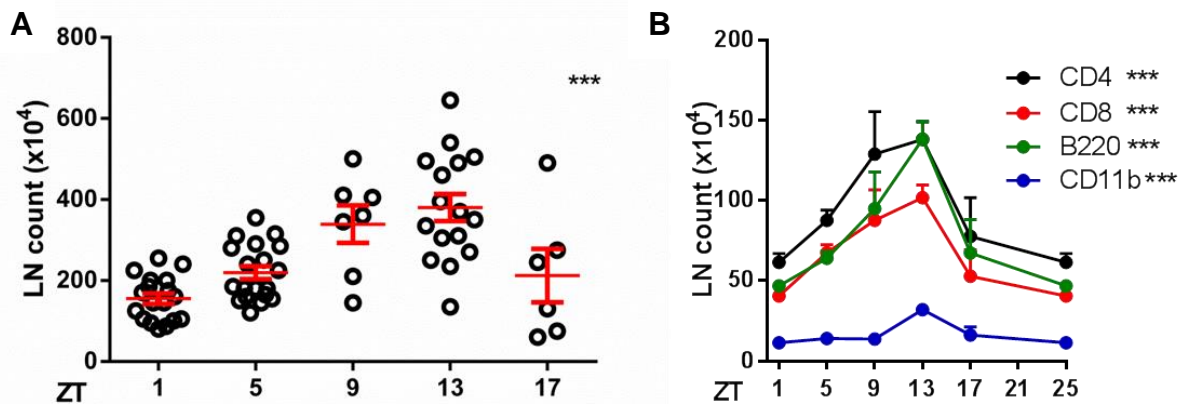


Figure 3.1 Oscillations in total cell counts and leukocyte subsets in inguinal lymph nodes

(A) Lymph nodes were harvested at different time-points during the day and cellular counts were obtained; n=6-19 mice, one way ANOVA (B) Leukocyte subsets in inguinal lymph nodes over 24 hours; n=4-15 mice, one way ANOVA; counts are plotted per single lymph node; ZT: *Zeitgeber* time. ***p<0.001.

Next, other skin draining lymph nodes (including axial and superficial cervical) and mesenteric lymph nodes were harvested, counted and analyzed for the distribution of leukocyte subsets (Figure 3.2). Similar oscillations could be observed for peripheral

and mesenteric lymph nodes as for inguinal lymph nodes, with leukocyte counts peaking around dark onset between ZT9 and ZT13 and troughing at ZT1, the onset of light.

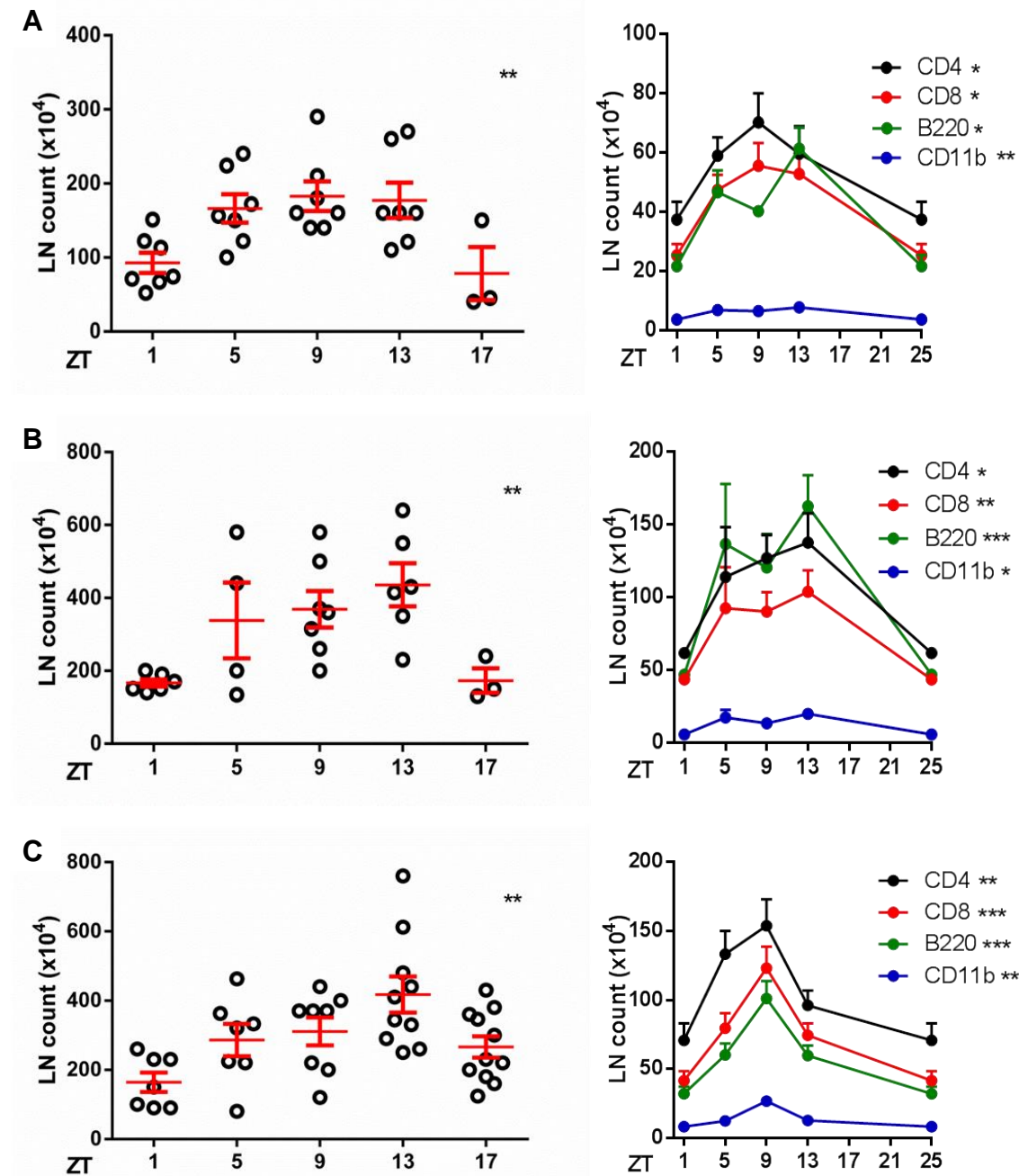


Figure 3.2 Cellular oscillations and leukocyte subsets of different peripheral lymph nodes

Cell counts in (A) axillary, (B) superficial cervical and (C) mesenteric lymph nodes with their respective counts of leukocyte subsets, counts are plotted per single lymph node; n=3-12 mice, one-way ANOVA. *p<0.05, **p<0.01, ***p<0.01.

3.1.2 Lymph node oscillations persist under altered light regimes

To investigate whether oscillations in cell counts are entrainable by environmental lighting conditions, mice were kept in different light regimes. Animals that were kept under normal 12h light:12h dark conditions (LD), were either put in constant darkness (DD) or exposed to a reversed light regime (DL) (Figure 3.3). In both cases (DD, and DL), rhythmic cell counts were sustained, indicating that they can be entrained by a *Zeitgeber* (in this case light) and that they are still observed in the absence of such a *Zeitgeber*. Both observations substantiated the bona fide circadian nature of the rhythm.

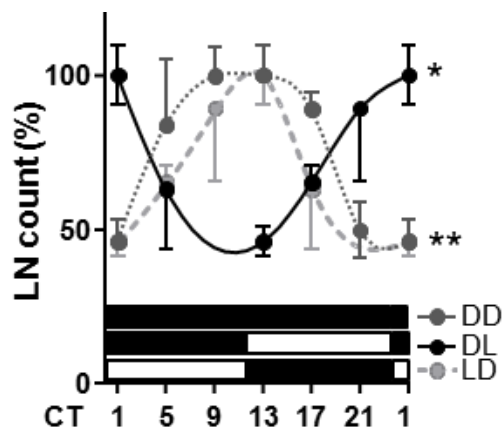


Figure 3.3 Rhythms in cell counts are sustained under different light regimes
 Lymph node oscillations under dark-dark (DD), dark-light (DL) and light-dark (LD) conditions, normalized to peak times; CT: circadian time, i.e. time in the absence of a *Zeitgeber*, in constant darkness; n=3-15, one-way ANOVA. *p<0.05, **p<0.01.

3.1.3 Dynamic egress and homing of cells into lymph nodes

The major contributors to lymph node counts are the homing of cells into the lymph node via HEVs and the egress of cells out of the lymph node into efferent lymphatic vessels. Therefore, both processes were blocked to determine the contribution of homing versus egress to the observed oscillations in lymph node cell counts.

For this purpose, homing was blocked with anti- α_L and anti- α_4 antibodies, as described previously (Lo et al. 2005), and cell counts were measured 6 hours, 12 hours and 24 hours post block. To block egress, FTY720 was administered and cell counts were measured in the same fashion as for the homing block experiments. As expected, blocking homing reduced cell counts, while blocking egress increased cell counts. Importantly, however, in both cases, oscillations in lymph node cell counts were abolished (Figure 3.4).

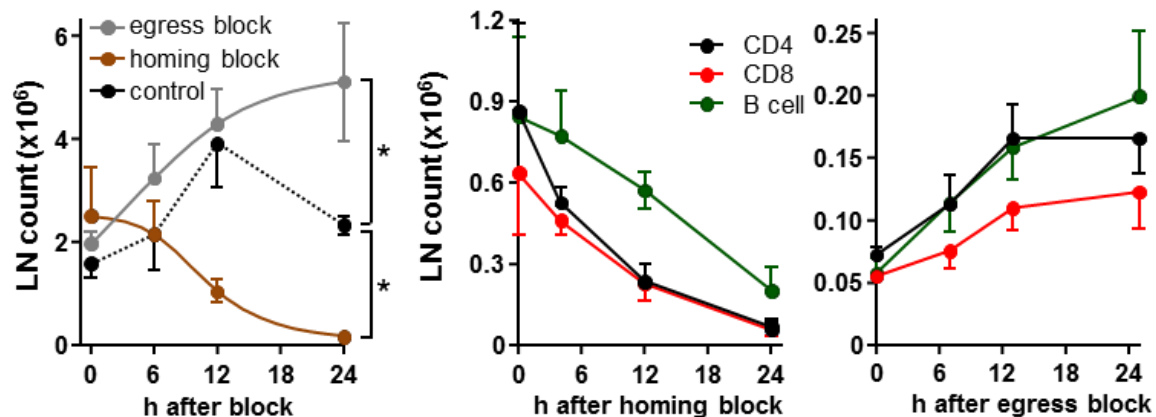


Figure 3.4 Homing and Egress block ablate oscillations in LN counts

Lymph node counts after homing (left panel, red line) or egress block (left panel, grey line) and the corresponding leukocyte subsets (middle: homing block, right: egress block); n=3-5 mice, one-way ANOVA with Tukey's multiple comparison test. *p<0.05.

A third process, which might affect lymph node cellularity is intranodal proliferation. For this purpose, proliferation was investigated by harvesting lymph nodes at two different time points, ZT5 and ZT13, and staining lymph node sections for Ki67. Ki67 is a nuclear protein, which is expressed in all phases of the cell cycle (G₁, S, G₂ and mitosis), except the resting phase, thus being an ideal marker for proliferation. As expected from the blocking experiments, the amount of proliferation as assessed by Ki67⁺ cells per lymph node was low. In addition, no effect of time-of-day was observed (Figure 3.5). Thus, proliferation at steady state within lymph nodes is low and does not account for the strong differences seen in overall cellularity across the day.

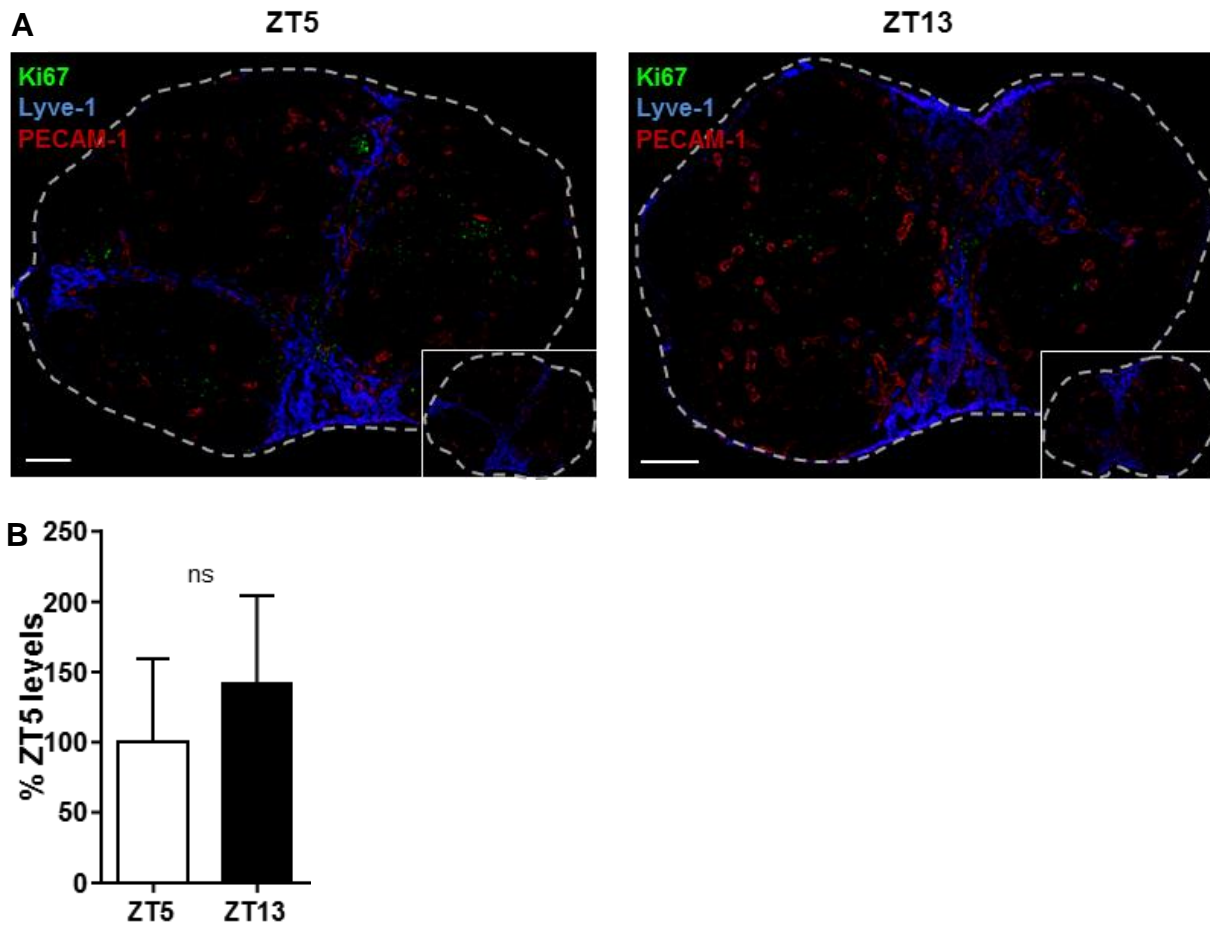


Figure 3.5 Steady-state proliferation within lymph nodes does not occur rhythmically
 (A) Sections of lymph nodes harvested at ZT5 and ZT13 and stained for Ki67, Lyve-1 (marker for lymphatic endothelium) and PECAM-1 (HEVs), inset: isotype stained control. Scale bars: 200 μ m. (B) Percentage of Ki67 $^{+}$ cells per lymph node, n=4-5 mice; unpaired student's t-test.

3.2 Homing of cells into lymph nodes is under circadian control

Homing of cells into lymph nodes via HEVs is dependent on various signals, including leukocyte dependent and endothelium-derived factors. Hence, the goal was to determine whether any of these factors was under circadian control and might contribute to the observed oscillations in lymph node counts.

3.2.1 Homing of cells into lymph nodes is time-of-day dependent

At first, we used adoptive transfer techniques to determine whether homing of cells into lymph nodes is dependent on the time of the day. We injected a mixture of splenocytes and lymphocytes (80:20 ratio) that were labeled with CFSE into recipient mice at different time points of the day and measured the amount of homed cells 2 hours afterwards via flow cytometry (Figure 3.6). Strong differences could be observed in the overall number of homed cells, as well as in the different leukocyte subsets, suggesting that leukocyte homing is under circadian control.

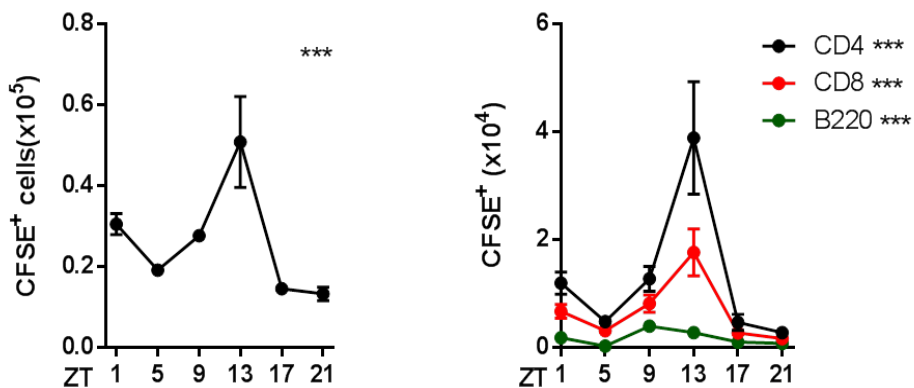


Figure 3.6 Lymph node homing is time-of-day dependent

Amount of CFSE⁺ in lymph nodes after 2 hours of homing at different time points of the day. For each time point, a specific ratio of splenocytes and lymphocytes was used (80:20); n=3-5, one-way ANOVA. ***p<0.001.

3.2.2 Rhythmic leukocyte homing is regulated by leukocyte- and endothelium-derived factors

The next aim was to determine the factors that contribute to time-of-day dependent differences in homing of cells to lymph nodes. To decipher the role of leukocyte versus microenvironment-derived factors, we used adoptive transfer techniques. In detail, we adoptively transferred cells harvested at ZT5 and ZT13 into recipient mice at either ZT5 or ZT13. By labeling donor cells with two different dyes, we were able to

see in the same mice the effect of changing leukocyte-intrinsic factors, whereas the usage of different recipient mice gave us a change in the microenvironment setup. Indeed, we saw differences in all four groups, covering all major leukocyte subsets (Figure 3.7).

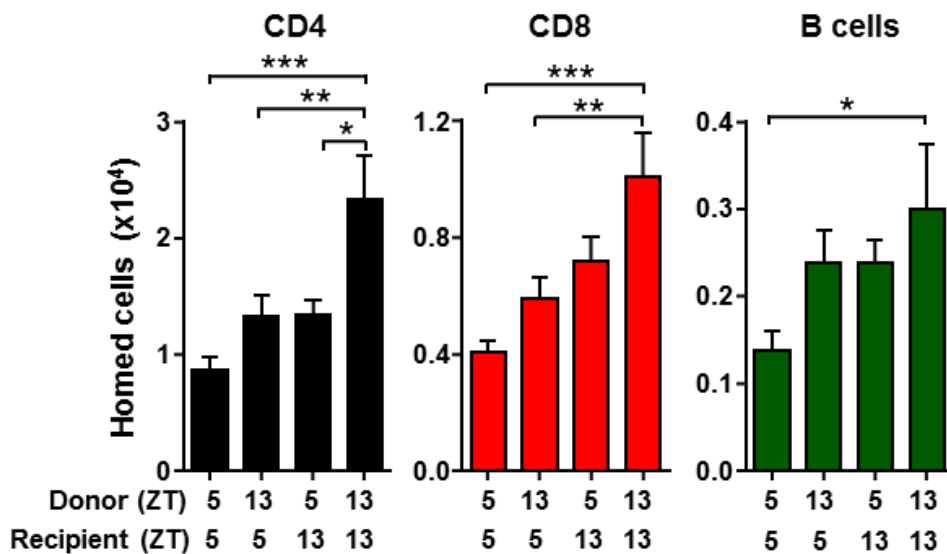


Figure 3.7 Leukocyte and endothelium-derived factors contribute to rhythmic LN homing

ZT5 and ZT13 harvested leukocytes were stained with the fluorescent dyes CFSE or CMTPX and adoptively transferred into ZT5 or ZT13 recipient mice. 2 hours after homing, the amount of homed (CFSE⁺/CMTPX⁺) cells was determined using flow cytometry. n=6-16 mice, one-way ANOVA with Tukey's multiple comparisons test. *p<0.05, **p<0.01, ***p<0.001.

As expected from the results shown in Figure 3.6, ZT5 cell transfer into ZT5 donors showed the lowest homing capacity, while ZT13 cells into ZT13 mice exhibited the highest amount of homed cells. Interestingly, intermediate levels of homing were observed for the ZT5 into ZT13 and ZT13 into ZT5 chimeric time points, suggesting contributing roles of both the microenvironment and the leukocyte in the rhythmic homing process.

Leukocytes express various chemokine receptors and adhesion molecules that take part actively in the leukocyte adhesion cascade. Therefore we aimed to investigate at different *Zeitgeber* times the expression of chemokine receptors and adhesion molecules on circulating cells in blood (Figure 3.8). In general, surface expression levels of pro-migratory factors did not oscillate strongly, although a trend was

observed for CCR7 expression levels. One reason for this observation might be that cells, which express a higher density of homing molecules towards the beginning of the active phase, have already homed to lymph nodes. Therefore, analysis of blood leukocyte subsets at this time point may not reveal the actual oscillations in homing molecules.

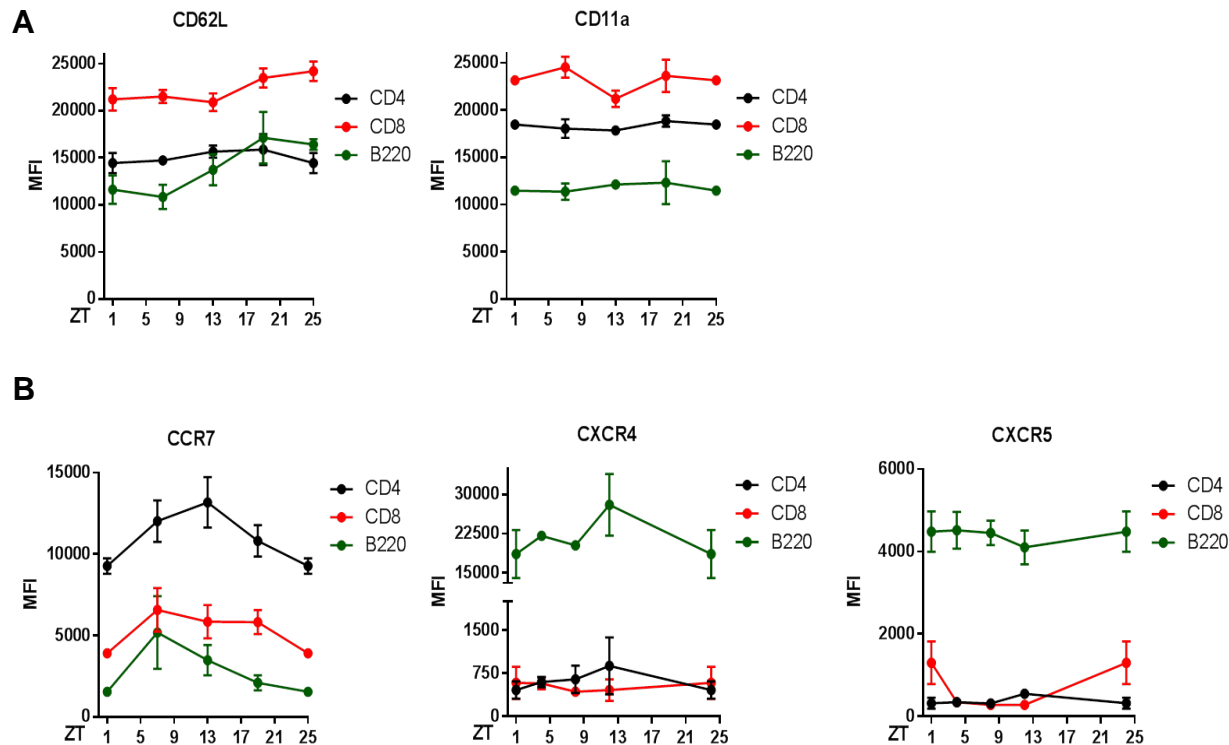


Figure 3.8 Integrin, selectin and chemokine receptor expression levels in blood
Mean fluorescence intensity (MFI) levels of adhesion molecules (A) and chemokine receptors (B) on the surface of leukocytes; n=3-6 mice, one-way ANOVA

Therefore, lymph nodes were harvested at different time points and stained for the same molecules as in Figure 3.8. Interestingly, the surface expression levels of CCR7 oscillated in a rhythmic fashion on all lymphocyte subsets in lymph nodes, whereas the expression levels of CXCR5, CXCR4, CD62L and CD11a showed either no oscillations or not for all lymphocyte subsets (Figure 3.9).

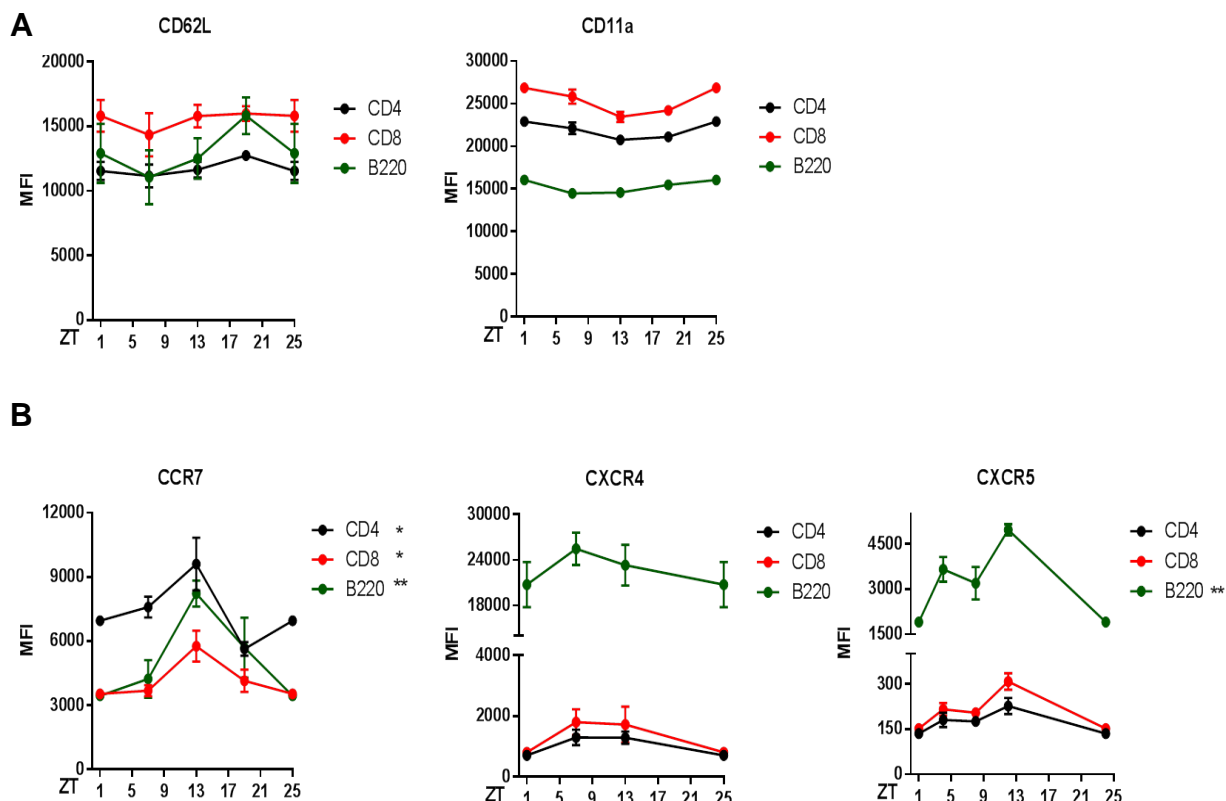


Figure 3.9 Integrin, selectin and chemokine receptor expression levels in lymph nodes
Lymph nodes were harvested and analyzed via flow cytometry for surface expression levels of adhesion molecules (A) and chemokine receptors (B) on lymphocyte subsets; n=3-5, one-way ANOVA. *p<0.05, **p<0.01.

As described above, time-of-day dependent differences in homing were due to contributions of both leukocyte and endothelium-derived signals. To investigate possible oscillations in factors regulating the microenvironment within lymph nodes, lymph nodes were harvested and cut in 10 μ m sections.

By the use of immunofluorescence markers, the MFI of adhesion molecules within HEVs was determined. Rhythmic oscillations could be observed for ICAM-1, VCAM-1 and Lyve-1, whereas the surface expression levels of PECAM-1 and PNAd remained stable (Figure 3.10).

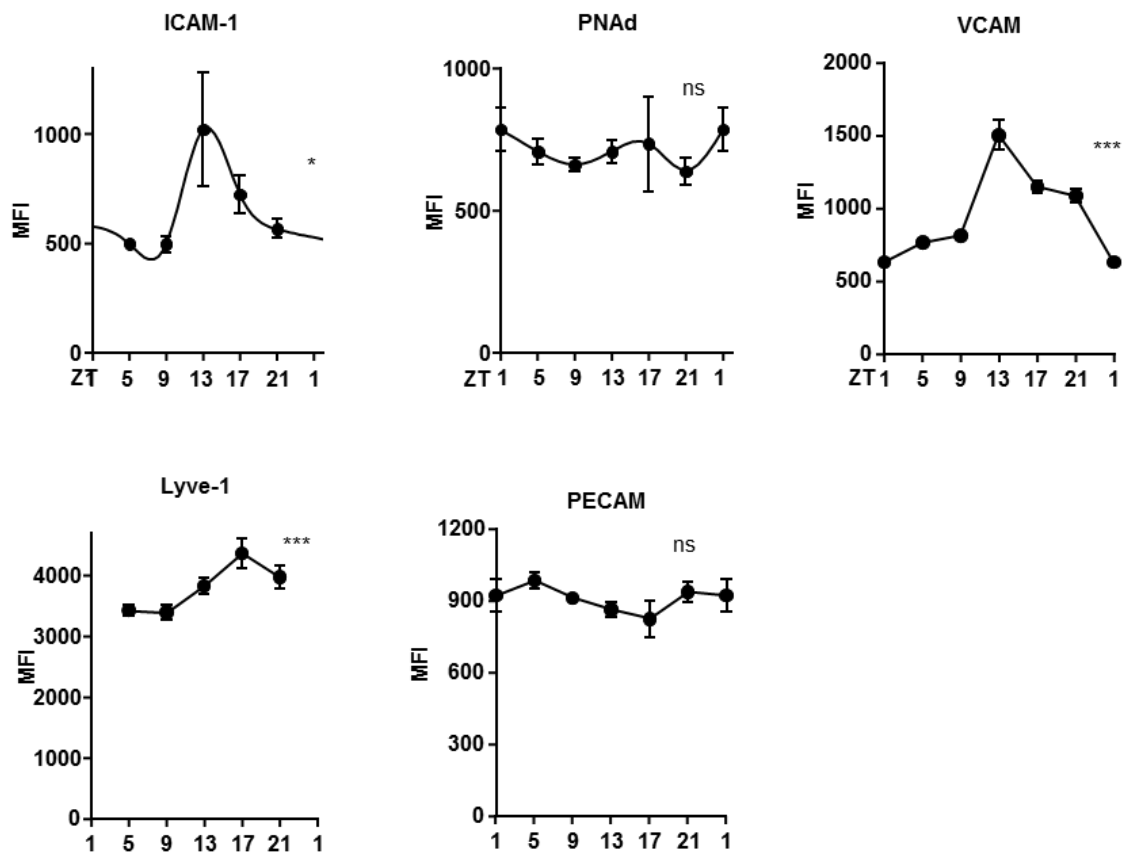


Figure 3.10 Expression levels of adhesion molecules on HEVs

MFI of different adhesion molecules within PECAM high areas (=HEVs) during 24 hours under constant darkness conditions; n=3-18 mice, one-way ANOVA. *p<0.05, ***p<0.001.

CCL21 is one of the most prominent chemokines regulating homing of cells into lymph nodes (Ansel et al. 2000; Lipp et al. 2016). Thus, both surface expression levels of CCL21 on HEVs and mRNA levels of whole lymph nodes were determined. Interestingly, oscillations could be observed for both determinants (Figure 3.11).

As leukocytes are gradient sensitive to the expression of CCL21, the gradient of the chemokine was analyzed within a distance of 100 µm starting from the border of HEVs. Indeed, also the gradient was significantly different over the course of a day (Figure 3.11). Towards the beginning of the active phase, CCL21 expression levels remained for a longer distance high compared to CCL21 levels during the resting phase. This phenomenon might lead to an additional boost for a more pronounced homing of cells towards the beginning of the active phase.

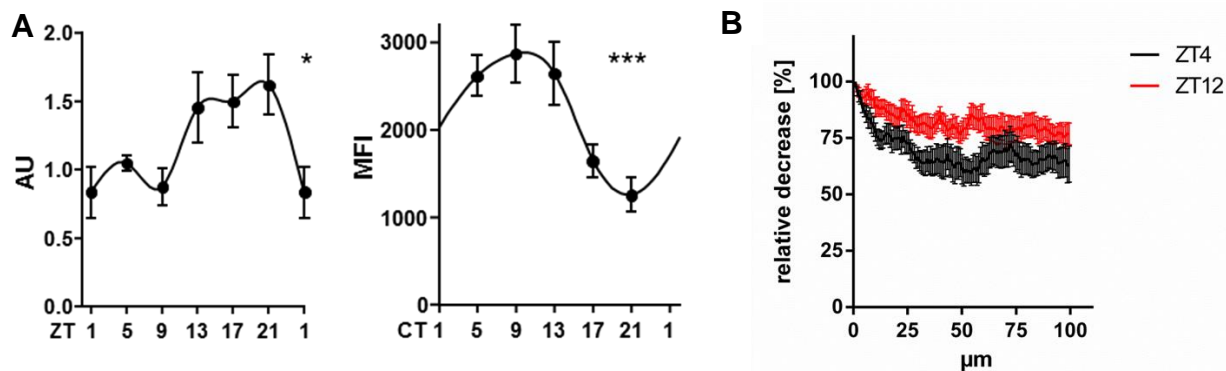


Figure 3.11 CCL21 expression levels oscillate within HEVs and lymph nodes

(A) Q-PCR analysis of CCL21 expression in lymph nodes over 24 hours; n=3-5 mice, one-way ANOVA (B) Surface expression levels of CCL21 on HEVs and their relative decrease 100 μ m aside of the HEV border; n=3-18 mice, one-way ANOVA. *p<0.05.

3.2.3 Rhythmic homing is dependent on circadian CCR7 expression

To investigate the role of rhythmic CCR7 expression in the described differences in homing potential, two approaches were taken, one by pharmacologically blocking chemokine receptor signaling and the other one by using genetically modified mice, which specifically lack CCR7 expression.

In order to downmodulate chemokine receptor signaling, lymphocytes were pulse-loaded for 10 min with pertussis toxin (PTX) prior to performing adoptive transfer experiments. This results in the ablation of G-protein coupled chemokine receptor function due to ADP-ribosylation of the $G_{\alpha i}$ -subunit, such as CCR7 (Lo et al. 2005). Leukocytes from two different *Zeitgeber* times were pre-treated with PTX and co-injected with PBS-treated cells. No differences were seen in the homing capacity of PTX-transferred cells – in contrast to PBS-treated cells (Figure 3.12). This data strengthens the fact that rhythmic expression/engagement of chemokine receptors is responsible for rhythmic homing.

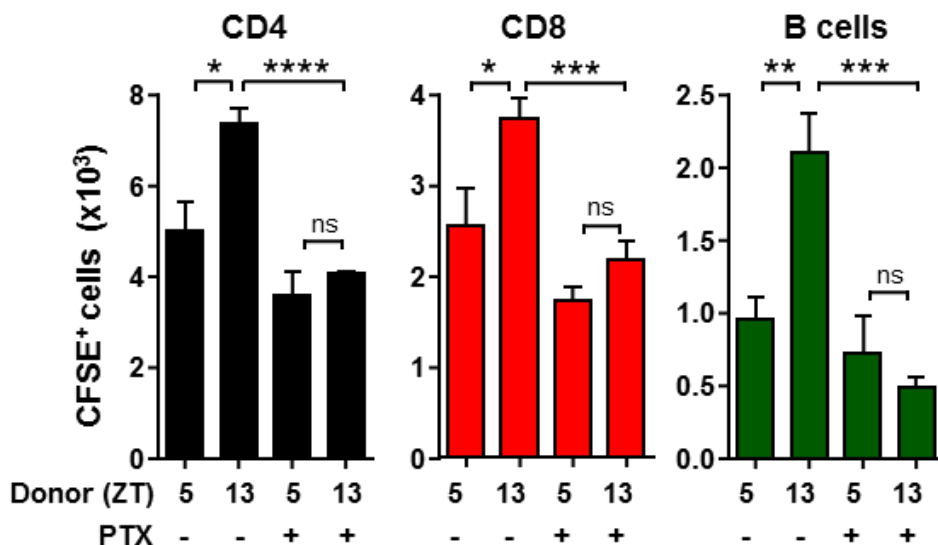


Figure 3.12 Rhythmic homing is blocked upon short PTX pre-treatment

Amount of homed cells in lymph nodes for donor cells harvested at ZT5 or ZT13. After labeling with fluorescent dyes, cells were either incubated with PBS or PTX for 10 minutes and injected into recipient mice; n=5 mice, unpaired student's t-test. *p<0.05, **p<0.01, ***p<0.001.

A further way to determine the role of CCR7 is by investigating *Ccr7*-deficient mice, which were generously provided by Prof. Dr. Reinhold Förster (MH Hannover). Total lymph node counts of these mice were analyzed for two Zeitgeber times, ZT1 and ZT9. In contrast to WT mice, neither total cell counts nor any leukocyte subset oscillated, while cell counts were overall diminished as expected (Förster et al. 1999). When rhythmic lymph node homing was performed in the same fashion as described above, adoptively transferred cells harvested from *Ccr7* KO mice and injected into WT recipients failed to show differences between the two Zeitgeber times (Figure 3.13).

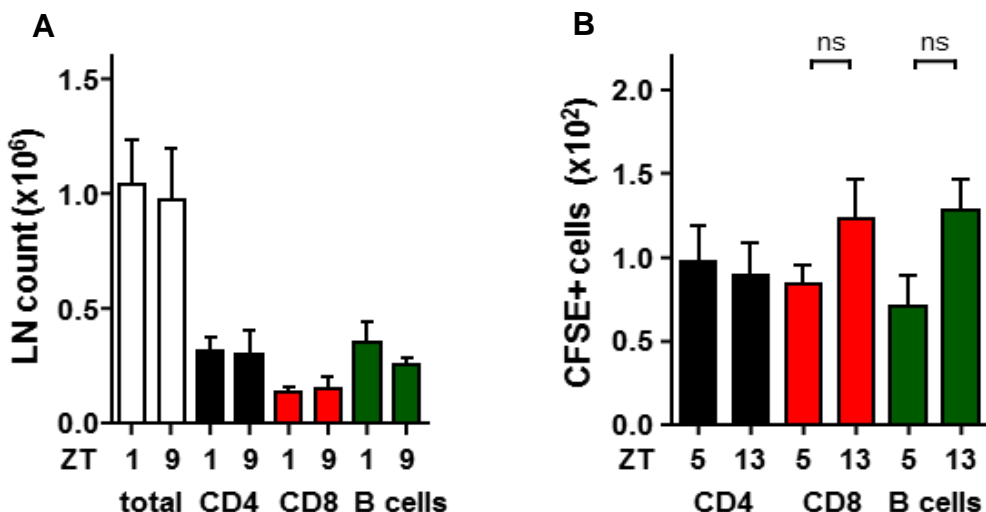


Figure 3.13 Lymph node cellularity and homing of *Ccr7* KO mice

(A) Inguinal lymph nodes of *Ccr7* -/- mice were harvested at different Zeitgeber times, counted and analyzed via flow cytometry. (B) *Ccr7* -/- cells from different Zeitgeber times were labeled with CFSE and CMTPX and injected into WT recipient mice. After 2 hours of homing, the amount of homed cells was analyzed via flow cytometry. n=4-6 mice, unpaired student's t-test

Together, these data show that time-of-day dependent differences in the homing capacity of leukocytes into the lymph node are dependent on rhythmic expression levels of CCR7.

3.3 Role of clock genes in leukocyte trafficking

3.3.1 Clock genes oscillate in lymph nodes

To address whether circadian clock genes oscillate in lymph nodes, inguinal lymph nodes were harvested and clock gene expression profiles were determined for the most prominent clock genes (Figure 3.14). All investigated genes in the molecular clock machinery oscillated significantly over 24 hours.

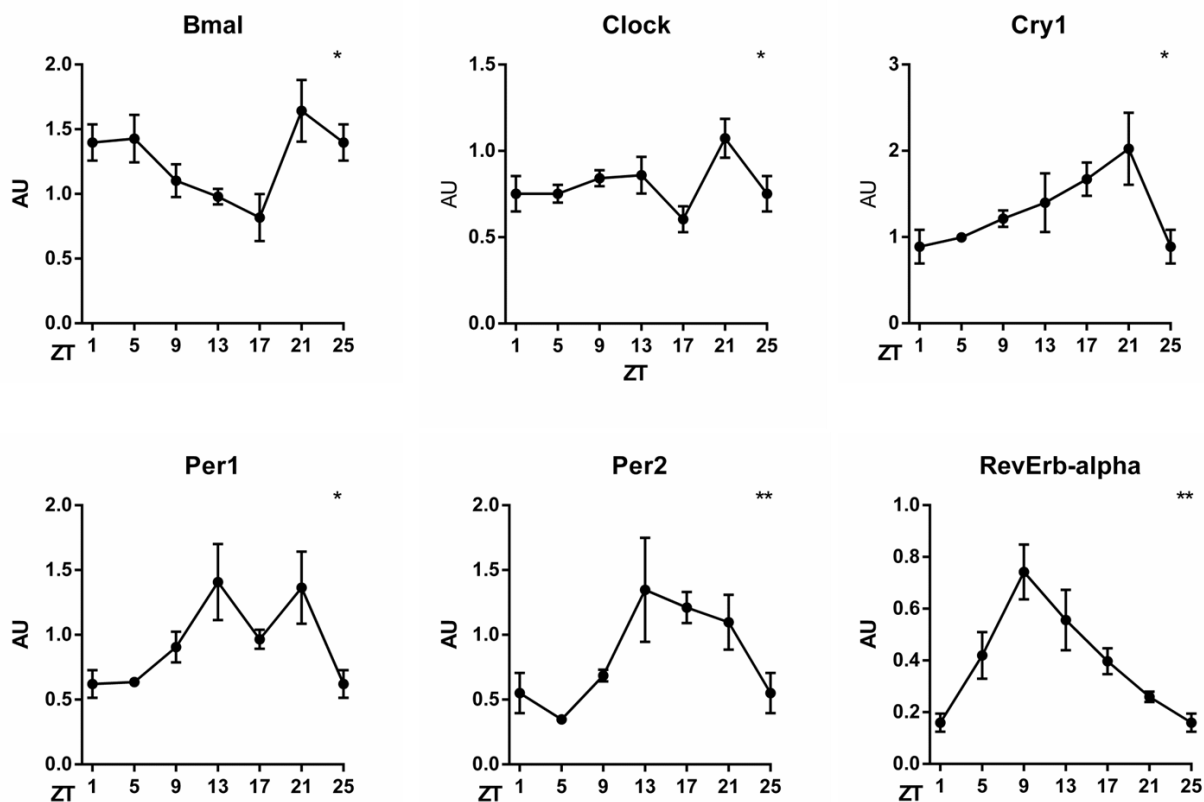


Figure 3.14 Expression profiles of clock genes in lymph nodes

Q-PCR analysis of circadian clock genes in inguinal lymph nodes over 24 hours; n=3-5 mice, one-way ANOVA. *p<0.05, **p<0.01.

3.3.2 Phenotype of T- and B-cell specific *Bmal1* knock-out mice

As described in the introduction, BMAL1 is a crucial protein for the molecular clock machinery. Furthermore, it is the only single gene whose knock-out results in complete loss of rhythmicity (Bunger et al. 2000). As our aim was to determine the role of BMAL1 in T-cell trafficking, *Bmal1*^{fl/fl} × *CD4cre* mice, which lack *Bmal1* expression in CD4 and CD8 T-cells were generated in our lab. Lymph nodes were harvested under steady-state conditions at four different time-points and leukocyte counts were obtained (Figure 3.15).

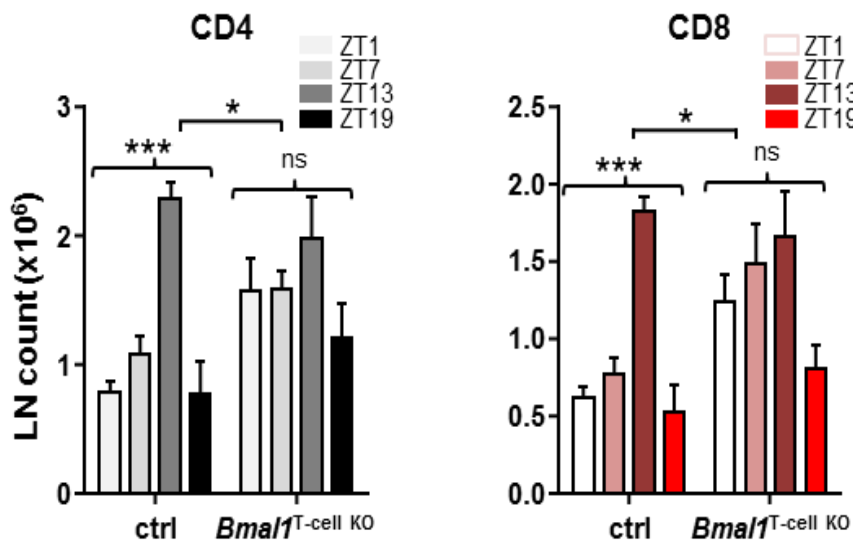


Figure 3.15 Leukocyte counts in T-cell specific *Bmal1* knock-out mice

Inguinal lymph nodes of *Bmal1*^{flox/flox} x *CD4cre* mice were harvested and analyzed for leukocyte subsets; n=3-9 mice, one-way and two-way ANOVA. *p<0.05, ***p<0.001.

Interestingly, leukocyte counts and the oscillation pattern were altered in inguinal lymph nodes, whereas spleen, thymus and bone marrow counts remained similar to control littermates (data not shown).

The same experiments were performed in *Bmal1*^{flox/flox} x *CD19cre* mice, which lack *Bmal1* expression in B-cells to exclusively determine the role of BMAL1 in B-cell trafficking (Figure 3.16).

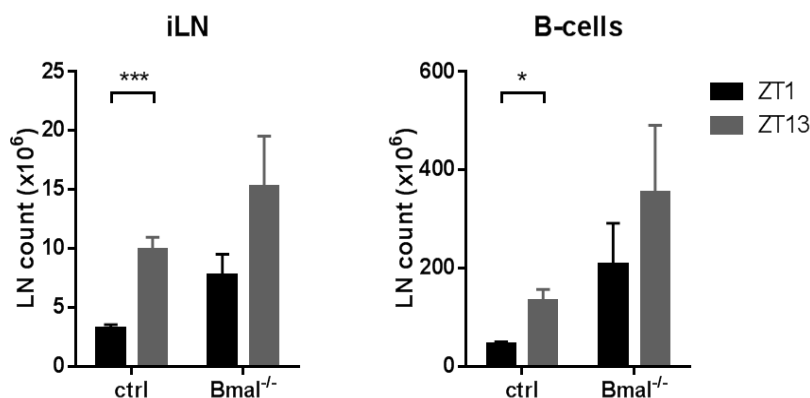


Figure 3.16 Leukocyte counts in B-cell specific *Bmal1* knock-out mice

Inguinal lymph node counts of *Bmal1*^{flox/flox} x *CD19cre* mice were harvested and analyzed for leukocyte subsets; n=4-5 mice, unpaired student's t-test. *p<0.05, ***p<0.001.

Similar to leukocyte counts in *Bmal1*^{flox/flox} *CD4cre* mice, cellularity in lymph nodes changed the strongest and the oscillation pattern was abandoned, whereas cellularity in other organs was unaffected (data not shown).

In a next step, donor leukocytes from *Bmal1* T-cell specific knock-out mice were harvested and injected into WT recipient mice to determine whether these donor cells exhibited an impaired rhythmic homing capacity. Indeed, leukocytes lacking *Bmal1* failed to show rhythmic differences in homing into lymph nodes compared to control cells (Figure 3.17). This suggested that a defect in *Bmal1* gene expression altered the expression profile of homing molecules such as CCR7.

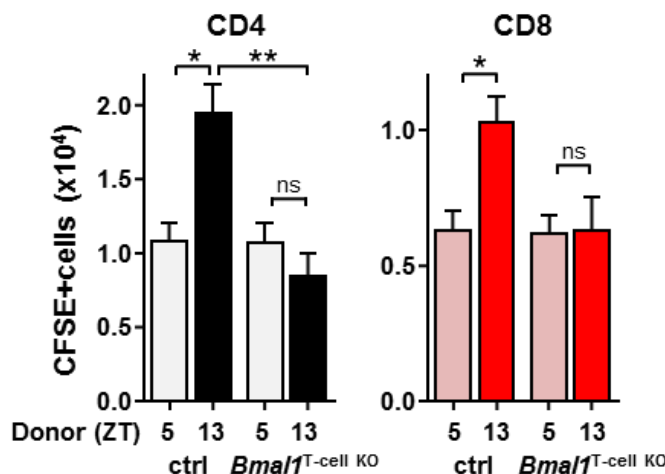


Figure 3.17 Lymph node homing of leukocytes harvested from control and T-cell-specific *Bmal1* knock-out mice

Lymph node homing of leukocytes harvested at different Zeitgeber times from control or *Bmal1* T cell specific knock-out mice into WT hosts. n=10-34 mice, one-way ANOVA with Tukey's multiple comparison test. *p<0.05 **p<0.01.

To verify this hypothesis, mRNA levels of *Ccr7* were investigated in isolated CD4 T-cells from control littermates and *Bmal1*^{flox/flox} *xCd4cre* mice. Indeed, *Ccr7* levels did oscillate in WT mice, whereas oscillations were significantly diminished in T-cells, which lacked *Bmal1* (Figure 3.18).

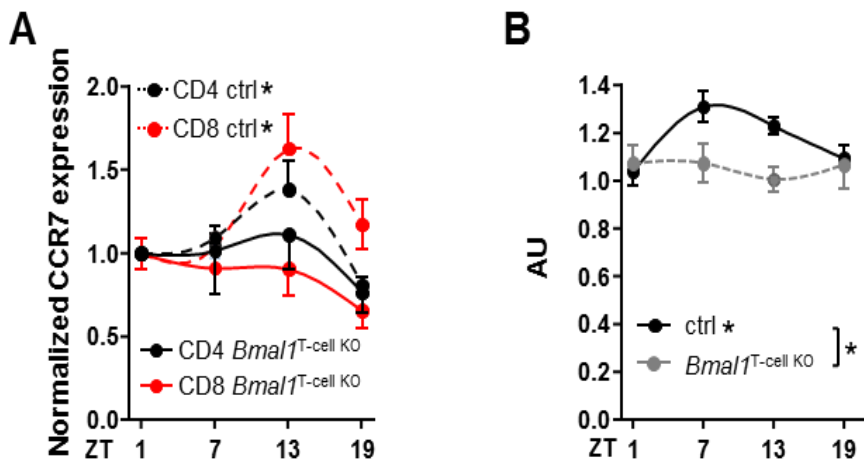


Figure 3.18 CCR7 surface expression and mRNA levels of control and T-cell-specific *Bmal1* KO mice

(A) CCR7 surface expression levels were analyzed via flow cytometry in control littermates and T-cell-specific *Bmal1* KO mice (B) Q-PCR analysis of *Ccr7* levels in isolated CD4 T-cells of control littermates and *Bmal1* deficient cells over 24 hours; n=3-5 mice, one-way and two-way ANOVA. *p<0.05.

Taken together, these data demonstrate that *Bmal1* plays a critical role in maintaining the rhythmic homing potential observed for leukocytes. If *Bmal1* gene expression is abolished, leukocyte fail to home into lymph nodes in a time-of-day dependent way.

3.4 Leukocyte egress into efferent lymphatic is under circadian control

3.4.1 Circadian oscillations in leukocyte numbers in lymph fluid

To determine whether leukocyte numbers in efferent lymph show rhythmic oscillations, a novel technique was established in order to cannulate lymphatic vessels. The advantage of this mesenteric lymph vessel cannulation is the tight control of the time scale of cannulation and the exclusion of contamination with blood, compared to other techniques that puncture the thoracic duct followed by peritoneal lavage (Matloubian et al. 2004). Of importance, there are no differences in

the amount of leukocytes harvested, when comparing our method to the previously described technique (data not shown).

As our previous data suggested, we also observed striking differences in the cellular counts within lymph fluid, where lymphocyte numbers peaked at ZT9 and exhibited a trough at ZT21 (Figure 3.19).

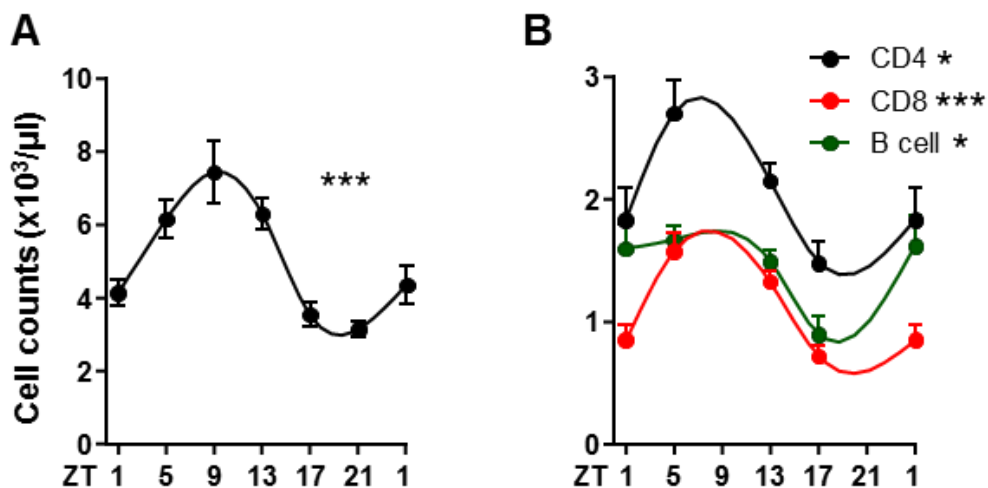


Figure 3.19 Leukocyte and lymphocyte numbers oscillate in lymph fluid

(A) Cell counts in efferent lymph fluid after 1 hour cannulation of a mesenteric efferent lymph vessel; n=6-33, one-way ANOVA (B) Lymphocyte subset numbers in efferent lymph over 24 hours; n=6-33, one-way ANOVA. *p<0.05, ***p<0.001.

As described for lymph node cellularity before, an important criterion for a circadian rhythm is its ability to persist at constant conditions, such as constant darkness.

We therefore transferred mice kept under normal light:dark conditions (LD) into constant darkness (DD) and measured lymph counts. Indeed, also under DD conditions lymphocyte counts remained oscillatory in efferent lymph (Figure 3.20). This demonstrated their *bona fide* endogenous circadian nature.

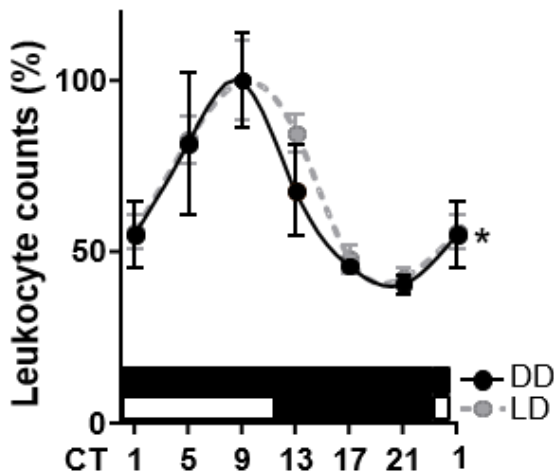


Figure 3.20 Lymph cell counts under constant darkness

Leukocyte numbers in efferent lymph under LD and DD conditions; n=3-37, one-way ANOVA. *p<0.05.

To exclude the possibility, that the observed oscillations in leukocyte counts were not due to potential time-of-day dependent differences in lymph flow, lymph was cannulated over one hour and lymphatic flow rate was quantified. Indeed, lymph flow was constant over the collected time points in anesthetized mice, demonstrating that oscillating numbers were caused by egress-mediated effects (Figure 3.21).

Time	ZT1	ZT7	ZT13	ZT21
Lymph volume (µl)	72 ± 5	70 ± 5	68 ± 4	79 ± 4
Lymph flow (µl/min)	1.2 ± 0.1	1.2 ± 0.1	1.1 ± 0.1	1.3 ± 0.1

Figure 3.21 Lymph flow is constant at different Zeitgeber times

Lymph volume and flow rate over different time points quantified over one hour of cannulation in anesthetized mice; n=7-22

3.4.2 Leukocyte half-life in LNs is time-of-day dependent

As time-of-day had a major influence on the LN homing and egress capacity of leukocytes, we investigated the possibility that leukocyte half-life, i.e. the time that a

leukocyte spends in the LN, is also dependent on the *Zeitgeber* time. Therefore, we carried out adoptive transfer experiments at ZT5 and ZT13 and - after two hours of homing - blocked any subsequent entering of lymphocytes into LN by administration of anti-integrin antibodies. Over the next 24 hours, lymph nodes and lymph was harvested at different times and the presence of both endogenous and adoptively transferred leukocyte subsets in LN and lymph were analyzed. Interestingly, at ZT13, endogenous cells remained significantly longer in the lymph node than at ZT5 (Figure 3.22). A similar, albeit weaker, effect was observed for transferred cells (Figure 3.23). This indicates that lymphocyte egress from lymph nodes into efferent lymphatic vessels is highly rhythmic.

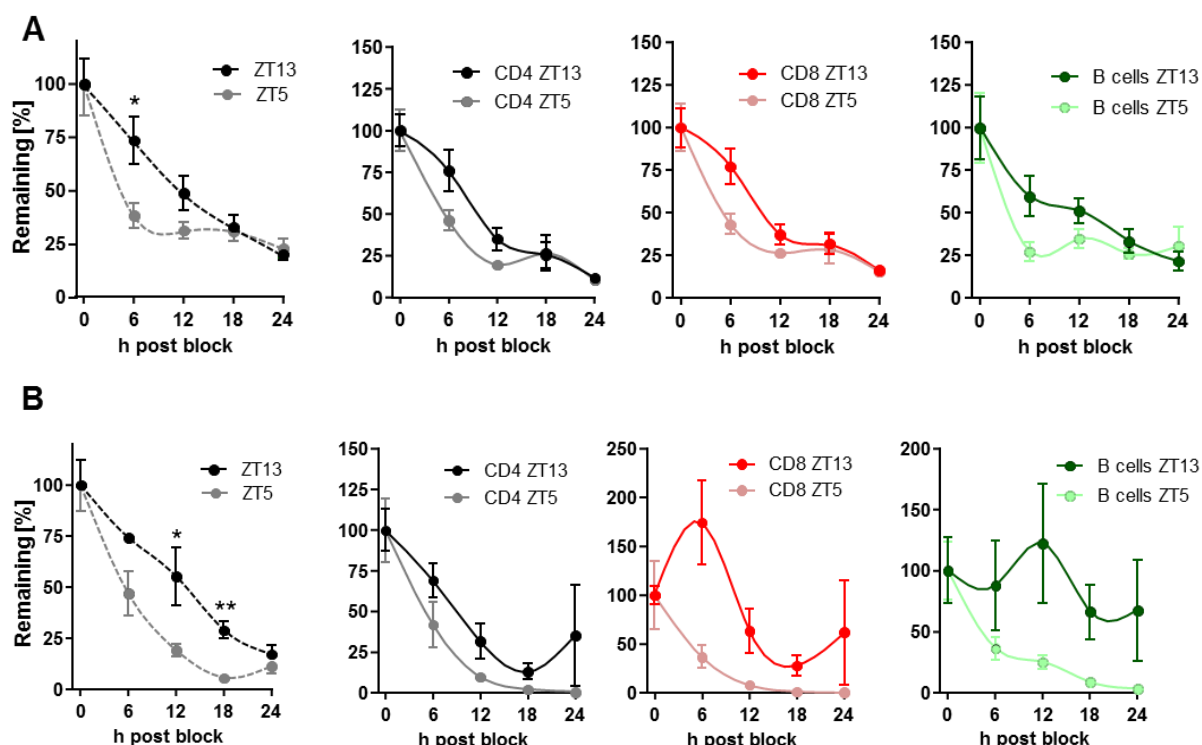


Figure 3.22 Analysis of remaining endogenous lymphocytes in lymph nodes and lymph after homing block

(A) Remaining percentage of lymphocyte subsets in lymph nodes over 24 hours after homing block at ZT5 and ZT13; n=3-10 mice, unpaired student's t-test (B) Remaining percentage of lymphocyte subsets in lymph over 24 hours after homing block at ZT5 and ZT13; n=3-6 mice, unpaired student's t-test. *p<0.05, **p<0.01.

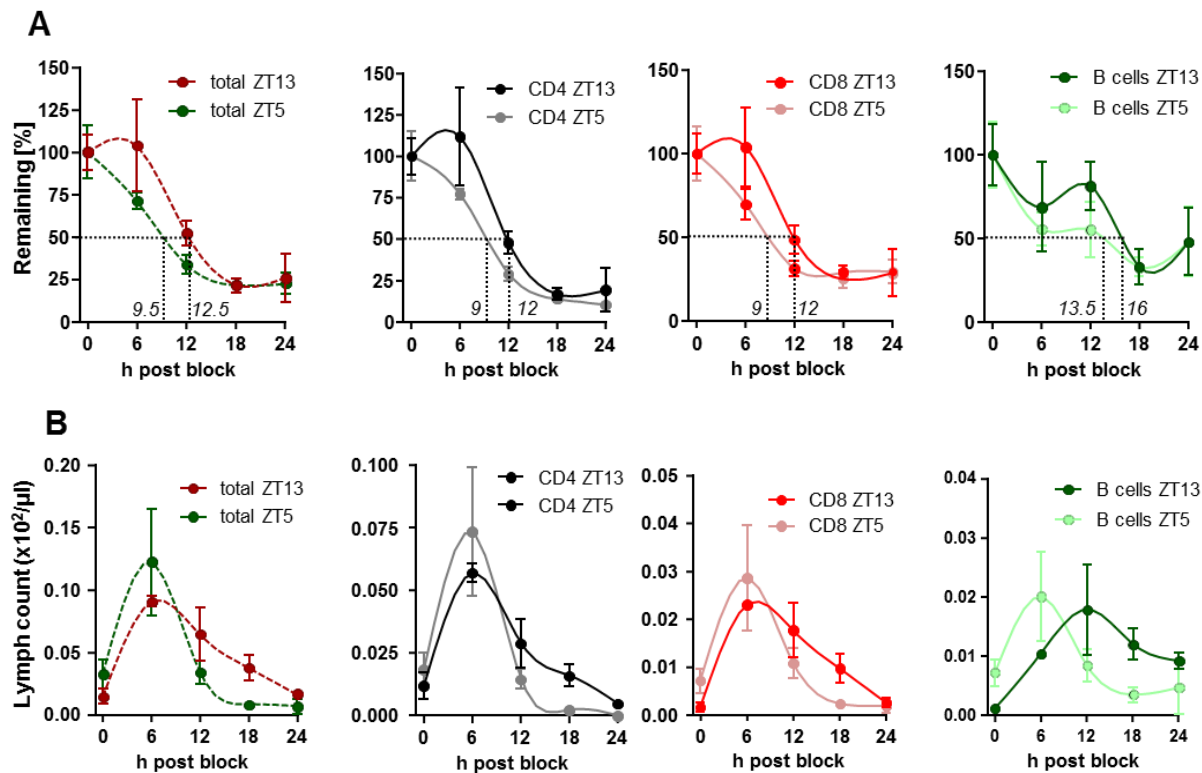


Figure 3.23 Half-life analysis of adoptively transferred cells in lymph nodes and lymph
 (A) Remaining percentage of adoptively transferred leukocytes at ZT5 and ZT13 recipients after homing block; n=3-10 mice (B) Total leukocyte and lymphocyte numbers in lymph after homing block was performed at ZT5 and ZT13; n=3-6 mice

3.4.3 Leukocyte egress and half-life is non-rhythmic in CD4 T lymphocytes lacking *Bmal1*

To investigate, whether the core clock protein BMAL1 regulates lymphocyte egress, lymph was drawn from *Bmal1*^{fl/fl} × CD4cre mice over different Zeitgeber times, counted and analyzed for leukocyte subsets via flow cytometry. Both for CD4 and CD8 T-cells, rhythmic oscillations in lymph counts were abolished (Figure 3.24).

This suggests that *Bmal1* is able to regulate the egress of cells from the lymph node into efferent lymphatic vessels.

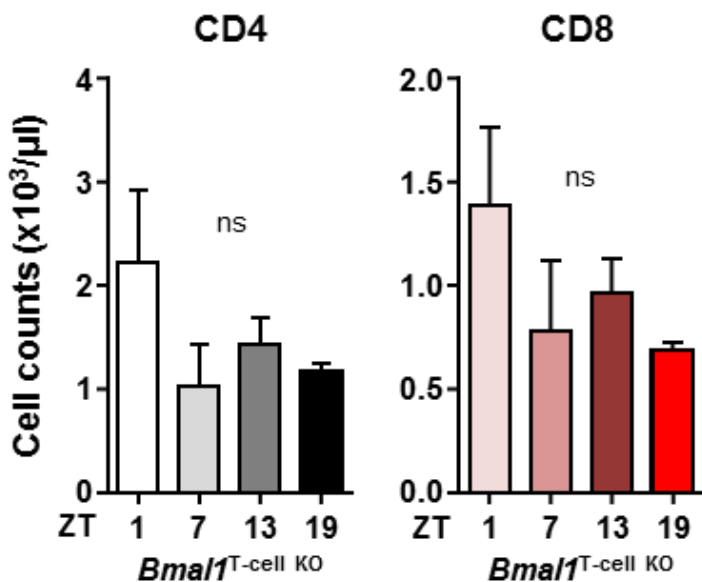


Figure 3.24 Leukocyte counts in lymph of T-cell-specific *Bmal1* KO mice

CD4 and CD8 T-cell counts in lymph drawn at different Zeitgeber times from *Bmal1*^{fl/fl} x *CD4cre* mice. n=3-8 mice, one-way ANOVA.

To determine, whether half-life of leukocytes in lymph nodes is under control of *Bmal1*, CD4 T-cells from *Bmal1*^{fl/fl} x *CD4cre* mice were isolated at two different Zeitgeber times and co-injected together with littermate controls into wild-type mice. Two and twelve hours after adoptive transfer, inguinal lymph nodes of recipient mice were harvested and analyzed for the amount of remaining cells (Figure 3.25). As expected, control ZT13 donor CD4 T-cells remained significantly longer in lymph nodes than ZT5 donor CD4 T-cells. In contrast, however, ZT5 and ZT13 CD4 T-cells lacking BMAL1 protein exhibited no time-of-day dependent differences. These results highlight the importance of a functional T cell clock for their rhythmic trafficking behavior.

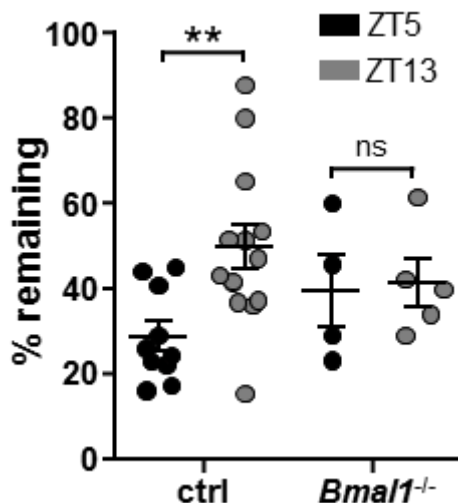


Figure 3.25 Impaired leukocyte dwell time in *Bmal1*-deficient CD4 T-cells

CD4 T-cells of littermate controls and *Bmal1*^{fl/fl} × CD4cre were isolated at ZT5 and ZT13 and injected into recipient mice. Two and twelve hours after transfer, the amount of labeled cells remaining in LN was analyzed using flow cytometry. Data points are shown as remaining cellular numbers (in %) in lymph nodes harvested twelve hours after transfer compared to two hours after transfer; n=4-13 mice, unpaired student's t-test. **p<0.01.

3.5 Rhythmic leukocyte egress is dependent on circadian *S1pr1* expression

The most important molecular pathway that regulates egress of leukocytes from lymph nodes into efferent lymphatic vessels is mediated via the S1P-S1P1 axis. Initially, we analyzed mRNA levels of all five known S1P receptors and observed rhythmic oscillations for all five receptors (Figure 3.26).

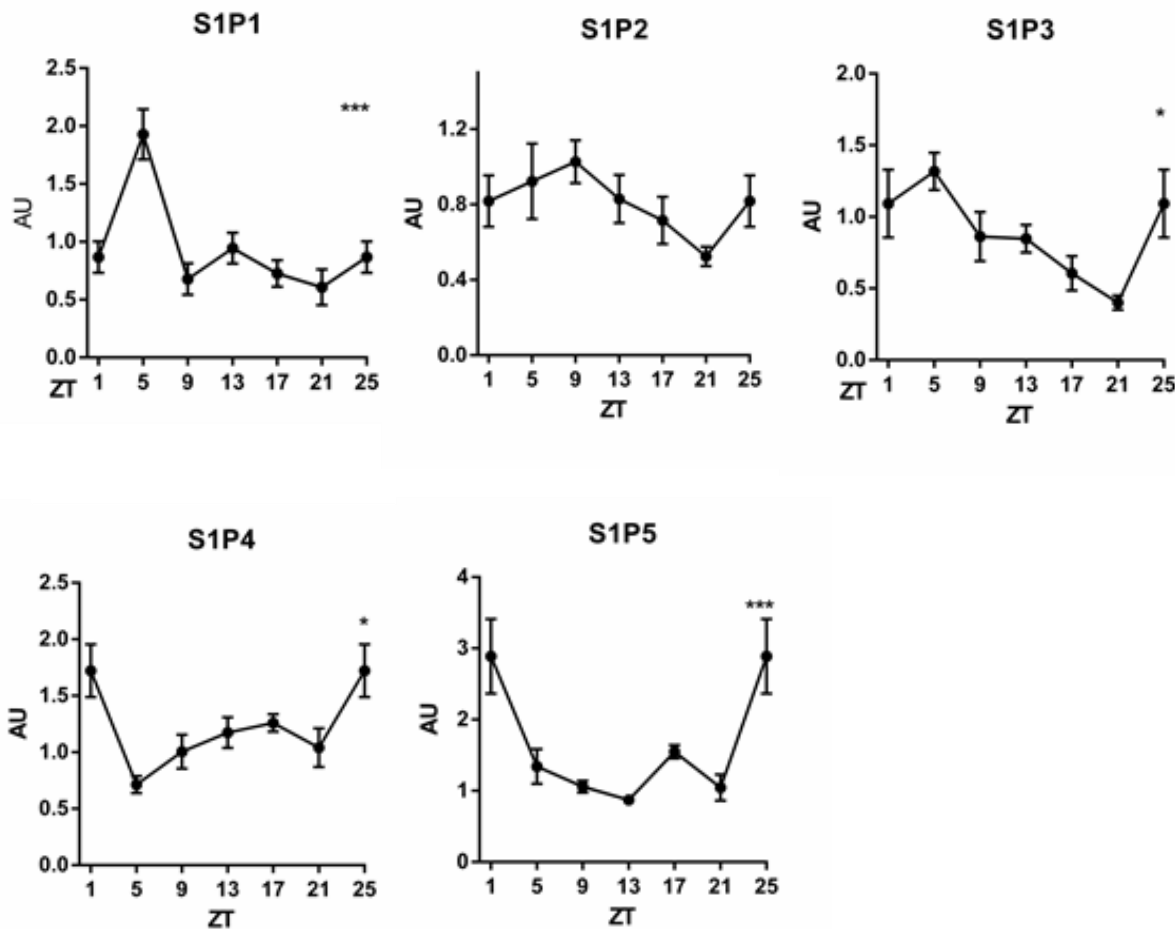


Figure 3.26 Q-PCR analysis of S1P1-5 receptors

Relative mRNA expression levels of S1P receptors harvested from inguinal lymph nodes over 24 hours; n=3-5 mice, one-way ANOVA. *p<0.05, ***p<0.001.

To investigate whether time-of-day changes in *S1pr1* expression levels caused the rhythms in lymph fluid cellularity we blocked leukocyte egress at different time-points of the day. This was achieved by injection of FTY720 40 minutes prior cannulation, an egress modulating drug that downmodulates S1P receptors (except S1P2). Indeed, lymph counts were differentially affected, depending on the time of day FTY720 was given, suggesting a time-of-day dependent sensitivity against the drug. This effect was also observed, when smaller doses of the drug were administered (Figure 3.27).

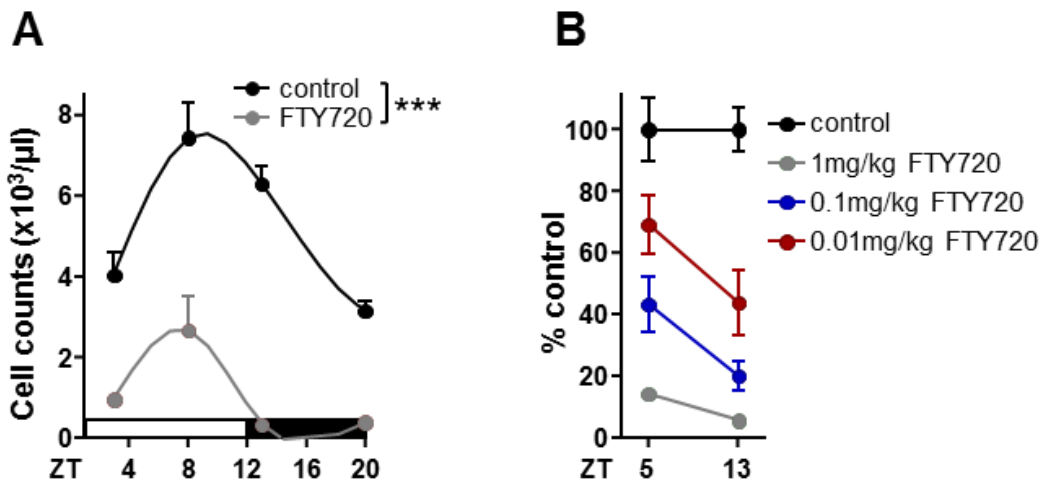


Figure 3.27 Time-of-day dependent sensitivity against FTY720

(A) Leukocyte counts in lymph fluid after blockade of S1P receptors at different time points of the day; n=3-33, two-way ANOVA (B) Effects of FTY720 titration at two different time-points, n=3-5 mice. ***p<0.001.

This indicated an important role for S1P1 in mediating rhythmic leukocyte egress. In fact, *S1pr1* levels do oscillate in CD4 T-cells corresponding to overall oscillations in lymph counts. These oscillations were abrogated in CD4 T-cells, which lack *Bmal1* expression (Figure 3.28).

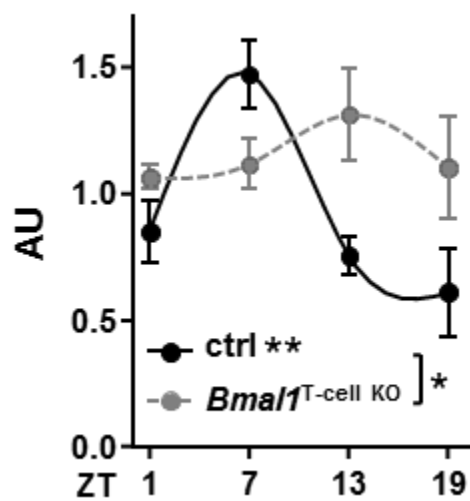


Figure 3.28 Q-PCR analysis of *S1pr1* levels in CD4 T-cells

S1pr1 mRNA levels were analyzed in CD4 T-cells in control and T-cell specific *Bmal1* KO mice. n=4-9 mice, one-way and two-way ANOVA. *p<0.05 **p<0.01.

To test whether also levels of S1P, the chemoattractant lipid that binds to S1P1, might be under circadian control, S1P levels in lymph and blood plasma were measured at different time-points of the day (Figure 3.29). In contrast to S1P receptor levels, concentration levels of S1P did not oscillate over the course of a day.

This demonstrates that expression levels of S1P1 regulate time-of-day differences in leukocyte egress.

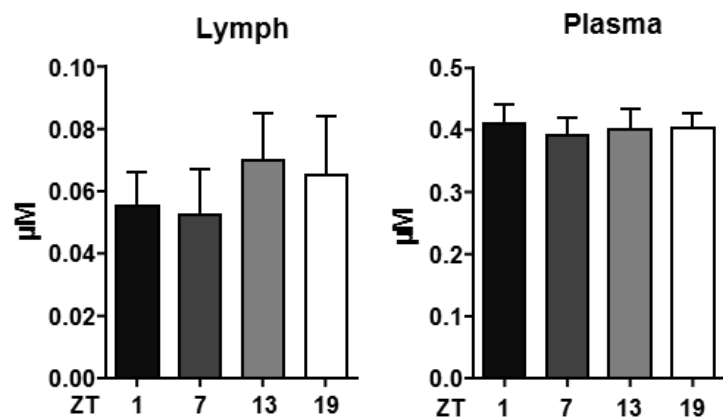


Figure 3.29 Lymph and Plasma S1P levels over 24 hours

Lymph and plasma samples were analyzed via mass spectrometry for levels of S1P, n=9-11 mice

3.5.1 Modulation of lymphocyte trafficking in *S1pr1* gene-targeted mice

S1P1 is a major regulator of rhythmic leukocyte egress. It has been previously reported that complete knock-out of S1P1 abolishes leukocyte egress entirely (Matloubian et al. 2004).

Therefore, we used heterozygous mice that lack one allele of the *S1pr1* gene, as it has been previously reported that *S1pr1^{fl/fl}* mice display haploinsufficiency (Pham et al. 2008). As expected, we did observe diminished leukocyte counts in blood (not shown) and lymph due to an impaired ability of leukocyte to leave the lymph node. Importantly, we observed non-rhythmic lymph node counts, whereas only CD8 T cells remained to show rhythmic but altered lymph counts (Figure 3.30).

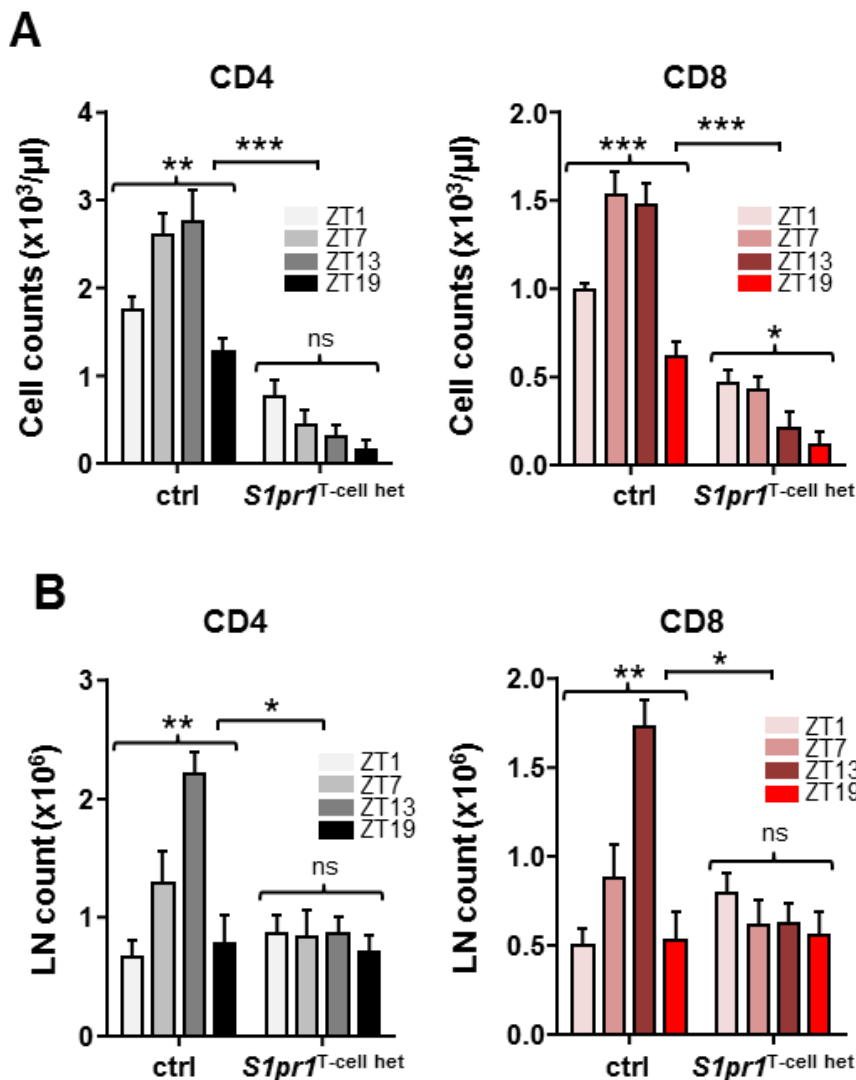


Figure 3.30 Leukocyte counts in T-cell-specific *S1pr1* heterozygous mice

Lymph (A) and inguinal lymph nodes (B) of *S1pr1*^{flx/+} x *CD4cre* mice were harvested and analyzed for leukocyte subsets; n=3-6 mice, one-way and two-way ANOVA. *p<0.05, **p<0.01, ***p<0.001.

As *S1pr1*^{flx/+} x *CD4cre* mice have reduced S1P1 receptor levels both on CD4 T-cells and CD8 T-cells due to T-cells undergoing a CD4-CD8 double positive developmental stage in the thymus, a different approach was used to target S1P1 function specifically in CD4 T-cells (Sharma & Zhu 2014). By breeding *S1pr1*^{flx/+} x *CD4ERT2* mice, these mice should lack partially the S1P1 receptor on CD4-T-cells after induction of the CRE recombinase and waiting the correct amount of time (Śledzińska et al. 2013). 5mg/day tamoxifen was given orally for five consecutive days and two weeks later, organs were harvested and analyzed for leukocyte counts (Figure 3.31). Instead of showing exclusively impaired CD4 T-cell numbers, CD8 T-

cell counts were also altered. This indicated that also CD8 T-cells were affected by the treatment, which could be due to an improper time point selected for harvest.

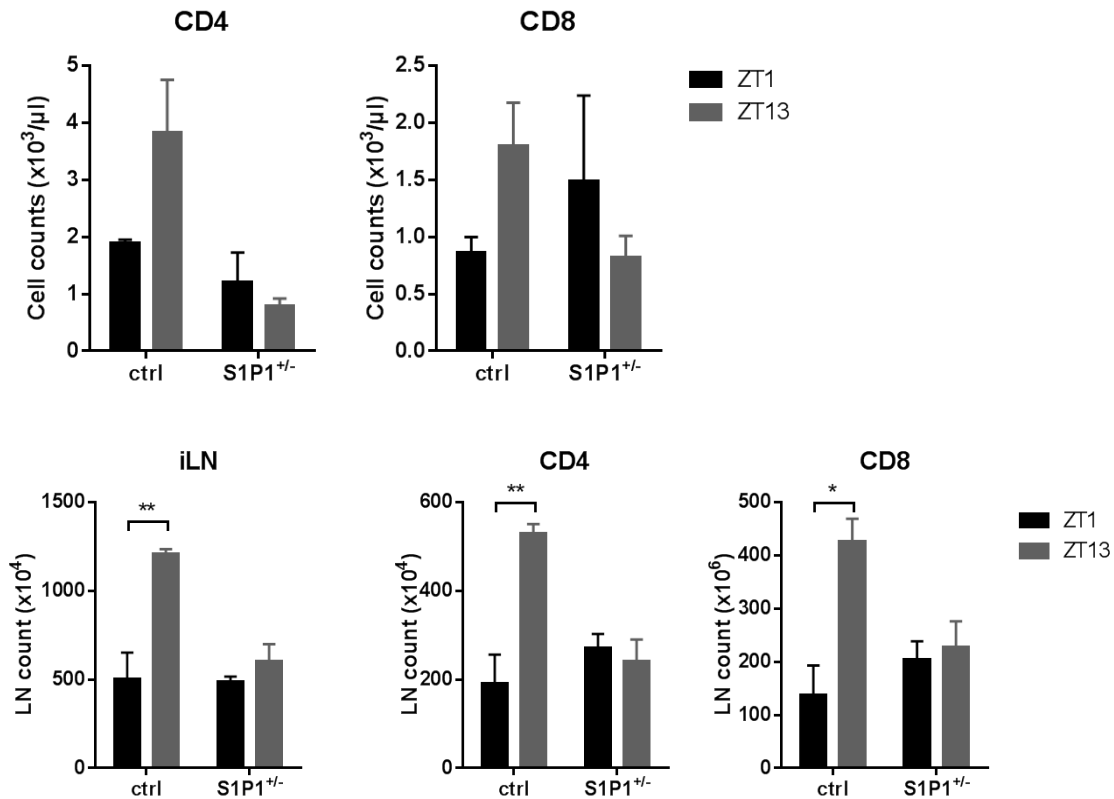


Figure 3.31 Leukocyte counts in $S1pr1 \times CD4$ inducible Cre mice

Leukocyte counts of organs harvested from $S1pr1^{flox/+} \times CD4ert2$ mice two weeks post tamoxifen treatment; n=3 mice, unpaired student's t-test. *p<0.05, **p<0.01.

4 Discussion

Circadian clocks have developed in unicellular and multicellular organisms during evolution to enable organisms to adapt optimally to environmental changes naturally occurring during the 24 hour light-dark cycle. In mammals, this evolution has led to the existence of the SCN, a central pacemaker which entrains pervasively expressed peripheral clocks in different organs and cell types. Furthermore, recent studies have strengthened the initial observations that integral parts of the immune system are under control of central or peripheral clocks, including immune responses to inflammatory diseases and adaptive immune responses against vaccines (Scheiermann et al. 2012; Long et al. 2016).

However, little is known to which extent peripheral clocks, which are known to be expressed in leukocytes (Bollinger et al. 2011; Hemmers & Rudensky 2015), might drive the migratory behavior of leukocytes under physiological and pathophysiological conditions in secondary lymphoid organs. Although it has been shown that molecular clock proteins are expressed in lymph nodes and spleen (Keller et al. 2009), the exact role of these proteins in lymphoid tissues remained unclear. Furthermore, controversial results have been published as to whether leukocyte numbers exhibit diurnal variation regarding their cell numbers in lymphoid tissues (Litvinenko et al. 2005; Fortier et al. 2011). The aim of this thesis was to investigate whether clocks in lymphocytes control the migratory behavior and functions of these cells and might thus play a role in the (patho)physiology of lymphatic organs.

The experimental work presented here unveiled that clock proteins regulate rhythmic expressions of proteins, which are crucial for the homing to and egress of leukocytes from lymph nodes. Under steady-state conditions, this results in higher expression of chemokine receptors (CCR7 and CXCR5), chemokines (CCL21) and adhesion molecules (ICAM-1 and VCAM-1), which leads to a higher homing capacity of leukocytes towards the beginning of the active phase. Furthermore it could also be shown that the expression profile of the main egress molecule S1P1 is also under circadian control and exhibits an inverted oscillation compared to the homing and retention factors. These opposite oscillation patterns determine the time-scale for a lymphocyte to enter, survey and finally leave lymph nodes.

Taken together, peripheral clocks modulate homing, dwell time and egress of leukocytes and thus actively shape rhythmic cellularity of lymph nodes. These rhythms were abolished by genetic disruption of T and B cell clocks. Moreover, these

rhythmic cellular oscillations contribute to understanding previously described circadian oscillations in the strength of adaptive immune responses.

4.1 Cellular oscillations of leukocyte numbers in lymph nodes

We initially determined cell counts of inguinal lymph nodes over multiple time points of the day, due to conflicting results in the literature. In accordance with data published by Litvinenko and colleagues, we detected a time-of-day dependent difference in the total cell counts of inguinal lymph nodes (Litvinenko et al. 2005). Furthermore, these oscillations in cell numbers were also detected in other skin draining and mesenteric lymph nodes, suggesting these oscillations to reflect a broad systemic phenomenon, which appears not to be restricted to the specific location of the lymphoid organ. To confer that these oscillations are *bona fide* circadian, i.e. persist under a changed light regime, mice were challenged either with a reversed dark/light cycle or kept in constant darkness. In both cases, oscillations in cell numbers of inguinal lymph nodes persisted, indicating their true circadian nature.

In a next step, the detailed cell composition of lymph nodes was determined. Due to the work of Fortier et al, it has been assumed, that lymphocyte subsets do not vary over the day in murine lymph nodes (Fortier et al. 2011). Recently, this assumption has been revoked by a study showing clear oscillations for major leukocyte subsets in lymph nodes (Suzuki et al. 2016). In accordance with the latter data, we also could determine significant differences in the cell numbers of CD4 T-cells, CD8 T- cells, B-cells and dendritic cells in all investigated lymph nodes. In general, leukocyte numbers increased towards the beginning of the active phase in these tissues, exhibiting a peak between ZT9 and ZT13, and decreasing towards the beginning of the resting phase, showing a trough at ZT1. Depending on the leukocyte subset, the time-of-day is therefore responsible for a 2-3 fold difference in total cell numbers. Interestingly, the peak of lymph node oscillations occurs 4-8 hours later to previously described oscillations in blood leukocyte counts (Scheiermann et al. 2013; Arjona et al. 2012; Curtis et al. 2014). It is remarkable, that other hematopoietic organs such as

the thymus and the spleen do not display perceptible oscillations in absolute numbers (data not shown).

Furthermore, it is well known, that overall numbers in bone marrow do not oscillate over 24 hours. Interestingly however, hematopoietic stem and progenitor cells (HSPCs) exhibit circadian differences in the mobilization into blood and the recruitment back into the bone marrow. Thereby, the release of HSCs from the bone-marrow into blood peaks 5 hours after the onset of light, similar to total leukocyte counts in blood (Méndez-Ferrer et al. 2008). In contrast, the recruitment of HSPCs to the bone marrow peaked one hour after the onset of darkness (Scheiermann et al. 2012), similar to the here observed peak in total leukocyte counts in lymph node. Mechanistically, both processes are mediated by a tissue specific circadian regulation of chemokine and endothelial cell adhesion molecules, as well as a circadian regulation of the adrenergic tone.

Therefore it appears that both homing of cells into the lymph node and egress from the lymph node might contribute to the observed oscillations in absolute cell counts. Indeed, both homing block (via HEVs) with anti-integrin antibodies and lymphocyte egress (via efferent lymphatic vessels) block with FTY720 ablated rhythmicity completely over 24 hours.

As the amount of intranodal proliferation did not change over the day, both homing and egress appear to be the main contributors to the observed oscillations in lymph node cellularity.

4.2 Control of lymph node cellularity by the circadian clock

4.2.1 Homing of cells into lymph nodes is under circadian control

To determine whether homing of leukocytes into lymph nodes is dependent on the time of the day, homing experiments were performed at different zeitgeber times. Indeed, up to 4 fold differences in the amount of homed cells were observed, where

leukocytes entered lymph nodes most prominently at the onset of the night phase (ZT13).

In order to enter lymph nodes, leukocytes undergo complex interactions with HEVs. This process is mediated by leukocyte-expressed factors, e.g. selectins (CD62L), integrins (CD11a) and chemokine receptors (CCR7, CXCR4, CXCR5), and endothelium-derived factors, e.g. adhesion molecules (ICAM-1, ICAM-2, VCAM-1) and chemokines (CCL21, CCL19, CXCL12, CXCL13) (Miyasaka & Tanaka 2004).

To decipher whether leukocyte-intrinsic or endothelium-derived signals contribute to the observed differences in homing potential, leukocytes were harvested from ZT5 or ZT13 donor mice and adoptively transferred at either ZT5 or ZT13 recipient mice. As expected, ZT5 cells into ZT5 mice exhibited the lowest homing capacity, whereas ZT13 cells into ZT13 mice showed the highest amount of homed cells. Interestingly, intermediate levels of homing capacity were observed both for ZT5 cells into ZT13 mice and ZT13 cells into ZT5 mice. A screen for promigratory factors on leukocytes revealed that exclusively the chemokine receptors CCR7 (for T and B cells) and CXCR5 (for B cells) exhibit rhythmic surface expression profiles, whereas other adhesion molecules (CXCR4, CD11a, CD62L) did not oscillate.

Several experiments performed within this thesis underscore the fact that CCR7 is a crucial determinant for rhythmic leukocyte homing.

First, rhythmic homing was blocked upon treatment of leukocytes with PTX, a chemical reagent, which abolishes $G_{\alpha i}$ protein-coupled receptor signalling. Second, *Ccr7*^{-/-} mice neither exhibited any oscillations in absolute cell counts nor in leukocyte subsets in lymph nodes. Third, CCR7 KO cells failed to show differences in the homing capacity between ZT5 and ZT13, in contrast to WT cells. Fourth, both CCR7 surface expression levels and mRNA levels do oscillate in leukocytes, peaking towards the beginning of the active phase when leukocyte homing is the highest.

As the function of CCR7 is dependent on chemokine ligands, CCL19 and CCL21 expression levels have been analyzed to test the hypothesis that the receptor as well as the ligand mediates rhythmic homing. Expression analyses of lymph nodes revealed that both mRNA levels and protein levels on HEVs of CCL21 oscillated over 24 hours, but not CCL19 (not shown).

As described before, BMAL1 is a crucial protein for the molecular clock machinery. Furthermore, it is the only single gene whose knock-out results in complete loss of rhythmicity (Bunger et al. 2000). However, few studies have focused on cell-type specific deletion of *Bmal1* to decipher its role in leukocyte trafficking. Nguyen and colleagues used mice which lack *Bmal1* in the myeloid lineage and showed that *Bmal1* controls trafficking of Ly6C^{hi} inflammatory monocytes by indirectly repressing the expression of CCL2, a chemokine which is expressed under inflammatory conditions (Druzd & Scheiermann 2013; Nguyen et al. 2013).

It was tempting to speculate, that *Bmal1* might regulate in a similar fashion the expression profiles of CCR7 or CCL21. To test this hypothesis we generated T and B cell specific knockout mice to elucidate the role of *Bmal1* on the regulation of leukocyte-derived molecules, which are involved in homing to lymph nodes.

Interestingly, both *Bmal1*^{flox/flox} x CD4cre mice and *Bmal1*^{flox/flox} x CD19cre mice do not exhibit rhythmic leukocyte counts in lymph nodes anymore, although blood leukocyte counts remain oscillatory. This suggests, that *Bmal1* plays indeed a crucial role in regulating lymph node cellularity. To determine, whether leukocytes, which lack *Bmal1* are less capable of homing into lymph nodes, adoptive transfer experiments were performed with leukocytes harvested from control and T-cell-specific *Bmal1* knock-out mice at different Zeitgeber times. In fact, leukocytes, which lack *Bmal1* fail to show time-of-day dependent differences in their homing potential. Mechanistically, leukocytes which lack *Bmal1* do not display rhythmic CCR7 surface expression levels on leukocytes, nor rhythmic mRNA levels.

As mentioned before, it might be possible that besides CCR7, the expression of the chemokine CCL21 is under rhythmic control, similar to the expression of CCL2 by *Bmal1* (Druzd & Scheiermann 2013; Nguyen et al. 2013). As CCL21 is produced by FRCs and endothelial cells in lymph nodes, the generation of *Bmal1*^{flox/flox} x Lyve-1 mice would be necessary to address this question. As both surface expression levels and mRNA levels of CCL21 in whole lymph nodes oscillated over the course of the day, a potential direct circadian regulation is feasible. Whether the adrenal axis governs this rhythmic expression, as has been shown for CXCL5 expression within the lung (Gibbs et al. 2014), or the sympathetic nervous system, as has been shown for both bone marrow and skeletal muscle (Méndez-Ferrer et al. 2008; Scheiermann et al. 2012), needs to be investigated in future experiments.

Taken together, the work presented in this thesis indicates that the expression profile of crucial molecules involved in leukocyte homing are regulated by the circadian clock and that thus the homing of cells into lymph nodes is time-of-day dependent.

4.2.2 Leukocyte egress into efferent lymphatic vessels is under circadian control

The egress of leukocytes from lymph nodes via efferent lymphatic vessels is, besides homing of cells into the organ, a further process that regulates lymph node cellularity.

Therefore, we investigated the possibility that lymphatic egress from lymph nodes is under circadian control by cannulating efferent lymphatic vessels. This hypothesis is supported by recent data from Suzuki et al., reporting that lymphocyte populations in lymph oscillate over 24 hours (Suzuki et al. 2016).

In fact, our data also show rhythms both for absolute leukocyte counts and for CD4 T-cells, CD8 T-cells and B-cells, peaking during the resting phase (ZT9) and exhibiting a trough at the end of the active phase (ZT21). Importantly, these rhythms were independent of lymph flow and, similar to lymph node counts, were *bona fide* circadian in nature as they persisted in constant darkness.

To examine, whether oscillations in lymph counts were truly attributable to rhythmic efflux of cells from lymph nodes and not due to rhythmic influx of cells into lymph nodes, we used an approach that has been previously described to determine leukocyte dwell time in lymph nodes (Mandl et al. 2012). In detail, we adoptively transferred leukocytes at different time points of the day, blocked lymph node homing 2 hours later via injection of blocking antibodies and harvested every 6 hours for 24 hours lymph nodes to quantify the amount of injected and endogenous leukocytes still present. Furthermore, lymph was drawn and analysed in the same manner.

Our data reveal that leukocytes injected at ZT13 remain significantly longer in lymph nodes and show a less rapid accumulation in lymph, compared to cells entering lymph nodes at ZT5. This results in longer lymph node half-lives of leukocytes injected at ZT13 (CD4: 12h, CD8: 12h, B cells: 16h) compared to ZT5 (CD4: 9h, CD8: 9h, B cells: 13.5h). Our observed transit rates for endogenous CD4 T- cells at

ZT13 match nicely previously described transit times, whereas we observed 6 hour shorter transit times for endogenous CD8 T cells (Mandl et al. 2012).

However, Mandl and colleagues use an exponential decay model to estimate transit times, i.e. a model in which T cells leave with a constant probability per unit time. Our data indicate though a time-dependent egress of leukocytes. Consequently, their mathematical model approach might lead to altered transit times as it is indeed the case. This hypothesis is strengthened by the fact that mice, which lack *Bmal1* in T- and B-cells do not exhibit any oscillations in lymph counts, confirming the importance of circadian clock proteins for lymphocyte egress. Furthermore, adoptively transferred CD4 T-cells, which lack *Bmal1* fail to show time-of-day differences in their lymph node transit time, highlighting the relevance of *Bmal1* in leukocyte trafficking.

In summary, our data demonstrate that egress of leukocytes from lymph nodes is highly rhythmic. Furthermore, the time-of-day entry of cells into lymph nodes determines their transit time, as leukocytes tend to survey the lymph node for 3 hours longer when entering the organ at the beginning of the active phase than entering during the rest phase. This observation may be due to it being more likely for an organism to encounter pathogens during the active phase than during the rest phase. Thus, leukocytes might increase their chances to encounter possible pathogens or antigens when they survey lymph nodes longer and at the right time.

4.2.3 Rhythmic leukocyte egress is dependent on circadian *S1pr1* expression

The group of Jason Cyster discovered over the last decade, that retention and egress of leukocytes in the lymph node is mainly modulated by the fine-tuned counterplay between CCR7 and S1P1 (Pham et al. 2008). As soon as S1P1 is upregulated on a leukocyte, the S1P1 signal overrides CCR7, a homing but also retention factor, and leukocyte egress is promoted (Cyster & Schwab 2012).

Thus, our hypothesis was that the expression of S1P1 might be also under circadian control and regulate leukocyte egress together with a rhythmic expression of CCR7.

To investigate the role of S1P1, we generated T-cell specific mice which were heterozygous for *S1PR1* in order to not abolish but only partially block leukocyte egress (Pham et al. 2008). These mice are known to have a gene-dosage-dependent cell trafficking defect due to haploinsufficiency (Matloubian et al. 2004; Lo et al. 2005). As expected, *S1pr1*^{T-cell het} mice do not display any oscillations in lymph node cellularity, but show altered lymph rhythmicity. A reason for still observing oscillations in lymph could be due to a still rhythmic expression of CCR7. As mentioned before, CCR7 is, also in *S1pr1*^{T-cell het} mice, able to indirectly modulate S1P1 levels. Thus, leukocyte counts in lymph fluid still do oscillate, however, in an altered fashion.

These data suggest, that S1P1 gene expression is indeed responsible for the observed oscillations in lymph counts and in regulating proper rhythmic leukocyte trafficking. Similar to the CCR7-CCL21 axis, S1P1 function is mediated by a chemoattractant lipid, S1P. It is known, that high S1P levels are able to downregulate S1P1 and a fine-tuned S1P gradient is crucial for leukocytes to exit lymph nodes (Schwab et al. 2005; Pappu et al. 2007). However, we did not detect any oscillations in S1P levels, neither in lymph nor in blood. Consequently, merely the receptor (S1P1) and not the ligand exhibits a rhythmic expression profile. This hypothesis is strengthened by the fact, that titrated amounts of FTY720, a drug which antagonizes S1P1 receptor function, demonstrate a clear time- and dose-dependent reduction of lymph cellularity with increased FTY720 concentrations.

In fact, we detected strong oscillations of *S1pr1* mRNA levels in isolated CD4 T-cells, peaking at ZT7 and coinciding with high lymph counts. Interestingly, these *S1pr1* oscillations were abolished in mice which lack the circadian core gene *Bmal1* in CD4 T-cells, indicating that *Bmal1* is able to regulate *S1pr1* expression. In fact, data which was generated in the lab of our collaborator Henrik Oster using a luciferase assay did show, that *Bmal1* is able to regulate S1P1 expression (Druzd et al. 2017). Although this data set suggests a negative regulation of *Bmal1*, this does not necessarily have to be the case, as clock mRNA and protein level rhythms usually do not occur at the same time but are often out of phase by several hours.

Chawla and colleagues describe that the cytokine genes *Ccl2* and *S100a8* are negatively regulated by BMAL1/CLOCK and these also exhibit only a slightly shifted profile to *Bmal1* - similar to *S1pr1* – peaking around ZT4 (Nguyen et al. 2013). The silencing of these cytokines occurs through the recruitment of a repressor complex to

the genes. The *S1pr1* gene exhibits several non-canonical E-boxes indicating a possibility that BMAL1/CLOCK heterodimers might also repress expression of *S1pr1* in this manner.

Taken together, our data demonstrate that a crucial gene, which regulates leukocyte egress is under circadian control. Interestingly, the *S1pr1* expression profile (high during the rest phase, low during active phase) is inverse to CCR7 oscillations (low during rest phase, high during active phase). These opposite rhythms make sense, as CCR7 can antagonize S1P1 function due to its role as a retention factor for leukocytes (Pham et al. 2008). Furthermore, the expression of CD69, a negative regulator of S1P1 (Shiow et al. 2006), is also inverse to the *S1pr1* expression profile. Although we did not investigate whether CD69 is also regulated by circadian genes, previously published studies suggest this mode of action. Specifically, the circadian gene *Per1* might be responsible for the upregulation of CD69 towards the beginning of the rest phase, as it downregulates the transcription factor Sox6, which itself is a negative regulator of CD69 (Le et al. 2013; Miyamoto et al. 2016). Altogether, a fine-tuned circadian machinery is responsible for the timing of leukocyte egress.

4.3 Outlook

Numerous studies have unravelled that integral parts of the innate immune system are under circadian control (Keller et al. 2009; Scheiermann et al. 2012; Nguyen et al. 2013; Gibbs et al. 2014). Although it has been recently shown that differentiation of leukocytes and critical factors of adaptive immunity are regulated by the circadian clock (Yu et al. 2013; Silver et al. 2012), little is known to what extent the circadian system orchestrates leukocyte trafficking.

The results of the work presented in this thesis expand our understanding of the mechanisms, which underlie leukocyte trafficking under steady-state and inflammatory conditions. Having established that the circadian clock in leukocytes drives rhythmic gene expression of pro-migratory molecules and together with rhythmic expression of endothelium-derived factors thus contributes to rhythmic leukocyte trafficking in lymph nodes, it would be beneficial to investigate the

contribution of other inputs to leukocyte trafficking. In fact, it has been recently reported that neural input to β 2-adrenergic receptors expressed on leukocytes regulates leukocyte egress from lymph nodes (Suzuki et al. 2016). It might be thus possible, that parts of the leukocyte adhesion cascade might be under control of different peripheral clocks, regulated by glucocorticoids or the sympathetic and parasympathetic nervous system as it has been shown for bone marrow and skeletal muscle (Scheiermann et al. 2012).

The work contained in this thesis has already been published within a larger project, investigating in addition to the molecular mechanism, which govern rhythmic leukocyte trafficking, the relevance of oscillatory lymph node counts for adaptive immune response and vaccination timing (Druzd et al. 2017). Within this paper, our data indicate that also the adaptive immune response to bacterial and viral infections is rhythmic. Furthermore, in a model of experimental autoimmune encephalomyelitis (EAE), immunization at the beginning of the active phase led to a higher immune response compared to immunization during the rest phase. Transferring this knowledge to humans, early morning hours should produce higher antibody titres. Indeed, preliminary studies could show that morning vaccination is associated with enhanced antibody responses (Phillips et al. 2008; Long et al. 2016).

In recent years, the term of chronopharmacology has become a new determinant in the treatment of diseases. In this context, research has provided evidence that the circadian system most prominently influences the activity of enzymes which are responsible for the metabolism of drugs, such as CYP P450 (Druzd et al. 2014). However, little is known to which extent diurnal differences in the expression profile of target molecules influence a drug's toxicity and efficacy. Our data indicate a time-of-day dependent sensitivity of Fingolimod, a drug, which has been used in the clinic since 2010 to treat multiple sclerosis. Due to the rhythmic expression profile of the drugs target, S1P1, treatment with 10% of the normal dose lead to a similar effect in leukopenia in our hands. Taking this knowledge into the daily clinical treatment routine could result in both lowering side-effects for the patient and lowering costs in healthcare. Hence, future research in the field of chronopharmacology will lead to improved therapeutic practises and the development of better drug strategies.

5 References

Ager, A. & May, M.J., 2015. Understanding high endothelial venules: Lessons for cancer immunology. *Oncoimmunology*, 4(6), p.e1008791.

Albrecht, U., 2012. Timing to Perfection: The Biology of Central and Peripheral Circadian Clocks. *Neuron*, 74(2), pp.246–260.

Alvarez, S.E. et al., 2010. Sphingosine-1-phosphate is a missing cofactor for the E3 ubiquitin ligase TRAF2. *Nature*, 465(7301), pp.1084–8.

von Andrian, U.H. & Mempel, T.R., 2003. Homing and cellular traffic in lymph nodes. *Nature reviews. Immunology*, 3(11), pp.867–78.

Ansel, K.M. et al., 2000. A chemokine-driven positive feedback loop organizes lymphoid follicles. *Nature*, 406(6793), pp.309–314.

Arjona, A. et al., 2012. Immunity's fourth dimension: Approaching the circadian-immune connection. *Trends in Immunology*, 33(12), pp.607–612.

Arjona, A. & Sarkar, D.K., 2008. Are circadian rhythms the code of hypothalamic-immune communication? Insights from natural killer cells. *Neurochemical Research*, 33(4), pp.708–718.

Arjona, A. & Sarkar, D.K., 2005. Circadian oscillations of clock genes, cytolytic factors, and cytokines in rat NK cells. *Journal of Immunology*, 174(12), pp.7618–7624.

Asfeldt, V.H., 1971. Plasma Corticosteroids in Normal Individuals: With Reference to the Orcadian Rhythm, ACTH Test, Insulin Test, and Dexamethasone Suppression Test. *Scandinavian Journal of Clinical and Laboratory Investigation*, 28(1), pp.61–70.

Bai, A. et al., 2007. Kruppel-like factor 2 controls T cell trafficking by activating L-selectin (CD62L) and sphingosine-1-phosphate receptor 1 transcription. *Journal of Immunology*, 178(12), pp.7632–7639.

Bai, Z. et al., 2013. Constitutive lymphocyte transmigration across the basal lamina of high endothelial venules is regulated by the autotaxin/lysophosphatidic acid axis. *J Immunol*, 190(5), pp.2036–2048.

Bajénoff, M. et al., 2006. Stromal Cell Networks Regulate Lymphocyte Entry, Migration, and Territoriality in Lymph Nodes. *Immunity*, 25(6), pp.989–1001.

Banerji, S. et al., 1999. LYVE-1, a new homologue of the CD44 glycoprotein, is a lymph-specific receptor for hyaluronan. *Journal of Cell Biology*, 144(4), pp.789–801.

Bollinger, T. et al., 2011. Circadian clocks in mouse and human CD4+ T cells. *PLoS ONE*, 6(12), pp.1–11.

Brinkmann, V. et al., 2010. Fingolimod (FTY720): discovery and development of an oral drug to treat multiple sclerosis. *Nature reviews. Drug discovery*, 9(11), pp.883–897.

Brown, S.A. et al., 2002. Rhythms of mammalian body temperature can sustain peripheral circadian clocks. *Current Biology*, 12(18), pp.1574–1583.

Bunger, M.K. et al., 2000. Mop3 is an essential component of the master circadian pacemaker in mammals. *Cell*, 103(7), pp.1009–1017.

Cahalan, M.D. & Parker, I., 2008. Choreography of Cell Motility and Interaction Dynamics Imaged by Two-Photon Microscopy in Lymphoid Organs. *Annual Review of Immunology*, 26(1), pp.585–626.

Carlson, C.M. et al., 2006. Kruppel-like factor 2 regulates thymocyte and T-cell migration. *Nature*, 442(7100), pp.299–302.

Choi, J.W. et al., 2011. FTY720 (fingolimod) efficacy in an animal model of multiple sclerosis requires astrocyte sphingosine 1-phosphate receptor 1 (S1P1) modulation. *Proceedings of the National Academy of Sciences of the United States of America*, 108(2), pp.751–6.

Cohen, J.N. et al., 2010. Lymph node-resident lymphatic endothelial cells mediate peripheral tolerance via Aire-independent direct antigen presentation. *The Journal of experimental medicine*, 207(4), pp.681–8.

Crosio, C. et al., 2000. Light induces chromatin modification in cells of the mammalian circadian clock. *Nature Neuroscience*, 2(12), pp.1241–1247.

Curtis, A.M. et al., 2014. Circadian Clock Proteins and Immunity. *Immunity*, 40(2), pp.178–186.

Cyster, J.G. & Schwab, S.R., 2012. Sphingosine-1-Phosphate and Lymphocyte Egress from Lymphoid Organs. *Annual Review of Immunology*, 30(1), pp.69–94.

Damiola, F. et al., 2000. Restricted feeding uncouples circadian oscillators in peripheral tissues from the central pacemaker in the suprachiasmatic nucleus. *Genes and Development*, 14(23), pp.2950–2961.

Darlington, T.K. et al., 1998. Closing the circadian loop: CLOCK-induced transcription of its own inhibitors per and tim. *Science*, 280(June), p.1599–603.

Dickmeis, T., 2009. Glucocorticoids and the circadian clock. *Journal of Endocrinology*, 200(1), pp.3–22.

Dimitrov, S. et al., 2009. Cortisol and epinephrine control opposing circadian rhythms in T cell subsets. *Cortisol and epinephrine control opposing circadian rhythms in T cell subsets.*, 113(21), pp.5134–5143.

Druzd, D. et al., 2017. Lymphocyte Circadian Clocks Control Lymph Node Trafficking and Adaptive Immune Responses. *Immunity*, 46(1), pp.120–132.

Druzd, D., de Juan, A. & Scheiermann, C., 2014. Circadian rhythms in leukocyte trafficking. *Seminars in Immunopathology*, 36, pp.149–162.

Druzd, D. & Scheiermann, C., 2013. Some Monocytes Got Rhythm. *Science*, 341(6153), pp.1462–1464.

Dunlap, J.C., 1999. Molecular bases for circadian clocks. *Cell*, 96(2), pp.271–290.

Elenkov, I.J., Chrousos, G.P. & Wilder, R.L., 2000. Neuroendocrine regulation of IL-12 and TNF-alpha/IL-10 balance. Clinical implications. *Ann N Y Acad Sci*, 917, pp.94–105.

Faroudi, M. et al., 2010. Critical roles for Rac GTPases in T cell migration to and within lymph nodes. *Blood*, 116(25), pp.5536–5547.

Fernandes, G. et al., 1976. Circadian rhythmic plaque-forming cell response of spleens from mice immunized with SRBC. *Journal of immunology (Baltimore, Md. : 1950)*, 117(3), pp.962–6.

Förster, R. et al., 1999. CCR7 coordinates the primary immune response by establishing functional microenvironments in secondary lymphoid organs. *Cell*,

99(1), pp.23–33.

Fortier, E.E. et al., 2011. Circadian variation of the response of T cells to antigen. *J Immunol*, 187(12), pp.6291–6300.

Fretham Stephanie, Derived copy of Anatomy of the Lymphatic and Immune Systems. OpenStax CNX. 17. Juli 2014 <http://cnx.org/contents/2c1d0878-e6c7-4cf0-929c-d68455988cc6@1>.

Gachon, F. et al., 2004. The mammalian circadian timing system: from gene expression to physiology. *Chromosoma*, 113(3), pp.103–12.

Gekakis, N. et al., 1998. Role of the CLOCK protein in the mammalian circadian mechanism. *Science (New York, N.Y.)*, 280(5369), pp.1564–1569.

Gibbs, J. et al., 2014. An epithelial circadian clock controls pulmonary inflammation and glucocorticoid action. *Nature medicine*, 20(8), pp.919–26.

Girard, J.-P., Moussion, C. & Förster, R., 2012. HEVs, lymphatics and homeostatic immune cell trafficking in lymph nodes. *Nature Reviews Immunology*, 12(11), pp.762–773.

Golan, K. et al., 2012. S1P promotes murine progenitor cell egress and mobilization via S1P 1-mediated ROS signaling and SDF-1 release. *Blood*, 119(11), pp.2478–2488.

Golombek, D. a & Rosenstein, R.E., 2010. Physiology of Circadian Entrainment. *Physiology Rev*, 90(3), pp.1063–1102.

Green, C.B., Takahashi, J.S. & Bass, J., 2008. The Meter of Metabolism. *Cell*, 134(5), pp.728–742.

Griffin, E.A., Staknis, D. & Weitz, C.J., 1999. Light-independent role of CRY1 and CRY2 in the mammalian circadian clock. *Science*, 286(5440), pp.768–771.

Hanson, M. et al., 2012. Crystal Structure of a Lipid G Protein – Coupled Receptor. *Science*, 335(February), pp.851–856.

Harikumar, K.B. et al., 2009. Corrected 16 october 2009; see last page. , 742(October), pp.1107–1111.

Hemmers, S. & Rudensky, A.Y., 2015. The Cell-Intrinsic Circadian Clock Is

Disposable for Lymphocyte Differentiation and Function. *Cell reports*, 11(9), pp.1339–49.

Herzog, B.H. et al., 2013. Podoplanin maintains high endothelial venule integrity by interacting with platelet CLEC-2. *Nature*, 502(7469), pp.105–109.

Hogenesch, J.B. et al., 1998. The basic-helix-loop-helix-PAS orphan MOP3 forms transcriptionally active complexes with circadian and hypoxia factors. *Proceedings of the National Academy of Sciences of the United States of America*, 95(10), pp.5474–9.

Ionac, M., 2003. One technique, two approaches, and results: Thoracic duct cannulation in small laboratory animals. *Microsurgery*, 23(3), pp.239–245.

J. L. Gowans, E.J.K., 1964. The Route of Re-Circulation of Lymphocytes in the Rat Author. *Proceedings of the Royal Society of London*, 159(975).

Jin, X. et al., 1999. A molecular mechanism regulating rhythmic output from the suprachiasmatic circadian clock. *Cell*, 96(1), pp.57–68.

Juarez, J.G. et al., 2012. Sphingosine-1-phosphate facilitates trafficking of hematopoietic stem cells and their mobilization by CXCR4 antagonists in mice. *Blood*, 119(3), pp.707–716.

Keller, M. et al., 2009. A circadian clock in macrophages controls inflammatory immune responses. *Proceedings of the National Academy of Sciences of the United States of America*, 106(50), pp.21407–12.

Kondo, T. et al., 1993. Circadian rhythms in prokaryotes: luciferase as a reporter of circadian gene expression in cyanobacteria. *Proc.Natl.Acad.Sci.USA*, 90(12), pp.5672–5676.

Kornmann, B. et al., 2007. System-driven and oscillator-dependent circadian transcription in mice with a conditionally active liver clock. *PLoS Biology*, 5(2), pp.0179–0189.

Labrecque, N. & Cermakian, N., 2015. Circadian Clocks in the Immune System. *Journal of biological rhythms*, 30(4), pp.277–90.

Le, N.Q. et al., 2013. Negative correlation between Per1 and Sox6 expression during chondrogenic differentiation in pre-chondrocytic ATDC5 cells. *Journal of*

pharmacological sciences, 122(4), pp.318–25.

Lee, M.J. et al., 1998. Sphingosine-1-phosphate as a ligand for the G protein-coupled receptor EDG-1. *Science*, 279(5356), pp.1552–1555.

Lipp, M. et al., 2016. Functional Microenvironments in Secondary Primary Immune Response by Establishing Pillars Article: CCR7 Coordinates the. *J Immunol The Journal of Immunology at UB Marburg on*, 196, pp.5–15.

Litvinenko, G.I. et al., 2005. Circadian dynamics of cell composition of the thymus and lymph nodes in mice normally, under conditions of permanent illumination, and after melatonin injection. *Bulletin of Experimental Biology and Medicine*, 140(2), pp.213–216.

Liu, Y. et al., 2000. Edg-1, the G protein-coupled receptor for sphingosine-1-phosphate, is essential for vascular maturation. *Journal of Clinical Investigation*, 106(8), pp.951–961.

Lo, C.G. et al., 2005. Cyclical modulation of sphingosine-1-phosphate receptor 1 surface expression during lymphocyte recirculation and relationship to lymphoid organ transit. *The Journal of experimental medicine*, 201(2), pp.291–301.

Long, J.E. et al., 2016. Morning vaccination enhances antibody response over afternoon vaccination: A cluster-randomised trial. *Vaccine*, 34(24), pp.2679–2685.

Louveau, A. et al., 2015. Structural and functional features of central nervous system lymphatic vessels. *Nature*, 523(7560), pp.337–41.

Maceyka, M. & Spiegel, S., 2014. Sphingolipid metabolites in inflammatory disease. *Nature*, 510(7503), pp.58–67.

Mandala, S. et al., 2002. Alteration of lymphocyte trafficking by sphingosine-1-phosphate receptor agonists. *Science (New York, N.Y.)*, 296(5566), pp.346–349.

Mandl, J.N. et al., 2012. Quantification of lymph node transit times reveals differences in antigen surveillance strategies of naive CD4+ and CD8+ T cells. *Proceedings of the National Academy of Sciences*, 109(44), pp.18036–18041.

Margaris, K.N. & Black, R. a, 2012. Modelling the lymphatic system : challenges and opportunities. *J R Soc Interface*, 9(69), pp.601–612.

Martinet, L. et al., 2011. Human solid tumors contain high endothelial venules: Association with T- and B-lymphocyte infiltration and favorable prognosis in breast cancer. *Cancer Research*, 71(17), pp.5678–5687.

Matloubian, M. et al., 2004. Lymphocyte egress from thymus and peripheral lymphoid organs is dependent on S1P receptor 1. *Nature*, 427(6972), pp.355–60.

Mempel, T.R., Henrickson, S.E. & Von Andrian, U.H., 2004. T-cell priming by dendritic cells in lymph nodes occurs in three distinct phases. *Nature*, 427(6970), pp.154–159.

Méndez-Ferrer, S. et al., 2008. Haematopoietic stem cell release is regulated by circadian oscillations. *Nature*, 452(7186), pp.442–447.

Miller, M.J. et al., 2002. Two-photon imaging of lymphocyte motility and antigen response in intact lymph node. *Science (New York, N.Y.)*, 296(5574), pp.1869–1873.

Mionnet, C. et al., 2011. High endothelial venules as traffic control points maintaining lymphocyte population homeostasis in lymph nodes. *High endothelial venules as traffic control points maintaining lymphocyte population homeostasis in lymph nodes.*, 118(23), pp.6115–6122.

Miyamoto, Y. et al., 2016. VCAM1 acts in parallel with CD69 and is required for the initiation of oligodendrocyte myelination. *Nature Communications*, 7, p.13478.

Miyasaka, M. & Tanaka, T., 2004. Lymphocyte trafficking across high endothelial venules: dogmas and enigmas. *Nature reviews. Immunology*, 4(5), pp.360–370.

Mukherji, A. et al., 2013. Homeostasis in intestinal epithelium is orchestrated by the circadian clock and microbiota cues transduced by TLRs. *Cell*, 153(4), pp.812–827.

Nader, N., Chrousos, G.P. & Kino, T., 2009. Circadian rhythm transcription factor CLOCK regulates the transcriptional activity of the glucocorticoid receptor by acetylating its hinge region lysine cluster: potential physiological implications. *Faseb J*, 23(5), pp.1572–1583.

Nguyen, K.D. et al., 2013. Circadian gene Bmal1 regulates diurnal oscillations of Ly6C(hi) inflammatory monocytes. *Science (New York, N.Y.)*, 341(6153),

pp.1483–8.

Nieminen, M. et al., 2006. Vimentin function in lymphocyte adhesion and transcellular migration. *Nature Cell Biology*, 8(2), pp.156–162.

Panda, S. et al., 2002. Coordinated transcription of key pathways in the mouse by the circadian clock. *Cell*, 109(3), pp.307–320.

Pappu, R. et al., 2007. Promotion of lymphocyte egress into blood and lymph by distinct sources of sphingosine-1-phosphate. *Science*, 316(5822), pp.295–298.

Pham, T.H.M. et al., 2010. Lymphatic endothelial cell sphingosine kinase activity is required for lymphocyte egress and lymphatic patterning. *The Journal of experimental medicine*, 207(1), pp.17–27.

Pham, T.H.M. et al., 2008. S1P1 Receptor Signaling Overrides Retention Mediated by G??i-Coupled Receptors to Promote T Cell Egress. *Immunity*, 28(1), pp.122–133.

Phillips, A.C. et al., 2008. Preliminary evidence that morning vaccination is associated with an enhanced antibody response in men. *Psychophysiology*, 45(4), pp.663–666.

Preitner, N. et al., 2002. The orphan nuclear receptor REV-ERB?? controls circadian transcription within the positive limb of the mammalian circadian oscillator. *Cell*, 110(2), pp.251–260.

Qi, H., 2006. Extrafollicular Activation of Lymph Node B Cells by Antigen-Bearing Dendritic Cells. *Science*, 312(5780), pp.1672–1676.

Ralph, M.R. et al., 1990. Transplanted suprachiasmatic nucleus determines circadian period. *Science (New York, N.Y.)*, 247(4945), pp.975–978.

Ramming, A. et al., 2012. Maturation-related histone modifications in the PU.1 promoter regulate Th9-cell development. *Blood*, 119(20), pp.4665–4674.

Saini, C. et al., 2012. 2012 - behavior and plasticity of mammalian circadian oscillators Simulated body temperature rhythms reveal the phase-shifting behavior and plasticity of mammalian circadian oscillators - U.pdf. , pp.567–580.

Scheiermann, C. et al., 2012. Adrenergic nerves govern circadian leukocyte

recruitment to tissues. *Immunity*, 37(2), pp.290–301.

Scheiermann, C., Kunisaki, Y. & Frenette, P.S., 2013. Circadian control of the immune system. *Nature reviews. Immunology*, 13(3), pp.190–8.

Schwab, S.R. et al., 2005. Lymphocyte sequestration through S1P lyase inhibition and disruption of S1P gradients. *Science (New York, N.Y.)*, 309(5741), pp.1735–9.

Sharma, S. & Zhu, J., 2014. Immunologic applications of conditional gene modification technology in the mouse. *Current protocols in immunology*, 105(4), pp.1–17.

Shiow, L.R. et al., 2006. CD69 acts downstream of interferon-alpha/beta to inhibit S1P1 and lymphocyte egress from lymphoid organs. *Nature*, 440(7083), pp.540–544.

Silver, A.C., Arjona, A., Hughes, M.E., et al., 2012. Circadian expression of clock genes in mouse macrophages, dendritic cells, and B cells. *Brain, Behavior, and Immunity*, 26(3), pp.407–413.

Silver, A.C., Arjona, A., Walker, W.E., et al., 2012. The Circadian Clock Controls Toll-like Receptor 9-Mediated Innate and Adaptive Immunity. *Immunity*, 36(2), pp.251–261.

Silver, R. et al., 1996. A diffusible coupling signal from the transplanted suprachiasmatic nucleus controlling circadian locomotor rhythms. *Nature*, 382(6594), pp.810–3.

Śledzińska, A. et al., 2013. TGF-β Signalling Is Required for CD4+ T Cell Homeostasis But Dispensable for Regulatory T Cell Function. *PLoS Biology*, 11(10).

Stokkan, K. et al., 2001. Entrainment of the Circadian Clock in the Liver by Feeding. *Science*, 291, pp.490–493.

Storch, K. et al., 2002. Extensive and divergent circadian gene expression in liver and heart. *Nature*, 417(May), p.78–83.

Sun, Y. et al., 2006. MOP3, a component of the molecular clock, regulates the development of B cells. *Immunology*, 119(4), pp.451–460.

Suzuki, K. et al., 2016. Adrenergic control of the adaptive immune response by diurnal lymphocyte recirculation through lymph nodes. *The Journal of Experimental Medicine*, p.jem.20160723.

Thaiss, C.A. et al., 2016. Microbiota Diurnal Rhythmicity Programs Host Transcriptome Oscillations. *Cell*, 167(6), p.1495–1510.e12.

Trevaskis, N.L., Kaminskas, L.M. & Porter, C.J.H., 2015. From sewer to saviour - targeting the lymphatic system to promote drug exposure and activity. *Nature reviews. Drug discovery*, 14(11), pp.781–803.

Ueda, H.R. et al., 2005. System-level identification of transcriptional circuits underlying mammalian circadian clocks. *Nature genetics*, 37(2), pp.187–92.

Umemoto, E. et al., 2006. Nepmucin, a novel HEV sialomucin, mediates L-selectin-dependent lymphocyte rolling and promotes lymphocyte adhesion under flow. *The Journal of experimental medicine*, 203(6), pp.1603–14.

Venkataraman, K. et al., 2008. Vascular endothelium as a contributor of plasma sphingosine 1-phosphate. *Circulation Research*, 102(6), pp.669–676.

Warnock, R. a et al., 1998. Molecular mechanisms of lymphocyte homing to peripheral lymph nodes. *The Journal of experimental medicine*, 187(2), pp.205–16.

Wigle, J.T. & Oliver, G., 1999. Prox1 function is required for the development of the murine lymphatic system. *Cell*, 98(6), pp.769–778.

Yang, X. et al., 2006. Nuclear Receptor Expression Links the Circadian Clock to Metabolism. *Cell*, 126(4), pp.801–810.

Yu, X. et al., 2013. TH17 cell differentiation is regulated by the circadian clock. *Science (New York, N.Y.)*, 342(6159), pp.727–30.

6 Appendix

6.1 Publications arising from this work

Druzd, D., Matveeva, O., Ince, L., Harrison, U., He, W., Schmal, C., Herz, H., Tsang, A., Kawakami, N., Leliavski, A., Uhl, O., Yao, L., Sander, L., Chen, C., Kraus, K., de Juan, A., Hergenhan, S., Ehlers, M., Koletzko, B., Haas, R., Solbach, W., Oster, H., and Scheiermann, C. (2017) Lymphocyte circadian clocks control lymph node trafficking and Adaptive Immune Responses. *Immunity*, 46(1), pp.120–132

Druzd, D., de Juan, A., and Scheiermann, C. Circadian rhythms in leukocyte trafficking. (2014) *Seminars in Immunopathology*, 36:149-62

Druzd, D. & Scheiermann, C. (2013) Some Monocytes Got Rhythm. *Science*, pp.1462–1464

Affidavit

Druzd, David Jakob

Surname, first name

Marchioninstrasse 27

Street

81377, Munich

Zip code, town

Germany

Country

I hereby declare, that the submitted thesis entitled

Control of lymphocyte trafficking through lymph nodes by the circadian clock

is my own work. I have only used the sources indicated and have not made unauthorised use of services of a third party. Where the work of others has been quoted or reproduced, the source is always given.

I further declare that the submitted thesis or parts thereof have not been presented as part of an examination degree to any other university.

Ort, Datum

Unterschrift, Doktorand